Final Report

GTO-19-C011 L2NAM1982F & L2NAM1984N
Data Reprocessing

For:
Energie Beheer Nederland B.V. (EBN)

December 2019

GEOFIZYKA TORUŃ
GRUPA PGNiG

Table of Contents

1. Introduction

The processing was performed under the “Agreement for the Processing of Seismic Data (Regional 2D Reprocessing of 1982/1984 NAM DEEP lines and Processing of the 2019 EBN 2D test line L2EBN2019SCAN001)” between EBN B.V. and Geofizyka Toruń S.A., Contract no. GTO-19-C011 dated February 2019.
The merged 1982/1984 NAM DEEP 2D line consists of 803,41 km (in total) of 2D data - single and triple (swath) lines acquired by Prakla in 1982 (446,70 km) and acquired by Prakla and G.S.I in 1984 (356,71 km) in central part of the Netherlands.
Processing was carried out by Geofizyka Torun in its processing center located in Toruń, Poland with SeisSpace software of Landmark, SUMMIG and VELANAL software of Techco Geophysical Services Ltd., GLI Hampson-Russell and GT’s proprietary tools and procedures.

The 1982/1984 NAM DEEP merged 2D line reprocessing project consists of the base processing sequence for entire dataset considered as a one volume from field data, final PreSTM and post-processing.

Separated NAM DEEP lines were delivered to GT included text navigation files, seismic data in SEG-D format, observer log files with comments and acquisition reports in PDF format.

A general location of L2NAM1982F lines is shown in the map at Fig.1 and location of L2NAM1984N lines is shown in the map at Fig.2 Coordinates were generated with use of following geodetic parameters:

Datum:	Amersfoort/RD New (EPSG28992)
Associated Ellipsoid:	Bessel 1841
Semi-main axis (*a*):	6377397.155
Hemisphere:	NE
Flattening (*f*):	1/299.1528128
Projection type:	Oblique Stereographic
Longitude of origin(λ_0):	05° 23' 15.50" E
Latitude of origin(φ_0):	52° 09' 22.178" N
False easting (FE):	155000
False northing (FNE):	463000
Scale factor (K):	0.9999079
Measurement unit:	International Meter.

Location of individual (single & triple) NAM DEEP lines and location of EBN TEST Line (L2EBN2019) are shown on Fig. 3.

Fig.1. General location of L2NAM1982F lines (from Agreement for the processing… . Appendix 2)

Fig.2. General location of L2NAM1984N lines (from Agreement for the processing… . Appendix 2)

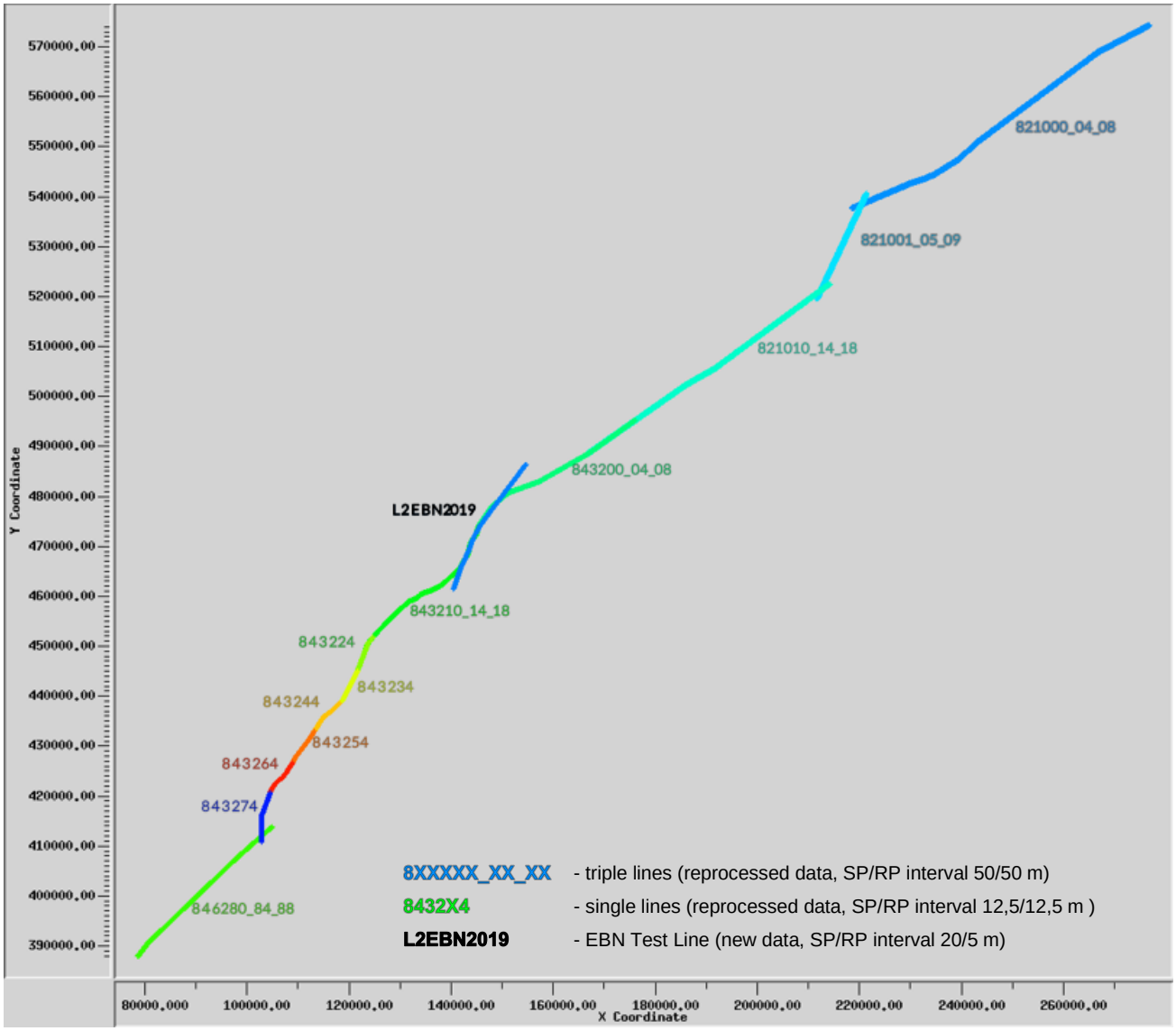

Fig. 3. NAM DEEP lines: six triple lines and six single lines merged give a 2D line from Bergen op Zoom (Zeeland) to Oudeschans (Groningen). L2EBN2019 test line (blue line) was processed separately.

1.1. Processing objectives

(from EBN Service Order Technical Specifications)

The 2019 EBN test line project, comprising acquisition, processing and interpretation of 2019 EBN test line, is a part of the work described in Contract no. GTO-19-C011 for Regional 2D Seismic Reprocessing of 1982/1984 NAM DEEP lines and Processing of the 2019 EBN 2D test line, which will comprise the reprocessing of vintage data as well as the acquisition of new 2D seismic data in areas with low data density. The aim is to decrease the subsurface uncertainty and hence shape the conditions needed for the successful development of geothermal projects in the area of interest

The purpose of the reprocessing was to test the feasibility and possible data improvements that can be achieved by applying state-of-the-art processing workflows to old vintage 2D seismic data. The NAM DEEP lines are of particular interest, as most of the data has been acquire with multiple shot & receiver lines, relatively large offsets and partly with deep shot holes and good size explosive charges.

1.2. Geological setting

(from EBN Service Order Technical Specifications)

1.2.1. Stratigraphy

The stratigraphic interval of interest ranges from Lower Carboniferous (Dinantian) carbonates at a depth of approximately 4500–6000 m to Cenozoic sands as shallow as 200 m below mean sea level (Van Adrichem Boogaert& Kouwe, 1993–1997). The primary targets for geothermal projects in the area are Lower Carboniferous carbonates and Permian (Rotliegend) sandstones. Secondary targets include Cenozoic sands, Zechstein carbonates, Triassic sandstones, Upper Jurassic/Lower Cretaceous sandstones and possibly Upper Cretaceous Chalk and Upper Carboniferous sandstones.

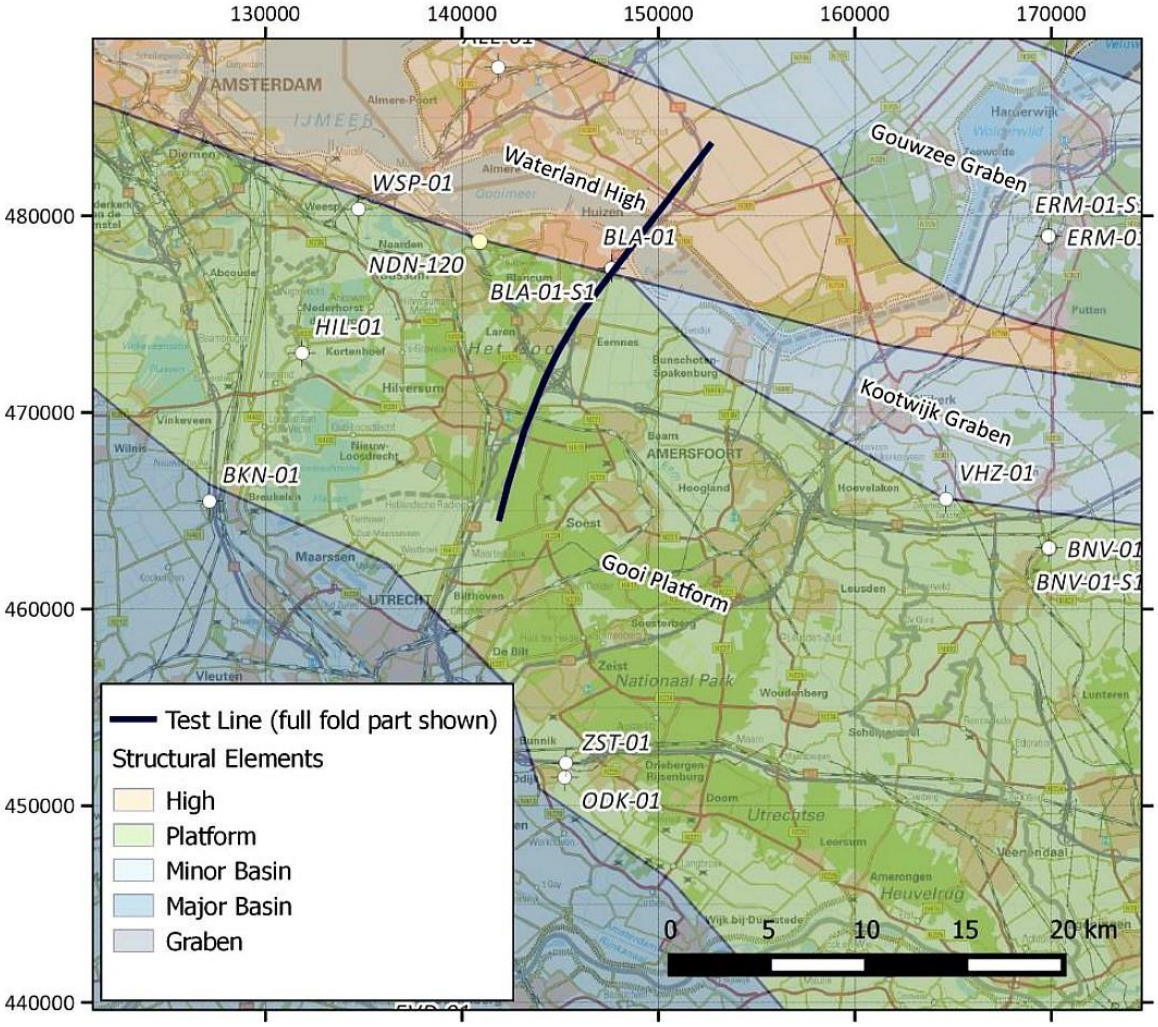

Fig. 4. Late Jurassic – Early Cretaceous structural elements in and around the 2019 EBN 2D test line (central part of the NAM DEEP line).

2019 EBN 2D test line that was acquired straddles the boundary between two structural features: the Waterland High in the north, and the Gooi Platform in the south (see Fig. 4). The line partly overlaps with an existing seismic line from the 1980s, an interpreted version of which is shown in Fig. 5. The Gooi Platform was subjected to moderate extension during the Mesozoic and to moderate inversion during the Cretaceous to Paleogene. Deformation of the Waterland High during these periods was minor. This results in distinct structural styles for the two domains.

From the limited amount of 2D data that is available in the vicinity of the seismic line it can be inferred that the Gooi Platform area is crosscut by WNW-ESE to NNW-SSE trending faults, with a spacing between faults of hundreds of metres to kilometres. These faults are interpreted to have been active as normal faults during the Mesozoic. During the Late Cretaceous to Paleogene the faults were reactivated as reverse and strike-slip faults, as indicated by the presence of flower structures.

From old to young the stratigraphy relevant for this test line is expected to consist of:

- Lower Carboniferous (Dinantian) carbonates and shales. Deposition of carbonates during this period, in either platform and / or basinal setting was related to a regional extension phase. Syn-sedimentary faults with offsets of hundreds of metres to kilometres may be present. Below the Waterland High a reflector is observed at a depth where the Dinantian is expected. Below the Gooi Platform no such reflector is present. It is at present unclear whether this is due to the absence of the Dinantian in a platform facies, or due to a limitation in data quality. One of the aims of the test line is to shed new light on this issue.
- An Upper Carboniferous siliciclastic sequence (sandstones, claystones and coal). The top of the Upper Carboniferous sequence was eroded along the Base Permian Unconformity (BPU) during the Late Carboniferous to Permian, following uplift related to the Variscan Orogeny.
- The Permian Rotliegend Slochteren Sandstone interval overlies the BPU. Its primary thickness in the Dutch onshore varies from about 150 m in the northwest to 0 m in the southeast. In the area of the test line a thickness of 50 to 150 m is expected.
- The Permian Zechstein interval is relatively thin in area C (compared to the Friesland – Groningen area). Main lithologies are carbonates, anhydrites and claystones with possibly minor amounts of rock salt in the northernmost section of the test line.
- The Lower Germanic Trias Group comprises the Lower Buntsandstein Formation including the Main Claystone Member (Geluk, 2007). This Group comprises interbedded claystones and sandstones. The Main Claystone Member is a laterally continuous and homogeneous stratigraphic interval. Seismic stacking velocities or log data from this unit can be used to estimate the maximum burial of Triassic and older units; in part of the area maximum burial is possibly higher than present-day burial, causing lateral velocity variations (Japsen, 2000).
- The Upper Germanic Trias Group comprises sandstones, claystones, carbonates and evaporites (predominantly anhydrites and some rock salt).
- The Lower Jurassic Altena Group consists of claystones.
- The Lower Cretaceous Rijnland Group consists predominantly of claystones with commonly a basal sandstone sequence. Locally, sand and claystones of the Schieland Group are present below the Rijnland Group. The Rijnland Group overlies a major unconformity. The presumed thickness of the removed section varies regionally; the deposits below the unconformity may by as young as the Upper Jurassic–Lower Cretaceous Schieland Group (if it was deposited) and as old as the Upper Carboniferous Limburg Group.
- The Upper Cretaceous Chalk Group consists, as the name suggests, almost exclusively of Chalk. It has a variable thickness caused by intraformational erosive events but predominantly the base

North Sea Supergroup Unconformity. The internal seismic velocity of this Chalk interval may vary considerably, both vertically and laterally. The formation is only expected in the southern segment of the test line.

- The uppermost lithostratigraphic group, the North Sea Supergroup consists primarily of unconsolidated sandstones and claystones. Its base is a major unconformity that progressively cuts down into the Triassic and results from a major tectonic inversion event and subsequent erosion.

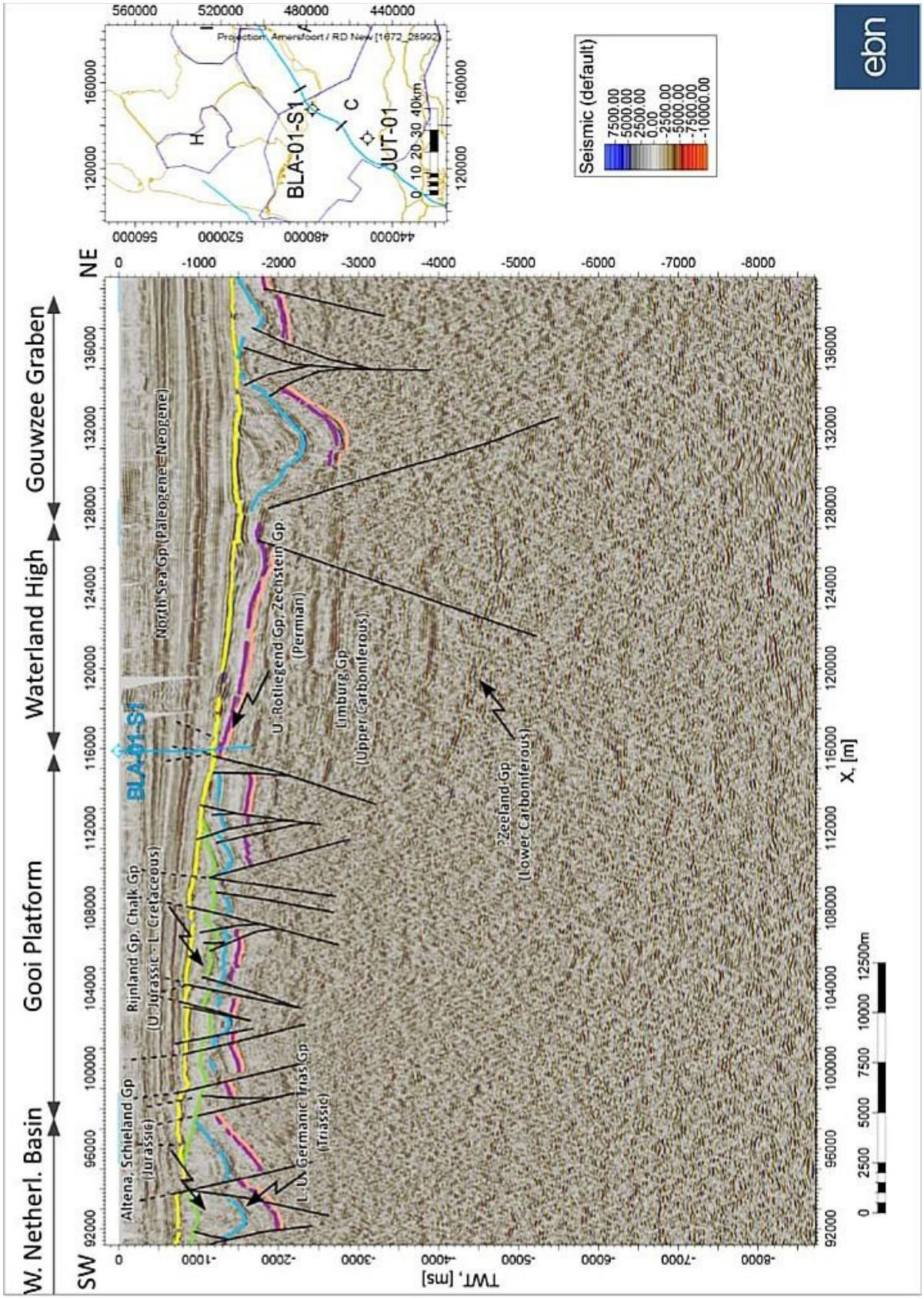

Fig. 5. Interpreted seismic section NAM-DEEP (central part of the line). An increase in acoustic impedance is represented by a negative number and displayed in red. The segment between X=104000 and 126000 m roughly corresponds to the seismic line that is to be acquired.

1.2.2. Shallow subsurface

The youngest sediments, part of the Upper North Sea Group, were deposited during the Quaternary period and constitute the near surface and soil profile, comprising sands, clays, peat and glacial deposits. The distribution of these sediments is well mapped in the publicly available models DGM v2.2 and GEOTOP (see https://www.dinoloket.nl/en/subsurface-models). The expected surface geology (Figure 6) of the test line up to a depth of 30 m can be divided in two parts: the part south of Laren and the northern half of the line.

The southern half of the line is located on the eastern flank of a hilly area called “Het Gooi”. The elevation at the test line ranges here between 0 and 5 m above sea level. The hills came into existence during the ice ages when Scandinavian sourced land ice pushed the frozen underground upwards. At the test line location this ice pushed deposits, mainly sands, can be encountered at a depth of 12–25 m below ground level. On top of these ice pushed sands, periglacial sands of the Drente Formation can be found, 8–15 m thick. These are capped by 3–10 m thick wind-blown sands of the Boxtel Formation. The groundwater level in this area is typically 0–1 m above sea level, so around 1–4 m below ground level.

The northern half of the line is located outside the ice pushed ridge and has Holocene deposits at surface. On top of the Drente Formation a 5–20 m thick Eem Formation can be found, which consists of marine sands and clays. The top of the Eem Formation is found 8–15 m below ground level. The Eem Formation is covered by around 8 m of wind-blown sands of the Boxtel Formation. A layer of a few meters of Holland peat is present on top of the Boxtel Formation, this peat is found at surface in the area north of Eemnes. At the northernmost part of the test line marine clayey or silty sands, up to 5 m thick are present. In the northern half of the line the ground water is typically found at 0–1 m below ground level.

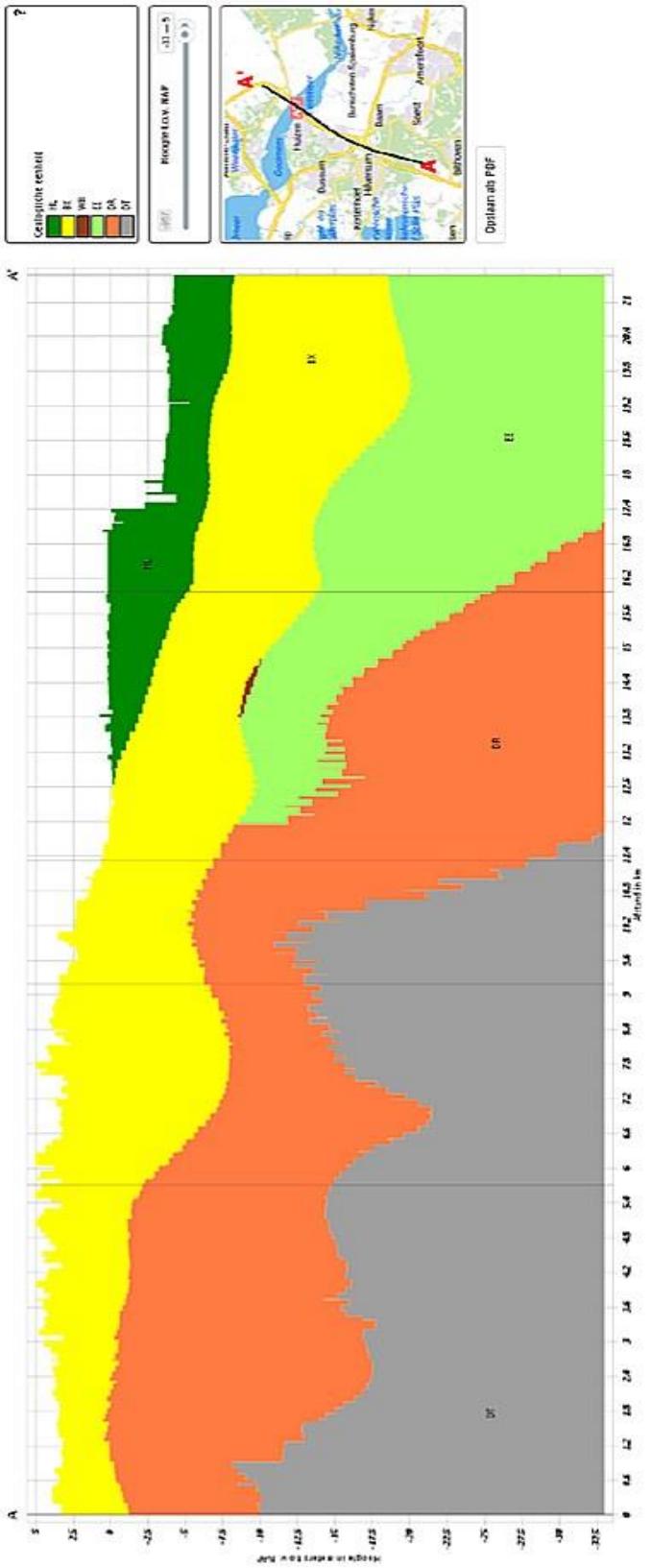

Fig. 6. Shallow geology along the 2019 EBN 2D test line (central part of NAM DEEP line). Source: DGM v. 2.2 (https://www.dinoloket.nl/en/subsurface-models). HL: Holocene, BX: Boxtel Formation, WB: Woudenberg Formation, EE: Eem Formation, DR: Drente Formation, DT: Ice Pushed Deposits.

1.3. Characterization of target interval

(from EBN Service Order Technical Specifications)

1.3.1 Primary targets

Rotliegend sandstones

The main uncertainties relevant to the assessment of the geothermal potential of the Rotliegend sandstones in the vicinity of the seismic line are:

- Reservoir quality. The wells in the southernmost part of area C show poor reservoir quality as a result of deep burial. The present-day depth is not excessive, but the reservoir has been buried deep prior to inversion, causing the reservoir to have a very poor transmissivity (< 2 Dm). Hence, it is essential to assess which areas were affected by inversion, and by how much.
- Thickness. On a regional scale the Rotliegend Group has an onlap configuration onto the London-Brabant-massif in the south. Its thickness is of the order of hundreds of metres in the north of the Netherlands, and zero in the south of the Netherlands. Local thickness variations may occur that are related to the topography at the time of deposition, which in turn resulted from Variscan faulting and folding, and from differential erosion of the Westphalian. Relatively shale prone intervals of the Westphalian subcrop are eroded more intensely at the BPU and consequently more accommodation space is created and thicker Rotliegend is expected (e.g., Mijnlieff & Geluk, 2008).

Lower Carboniferous (Dinantian) carbonates

The presence of Lower Carboniferous (Dinantian) carbonates has not yet been proven in the area with a well. Their presence is inferred (Figure 7) from the fact that the central part of the area was a high from Westphalian (Late Carboniferous) to Cenozoic times. Based on the assumption that highs are generally long-lived, a fault-bounded high with a carbonate build-up on top is inferred, which would have been surrounded by deeper water (Pagnier et al., 2002; Geluk et al., 2007; Van Hulten& Poty, 2008; Boxem et al., 2016). The presence of an Early Carboniferous fault-bounded high and thus carbonate platforms is estimated based on the subcrop pattern at BPU-level; regions where relatively old Westphalian (A or B) subcrops the Base Permian Unconformity are taken to indicate the presence of a Dinantian carbonate build-up; the surrounding basinal deposits are expected to compact more easily, allowing for the preservation of a thicker section of Westphalian (Van Hulten& Poty, 2008). This assumes that Variscan inversion was of secondary importance for the subcrop pattern (e.g., Pagnier et al., 2002), an assumption that can be challenged (e.g. Kombrink, 2008). The outline in Figure 7 is based on the present-day preservation of the Late Cretaceous Chalk Group, based on the assumption that the underlying Lower Carboniferous carbonate platform prevented inversion here during the Cenozoic, preserving the Chalk.

To test these hypotheses, improved subsurface data is required. The presently available seismic data does not image depths (4–7,5 km) at which the Dinantian is expected and no wells are drilled in this area to these depths.

1.3.2 Secondary targets

Secondary geothermal targets in area C are Zechstein Carbonates, Triassic sandstones, Upper Jurassic / Lower Cretaceous sandstones and Cenozoic sands.

Zechstein Carbonates

Locally, Zechstein carbonates are proven gas reservoirs. It appears that the permeable intervals are either facies related or result from fracturing or leaching. Permeable facies include slope and platform facies including collapse breccias. From regional mapping (Geluk, 2007) it may be concluded that the Zechstein -1 and -3 carbonate sequences may have some potential in area C. Large scale leaching may have occurred around the Maasbommel High, below the Kimmerian Unconformity and potentially in the area of Amsterdam below the Kimmerian and Laramide Unconformities.

Triassic Sandstones

Where present, Triassic sandstones may provide a geothermal reservoir. However, in the study area only thin sands are expected. To the south they increase in thickness and there the Röt interval is present in a fringe sandstone facies as well. As is the case with the Rotliegend the Triassic reservoirs have been uplifted during inversion and suffer from poor reservoir quality as a result from deep maximum burial (see also 1.3.1 Primary targets - Rotliegend sandstones). As for the Zechstein, the Triassic sandstones may have been locally leached below the Kimmerian and Laramide Unconformities.

Vlieland Sandstone

Within the larger surroundings of area C the Upper Jurassic / Lower Cretaceous strata, amongst which the Vlieland Sandstone Formation, proves to be a prolific reservoir for both hydrocarbons and geothermal resources. There is a very general rule of thumb stating that a relation exists between the total thickness of the Vlieland Subgroup (KNN) and the presence of a basal sandstone interval. Within the vicinity of the line the thickness of this stratigraphic interval is limited and thus only modest amounts of sand are expected.

Cenozoic sands

Data availability to support the geothermal potential of the Cenozoic below 200 m are few and far between, even though all oil and gas wells drilled through this interval. This is due to the fact that data acquisition (logging) in this interval was limited to the bare minimum. Additionally, the well density in area C is very low. The first prerequisite for assessing the geothermal potential or the potential for heat storage/buffering, is a reliable reservoir delineation of the main sand packages such as the Brussels Sand Member. Focus should be on the seismic recognition of these intervals and the identification of intra-Cenozoic truncation surfaces under which the potential reservoir zone may not be present due to erosion. In the southern part of the planned line a large part of the Middle and Lower North Sea interval has been eroded/has not been deposited. Chances of encountering reservoir sands are better towards the northeast, where the stratigraphic interval is more complete.

Other secondary targets

The possible secondary targets Chalk and Westphalian (Upper Carboniferous) are present in area C but matrix porosity and permeability of these potential reservoir units is generally expected to be very low.

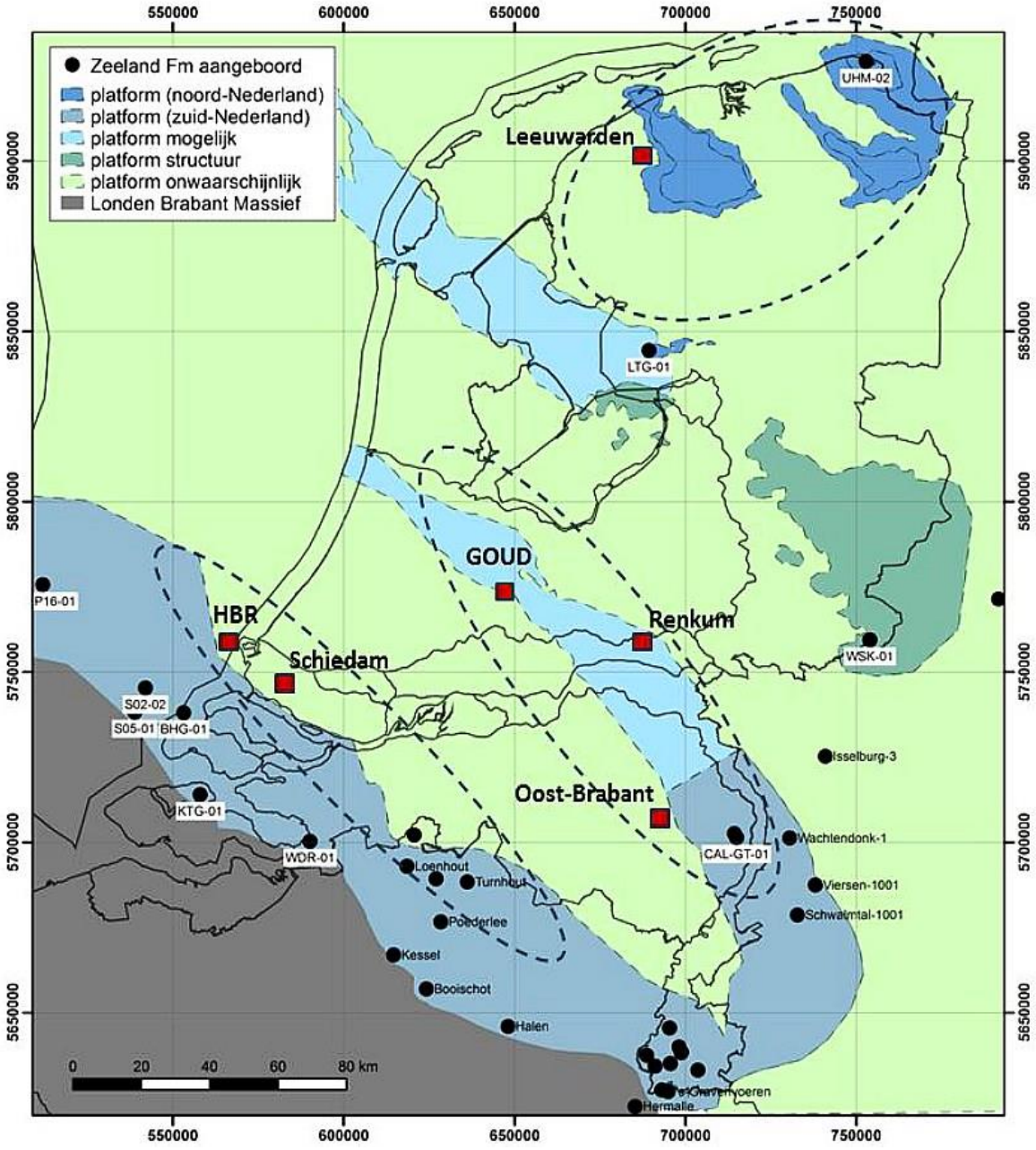

Fig. 7. Facies map of the Dinantian (Early Carboniferous) from Boxem et al. (2016). “Platform mogelijk”: platform possible, “Platform structuur”: platform structure, “Platform onwaarschijnlijk”: platform unlikely, “Zeeland Formatie aangeboord”: Zeeland Fm encountered in well.

1.4. Key personnel

Key GT's personnel involved in seismic data reprocessing of the NAM-DEEP line were following persons:

Krzysztof Kolasiński	Seismic Data Processing Department Manager
Seweryn Tlałka	Deputy Manager/ Chief Technologist
Jacek Biesaga	Processing Group Manager
Marek Popielarski	Team Leader (NAM-DEEP project)/ Senior Processing Specialist
Piotr Wędrowski	Senior Processing Specialist
Rafał Zalewski	Processing Specialist
Marcin Osiński	Processing Specialist
Anna Zduniak	Processing Specialist
Piotr Idzikowski	Seismic Databases Manager
Anna Machalska	Technical Support
Ireneusz Gorczyca	Technical Support
Henryk Kowalski	R&D Manager
Grzegorz Ząbik	R&D Senior Processing Specialist

On behalf of EBN the work was supervised by:

Johannes Rehling	Technical Representative
Audrey Roustiau	Deputy Technical Representative.

2. Acquisition summary

The 1982 NAM-DEEP lines have been acquired as swath lines (3 shot lines and 3 receiver lines parallel to each other). All receivers were recording all shots, even though the shot increment per individual lines within a swath was varying.

The 1984 NAM-DEEP lines have been acquired with varying acquisition parameters. Some of lines were shot as swath while other were shot as single lines.

Detailed description of acquisition parameters is presented in Table 1.

1984 NAM-DEEP single lines

Line No	SP Range		Length (km)	No of Traces	Nominal Fold in 25m bin	Record Length (s)	Sampling Rate (ms)	Shot Interval (m)	Group Interval (m)	Spread Type	Far Offset (m)	Near Offset (m)	Geophone Array (m)	No of Geophones per Group	Geophone Type	Source	Antialias filter (Hz)	Instruments
843224	1028,5	1888,5	10,75	288	576	10	4	12,5	12,5	Off-End	3593,75	12,5	15,4	12	SM-4	Dynamite	Out-62.5/72	SN-348
843234	1288,5	1888,5	7,50	288	576	10	4	12,5	12,5	Off-End	3593,75	12,5	15,4	12	SM-4	Dynamite	Out-62.5/72	SN-348
843244	1289,5	1582,5	3,66	288	576	10	4	12,5	12,5	Off-End	3593,75	12,5	15,4	12	SM-4	Dynamite	Out-62.5/72	SN-348
	1582,5	1888,5	3,83	288	576	10	4	12,5	12,5	Asymmetrical	3581,25	218,75	15,4	12	SM-4	Dynamite	Out-62.5/72	SN-348
843254	1289,5	1888,5	7,49	288	576	10	4	12,5	12,5	Asymmetrical	3581,25	218,75	15,4	12	SM-4	Dynamite	Out-62.5/72	SN-348
843264	1077,5	1888,5	10,14	288	576	10	4	12,5	12,5	Asymmetrical	3581,25	218,75	15,4	12	SM-4	Dynamite	Out-62.5/72	SN-348
843274	1289,5	1853,5	7,05	288	576	10	4	12,5	12,5	Asymmetrical	3581,25	218,75	15,4	12	SM-4	Dynamite	Out-62.5/72	SN-348
Total km.:			50,41															

1982/1984 NAM-DEEP swath lines

Line No	SP Range		Length (km)	No of Traces	Nominal Fold in 25m bin	Record Length (s)	Sampling Rate (ms)	Shot Interval (m)	Group Interval (m)	Spread Type	Far Offset (m)	Near Offset (m)	Geophone Array (m)	No of Geophones per Group	Geophone Type	Source	Antialias filter (Hz)	Instruments
821000/1004/1008	3615	4955	201,00	3 x 120	360	10	4	50	50	Off-End	5975	25	45,8	12	SM-4	Dynamite	Out-125/72	SN-348
821001/1005/1009	3081	3550	70,35	3 x 120	360	10	4	50	50	Off-End	5975	25	45,8	12	SM-4	Dynamite	Out-125/72	SN-348
821010/1014/1018	1879	3048	175,35	3 x 120	360	10	4	50	50	Off-End	5975	25	45,8	12	SM-4	Dynamite	Out-125/72	SN-348
843200/204/208	95	845	112,50	3 x 96	432	10	4	50	50	Off-End	4775	25	45,8	12	SM-4	Dynamite	Out-62.5/72	SN-348
843210/214/218	96	701	90,75	3 x 96	432	10	4	50	50	Off-End	4775	25	45,8	12	SM-4	Dynamite	Out-62.5/72	SN-348
846280/284/288	50	737	103,05	3 x 100	450	10	4	50	50	Off-End	4975	25	45,8	12	SM-4	Dynamite	Out-125/72	SN-348
Total km.:			753,00															

Table 1. Acquisition parameters of NAM-DEEP 2D lines.

3. Processing summary

The processing sequence and parameters were tested on shot records, CMP gathers and control sections. The processing sequence and parameters of particular procedures were arranged with active participation of EBN representative who had decisive influence on final scheme of conducted works. The processing flowcharts are shown on Fig. 8, and 9.

General list of performed procedures on the 2019 EBN test line is as follows:

1. Loading data to processing.
2. Manual geometry preparing
3. Loading geometry to trace headers & QC.
4. Merging single and triple lines into one 2D line
5. Trace edition (automatic)
6. Automatic First Break picking.
7. Base static correction calculation
8. Spherical divergence correction.
9. Coherent noise attenuation in shot domain.
10. Random noise attenuation in shot and receiver domain.
11. Instrument &Geophone dephasing.
12. 1st pass of surface-consistent trace amplitude scaling (SCAC 1).
13. Phase and amplitude inverse Q-compensation.
14. Surface-consistent spiking deconvolution.
15. 2nd pass of surface-consistent trace amplitude scaling (SCAC 2).
16. Base static correction application.
17. Velocity analysis.
18. Residual static corrections calculation and application.
19. Multiple reflection attenuation.
20. Data interpolation.
21. Preparing data for PreSTM.
22. Final pre-migration velocity analysis.
23. 1st pass of Pre-Stack Time Migration for velocity analysis.
24. 1st iteration of migration velocity analysis
25. 2nd pass of Pre-Stack Time Migration for velocity analysis.
26. 2nd iteration of migration velocity analysis.
27. Final iteration of VTI Pre-Stack Time Migration
28. Final velocity analysis (3rd iteration of migration velocity analysis).
29. Final post-migration multiple reflection attenuation.
30. Residual coherent (linear) noise attenuation – two passes.
31. Trim statics.
32. Trace muting.
33. Final PreSTM stacking.
34. Final post-stack processing.

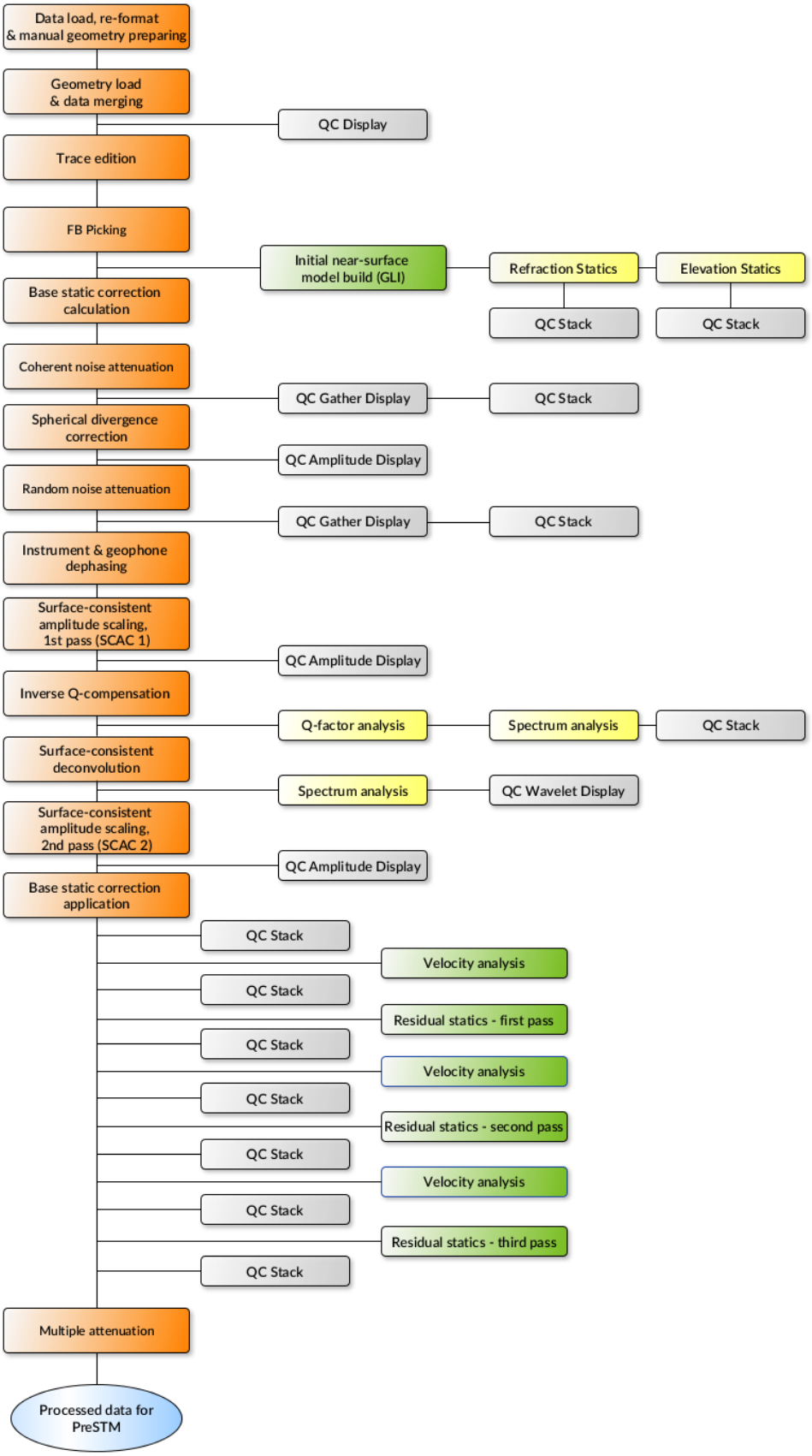

Fig. 8. Flowchart of Base Processing sequence before Pre-Stack Time Migration.

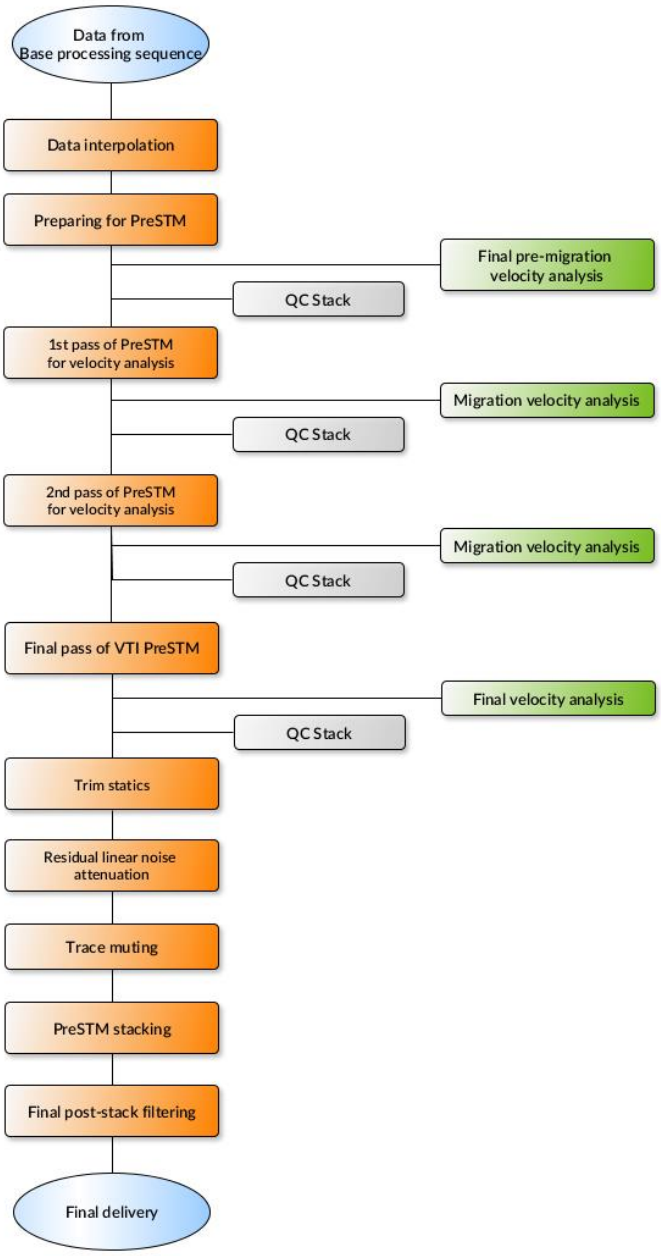

Fig. 9. Flowchart of pre-migration phase of time processing.

4. Project management

The responsibility for contact with EBN was carried by two persons: Team Leader and Processing Group Manager. The Team Leader gathered information from executive staff and prepared weekly reports containing detailed status of processing. Weekly reports were sent to client every Tuesday with information about achievements of the previous week. The usual form of contact was Webex meetings arranged every Wednesday with presence of EBN Representatives, Team Leader, Processing Group Manager and executive staff persons depending on issues discussed.
All decisions made during the meetings were specified in “Minutes of the Meeting” documents which were later created and agreed by both parties.

There were two meetings in Torun and 27 Webex meetings, the “Minutes of the Meeting” documents were sent to the Client via e-mail and are stored on CD with this report.

Base Processing Sequence for entire dataset from data input to Pre-Stack Time Migration – commenced in April 2019 and completed in December 2019.

5. Testing

The processing sequence and parameters were tested on selected shot records, CMP gathers and control sections. For certain tests plots of amplitudes or other attributes were produced.
Testing was carried out on the part of merged NAM DEEP Line corresponding to EBN Test Line. The pictures placed in this report also refer to this part – CDP range: 3924-5156, full CDP range is 2-11172. Tests were prepared in the form of PowerPoint presentations, shown and discussed during Webex meetings and delivered to EBN via SFTP at the start of the project and later via OneDrive. The work flowchart is shown on figures Fig. 8 - Fig. 9. The final processing sequence along with parameters is described in 6th section of this report. The PowerPoint presentations containing tests were posted on FTP site and OneDrive and are stored on CD with this report.

6. Production QC

The sequence of seismic data processing for the implementation of the tasks set was determined on the basis of tests performed after approval by EBN. The work on the project consisted of Base Processing Sequence for entire dataset with Pre-Stack Time Migration and post-processing,

The next subsections contain detailed description of used procedures with parameters.

6.1. Base Processing Sequence with Pre-STM and post-processing

Processing Sequence before Pre-Stack Time Migration:

- Input data and reformat to SeisSpace internal format,
- Manual geometry preparing
- Geometry assignment with detailed QC carried out,
- Merging single and triple lines into one 2D line
- Noisy trace editing and bad records elimination,
- Manual first-break picking in offset range 0-2000 m,
- Near-surface model building and base static corrections calculation:
  - initial refraction model calculation with use of General Linear Inversion (GLI),
  - long and short component calculation,
  - grid spacing equal to CDP bin size,
  - velocity smoothing window 1200 m (horizontal) and 600 m (vertical),
- Ground-roll attenuation in shot domain

  Ground Roll Removal:
  - filter width: 11 traces,
  - frequencies: 0-16 Hz,
  - number of frequency bands: 4,
  - windowed application (only for ground-roll),

- Shot-domain de-spike and high-threshold anomalous amplitude suppression in bottom part of the data *(De-burst energy scaling ST)*:
  - window length: 100 ms,
  - window width: 22,
  - percentage threshold: 750 %,
- Receiver-domain de-spike and high-threshold anomalous amplitude suppression in bottom part of the data *(De-burst energy scaling ST)*:
  - window length: 100 ms,
  - window width: 22,
  - percentage threshold: 500 %,
- Spherical divergence correction *(True Amplitude Recovery)*:
  - gain function $g(t) = t^{1.3}$,
- Instrument and geophone dephasing on basis of known receiver characteristic,
- Surface consistent amplitude scaling (1st pass):
  - decomposition: source, receiver, offset,
  - application: shot, receiver,
- Inverse phase and amplitude Q-compensation:
  - attenuation dispersion formula: Futterman
  - frequency of Q model: 40 Hz,
  - reference frequency: 15 Hz,
  - max. gain: 15 dB,
  - type of Q value: effective Q,
  - Q value: 100,
- Surface consistent predictive deconvolution, calculated in single time window:
  - decomposition: source, receiver, offset, CMP,
  - application: shot, receiver,
  - operator length: 160 ms,
  - percentage pre-whitening: 0.1 %,
  - prediction distance: 16 ms,
- Surface consistent amplitude scaling (2nd pass):
  - decomposition: source, receiver, offset,
  - application: shot, receiver,
- Base static correction application:
  - application of long-wavelength and short-wavelength refraction static corrections,
- Interactive velocity analysis (1st pass):
  - grid density: 1000 m,
  - used super-gather size: 11 CMP bins,
- Residual statics (I) corrections calculation and application *(Max. Power Autostatics)*:
  - smash length: 5 CMP bins,

- maximum time shift: ± 100 ms.
- time gate width: 3000 ms,

- Interactive velocity analysis (2nd pass):
  - grid density: 500 m,
  - used super-gather size: 11 CMP bins,
- Residual statics (II) corrections calculation and application *(Max. Power Autostatics)*:
  - smash length: 5 CMP bins,
  - maximum time shift: ± 60 ms,
  - time gate width: 2000 ms,
- Interactive velocity analysis (3rd pass):
  - grid density: 500 m,
  - used super-gather size: 11 CMP bins,
- Residual statics (III) corrections calculation and application *(Max. Power Autostatics)*:
  - smash length: 5 CMP bins,
  - maximum time shift: ± 30 ms,
  - time gate width: 1500 ms,
- Multiple reflection attenuation *(Radon Filter)*:
  - number of P-values: 160
  - P-values range: -100 – 400 ms,
  - reference offset for P-values: 2500 m,
  - frequency range of interest: 6-90 Hz,
  - type of transform: Parabolic,

Pre-Stack Time Migration sequence:

- Trace interpolation *(LSS Trace Interpolation)*:
  - number of dips for interpolation: 17,
  - dip range for interpolation: +/- 3 ms/trace,
  - max. distance for interpolation: 31 traces,
- Final pre-migration interactive dense velocity analysis:
  - grid density: 250 m,
  - used super-gather size: 5 CMP bins,
- 1st pass of Kirchhoff PreSTM for velocity analysis:
  - migration angle: 30.0 deg,
  - antialias percentage: 100.0,
  - half aperture: 3000 m,
- 1st pass of migration velocity analysis:
  - grid density: 250 m,
  - used super-gather size: 5 CMP bins,

- 2nd pass of Kirchhoff PreSTM for velocity analysis:
  - migration angle: 30.0 deg,
  - antialias percentage: 100.0,
  - half aperture: 3000 m,
- 2nd pass of migration velocity analysis:
  - grid density: 250 m,
  - used super-gather size: 5 CMP bins,
- Final Kirchhoff VTI PreSTM:
  - migration angle: 30.0 deg,
  - antialias percentage: 100.0,
  - half aperture: 3000 m,
- Final velocity analysis (3rd pass of migration velocity analysis):
  - grid density: 250 m,
  - used super-gather size: 5 CMP bins,
- Final residual multiple reflection attenuation *(Radon Filter)*:
  - number of P-values: 800,
  - P-values range: -100-400 ms,
  - reference offset for P-values: 1500 m,
  - frequency range of interest: 6-90 Hz,
  - type of transform: Parabolic
- Final coherent noise attenuation (*Radon Filter* applied twice in cascade mode):

  1st iteration:
  - number of P-values: 1201,
  - P-values range: 250 - 4000 ms,
  - reference offset for P-values: 3000 m,
  - frequency range of interest: 0-25 Hz,
  - type of transform: Linear,

  2nd iteration:
  - number of P-values: 1201,
  - P-values range: 200 - 5500 ms,
  - reference offset for P-values: 3000 m,
  - frequency range of interest: 0-20 Hz,
  - type of transform: Linear,
- Residual static corrections in CMP gathers (*External Model Trim Statics*):
  - max. static shift: ± 4 ms,
- Final post-migration (residual) velocity analysis:
  - grid density: 250 m,
  - used super-gather size: 5 CMP bins,
- Trace muting analysis and application (for full offset range PreSTM stack),
- Percentage mute application (for percentage offset limited PreSTM stacks),

- Final PreSTM stacking,
- Post-Stack S/N Enhancement (*Dip Scan Stack*)
  - aperture size 5 traces
  - dip range (min/max) +/-12ms
- Spectral enhancement (*Spectral Shaping*),
- Final post-stack filtering in 6 time windows (*Bandpass Filter*):

Time window:	Filter frequency values:
0 – 1000 ms	4-8-90-130 Hz,
1000 – 2000 ms	4-6-85-110 Hz,
2000 – 3000 ms	4-6-64-76 Hz,
3000 – 5000 ms	4-6-32-44 Hz,
5000 – 7000 ms	4-6-28-36 Hz,
7000 – 10000 ms	4-6-24-32 Hz,

- Final post-stack dynamic scaling – only for additional version with S/N ratio enhancement (*Automatic Gain Control*):
  - type of AGC scalar: Mean,
  - AGC operator length: 500 ms,
- Polarity reverse in order to correspond to European SEG Standard.

6.2. Offset Stacks

At the Client's additional request following offset stacks (final sections after PreSTM) were produced, dividing the pre-stack data into three (3) offset ranges:

- "Near" for 33,3% of mute offset
- "Mid" for mute offset between 33,3% and 66,7%
- "Far" for mute offset between 66,7% and 100%.

Offset stacks were produced and sent to the Client for Basic Processing

For more information see point. 8.11

7. Deliverables

ASCII Output Archiving Products:

NAM_DEEP_Line_Muting.txt	Final outer muting
NAM_DEEP_Line_Velocities_before_Migration.txt	Stacking Velocities before Migration, datum: 0m NAP
NAM_DEEP_Line_Velocities_Final_Migration.txt	PreSTM velocities, datum: 0m NAP
NAM_DEEP_Line_Velocities_Final_Migration_Stacking.txt	Final Stacking Velocities, datum: 0m NAP
NAM_DEEP_Line_Final_ETA.txt	ETA parameter, datum: 0m NAP

SEGY Output Archiving Products:

NAM_DEEP_Line_Velocities_before_Migration.sgy	Stacking Velocities before Migration, datum: 0m NAP
NAM_DEEP_Line_Velocities_Final_Migration.sgy	PreSTM velocities, datum: 0m NAP
NAM_DEEP_Line_Velocities_Final_Migration_Stacking.sgy	Final Stacking Velocities, datum: 0m NAP
NAM_DEEP_Line_Final_ETA.sgy	ETA parameter, datum: 0m NAP

SEGY Seismic Pre-Stack Output Archiving Products:

NAM_DEEP_Line_Gathers_Shots_After_Identing.sgy	Shots after identing
NAM_DEEP_Line_Gathers_CDP_After_Denoise.sgy	CDP gathers after denoise
NAM_DEEP_Line_Gathers_CDP_Before_PreSTM.sgy	CDP gathers as input to migration
NAM_DEEP_Line_Gathers_CDP-VTI_PreSTM.sgy	CDP gathers just after VTI PreSTM
NAM_DEEP_Line_Gathers_CDP_FINAL-VTI_PreSTM.sgy	CDP gathers processed after VTI PreSTM

SEGY Seismic Full Stack Output Archiving Products:

NAM_DEEP_Line_Stack_After_Denoise.sgy - Stack after denoise

NAM_DEEP_Line_Stack_Before_PreSTM.sgy - Stack before PreSTM

NAM_DEEP_Line_Stack_Final-VTI_PreSTM_AGC_ROT.sgy - Final full PreSTM (including spectral shaping & TVF), with post-migration pre-stack & post-stack scaling, with phase rotation

NAM_DEEP_Line_Stack_Final-VTI_PreSTM_AGC.sgy - Final full PreSTM (including spectral shaping & TVF), with post-migration pre-stack & post-stack scaling, without phase rotation

NAM_DEEP_Line_Stack_Final-VTI_PreSTM_ROT.sgy - Final full PreSTM (including spectral shaping & TVF), without pre-migration scaling, with phase rotation

NAM_DEEP_Line_Stack_Final-VTI_PreSTM.sgy - Final full PreSTM (including spectral shaping & TVF), without pre-migration scaling, without phase rotation

NAM_DEEP_Line_Stack_Raw-VTI_PreSTM_AGC_ROT.sgy - Raw full PreSTM (excluding spectral shaping & TVF), with post-migration pre-stack & post-stack scaling, with phase rotation

NAM_DEEP_Line_Stack_Raw-VTI_PreSTM_AGC.sgy - Raw full PreSTM (excluding spectral shaping & TVF), with post-migration pre-stack & post-stack scaling, without phase rotation

NAM_DEEP_Line_Stack_Raw-VTI_PreSTM_ROT.sgy - Raw full PreSTM (excluding spectral shaping & TVF), without pre-migration scaling, with phase rotation

NAM_DEEP_Line_Stack_Raw-VTI_PreSTM.sgy - Raw full PreSTM (excluding spectral shaping & TVF), without pre-migration scaling, without phase rotation

SEGY Seismic Offset Stack Output Archiving Products:

NAM_DEEP_Line_Stack_Final-VTI_PreSTM_AGC_far_offsets.sgy - Final far offsets PreSTM (including spectral shaping & TVF), with post-migration pre-stack & post-stack scaling, without phase rotation

NAM_DEEP_Line_Stack_Final-VTI_PreSTM_AGC_mid_offsets.sgy - Final mid offsets PreSTM (including spectral shaping & TVF), with post-migration pre-stack & post-stack scaling, without phase rotation

NAM_DEEP_Line_Stack_Final-VTI_PreSTM_AGC_near_offsets.sgy - Final near offsets PreSTM (including spectral shaping & TVF), with post-migration pre-stack & post-stack scaling, without phase rotation

NAM_DEEP_Line_Stack_Final-VTI_PreSTM_AGC_ROT_far_offsets.sgy - Final far offsets PreSTM (including spectral shaping & TVF), with post-migration pre-stack & post-stack scaling, with phase rotation

NAM_DEEP_Line_Stack_Final-VTI_PreSTM_AGC_ROT_mid_offsets.sgy - Final mid offsets PreSTM (including spectral shaping & TVF), with post-migration pre-stack & post-stack scaling, with phase rotation

NAM_DEEP_Line_Stack_Final-VTI_PreSTM_AGC_ROT_near_offsets.sgy - Final near offsets PreSTM (including spectral shaping & TVF), with post-migration pre-stack & post-stack scaling, with phase rotation

NAM_DEEP_Line_Stack_Final-VTI_PreSTM_far_offsets.sgy - Final far offsets PreSTM (including spectral shaping & TVF), without pre-migration scaling, without phase rotation

NAM_DEEP_Line_Stack_Final-VTI_PreSTM_mid_offsets.sgy - Final mid offsets PreSTM (including spectral shaping & TVF), without pre-migration scaling, without phase rotation

NAM_DEEP_Line_Stack_Final-VTI_PreSTM_near_offsets.sgy - Final near offsets PreSTM (including spectral shaping & TVF), without pre-migration scaling, without phase rotation

NAM_DEEP_Line_Stack_Final-VTI_PreSTM_ROT_far_offsets.sgy - Final far offsets PreSTM (including spectral shaping & TVF), without pre-migration scaling, with phase rotation

NAM_DEEP_Line_Stack_Final-VTI_PreSTM_ROT_mid_offsets.sgy - Final mid offsets PreSTM (including spectral shaping & TVF), without pre-migration scaling, with phase rotation

NAM_DEEP_Line_Stack_Final-VTI_PreSTM_ROT_near_offsets.sgy - Final near offsets PreSTM (including spectral shaping & TVF), without pre-migration scaling, with phase rotation

NAM_DEEP_Line_Stack_Raw-VTI_PreSTM_AGC_far_offsets.sgy - Raw far offsets PreSTM (excluding spectral shaping & TVF), with post-migration pre-stack & post-stack scaling, without phase rotation

NAM_DEEP_Line_Stack_Raw-VTI_PreSTM_AGC_mid_offsets.sgy - Raw mid offsets PreSTM (excluding spectral shaping & TVF), with post-migration pre-stack & post-stack scaling, without phase rotation

NAM_DEEP_Line_Stack_Raw-VTI_PreSTM_AGC_near_offsets.sgy - Raw near offsets PreSTM (excluding spectral shaping & TVF), with post-migration pre-stack & post-stack scaling, without phase rotation

NAM_DEEP_Line_Stack_Raw-VTI_PreSTM_AGC_ROT_far_offsets.sgy - Raw far offsets PreSTM (excluding spectral shaping & TVF), with post-migration pre-stack & post-stack scaling, with phase rotation

NAM_DEEP_Line_Stack_Raw-VTI_PreSTM_AGC_ROT_mid_offsets.sgy - Raw mid offsets PreSTM (excluding spectral shaping & TVF), with post-migration pre-stack & post-stack scaling, with phase rotation

NAM_DEEP_Line_Stack_Raw-VTI_PreSTM_AGC_ROT_near_offsets.sgy - Raw near offsets PreSTM (excluding spectral shaping & TVF), with post-migration pre-stack & post-stack scaling, with phase rotation

NAM_DEEP_Line_Stack_Raw-VTI_PreSTM_far_offsets.sgy - Raw far offsets PreSTM (excluding spectral shaping & TVF), without pre-migration scaling, without phase rotation

NAM_DEEP_Line_Stack_Raw-VTI_PreSTM_mid_offsets.sgy - Raw mid offsets PreSTM (excluding spectral shaping & TVF), without pre-migration scaling, without phase rotation

NAM_DEEP_Line_Stack_Raw-VTI_PreSTM_near_offsets.sgy - Raw near offsets PreSTM (excluding spectral shaping & TVF), without pre-migration scaling, without phase rotation

NAM_DEEP_Line_Stack_Raw-VTI_PreSTM_ROT_far_offsets.sgy - Raw far offsets PreSTM (excluding spectral shaping & TVF), without pre-migration scaling, with phase rotation

NAM_DEEP_Line_Stack_Raw-VTI_PreSTM_ROT_mid_offsets.sgy - Raw mid offsets PreSTM (excluding spectral shaping & TVF), without pre-migration scaling, with phase rotation

NAM_DEEP_Line_Stack_Raw-VTI_PreSTM_ROT_near_offsets.sgy - Raw near offsets PreSTM (excluding spectral shaping & TVF), without pre-migration scaling, with phase rotation

8. Details of selected processing procedures

8.1. Noisy traces/bad records edition

Initial trace edition was performed during QC at preliminary stage of processing. The main task of this procedure was to eliminate the following groups of traces:

- noisy with no chance to suppress noise,
- zero amplitude (containing no data).

Preliminarily the number of non-zero traces was estimated at 4,202,167. However, at the early stage of processing few additional records were identified as corrupted like files 654, 655, 1040, 1041 on line 821010_14_18. In this case the record is stuck together with previous or next one with no possibility to distinguish which one is correct and merge of navigation properly. Automatic edition was checked and an additional number of the most noisy traces have been edited and excluded from further processing.

Total traces input:	4,199,287
Total traces in 400/25 grid	4,117,514
Live traces after editing:	3,909,099
Number of traces rejected:	208,415
Percentage of traces rejected:	5,06%

Results of trace editing/bad records elimination on stacked section are presented on Fig. 10.

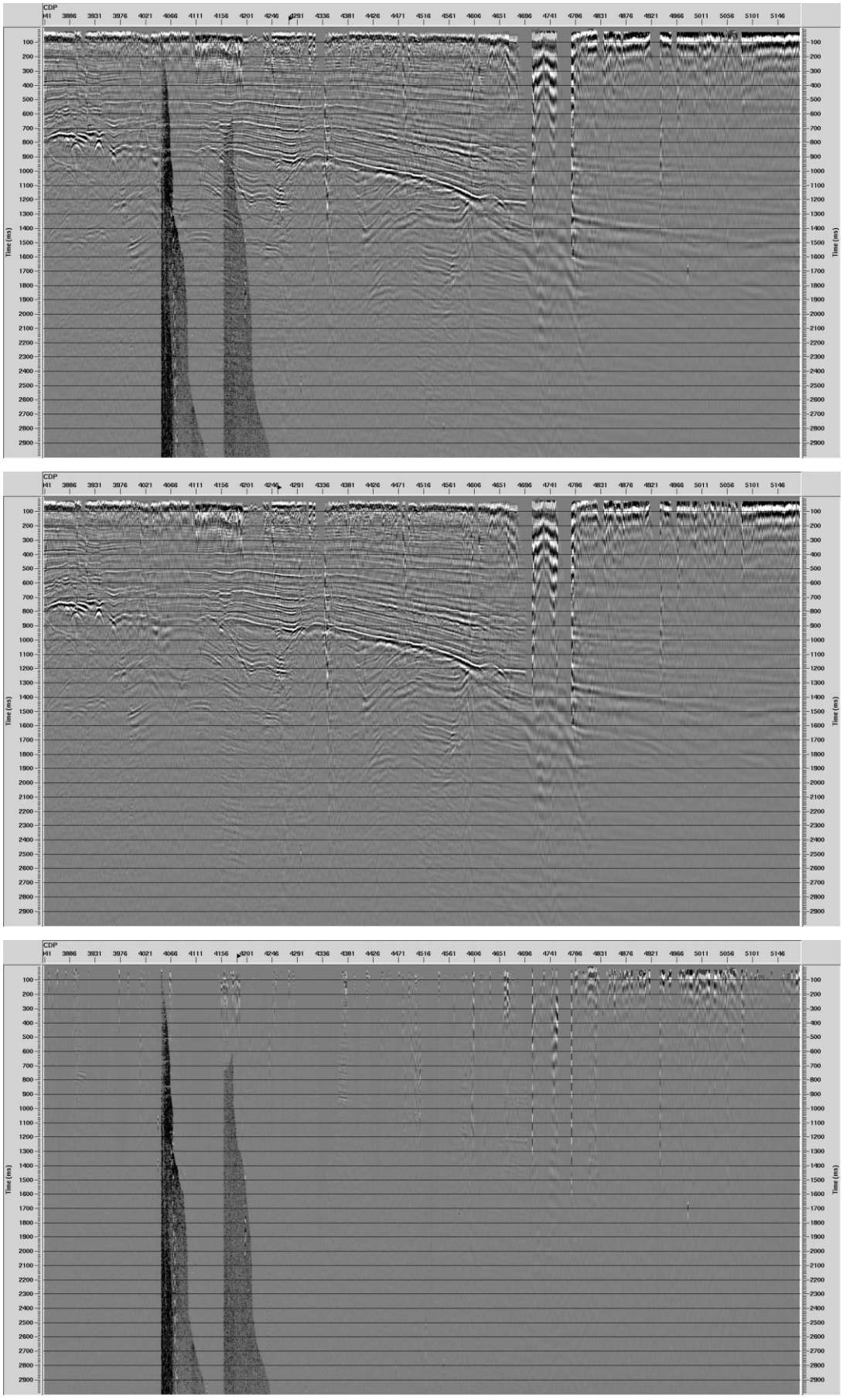

Fig. 10. Raw stacked section: before noisy traces elimination (top), after noisy traces elimination (middle) and difference between stacks with and without noisy traces (bottom). Trace length 3 s.

8.2. Near surface model build and base static correction calculation

For the near surface model build GLI 2D/3D (a software by Hampson-Russell) was used. Refraction Static Computation was made on the basis of the first break picks. After tests and consulting with the EBN, offset range from 0 m to 2000 m was selected for further analysis. First breaks initially were picked in automatic manner and corrected manually.

Initial near surface model was created based on information (velocity and thickness) from discrete locations of Control Points summarizing the first break picking at the certain radius. In the following step obtained model is updated in the iterative mode to get the minimum error between times derived from the model and the arrival time from the real first break picks. Once the convergence is achieved, refraction static is computed using the pseudo datum calculation method. A replacement velocity of 1800 m/s and the reference datum NAP were used.

The best results were achieved with use of Generalized Linear Inversion (GLI) method for the following near surface model:

- number of layers below the weathering zone: 1,
- elevation range: -6 – +20 m above NAP,
- V0 – velocity of shallowest layer: 800 m/s,
- V1 – velocity of 1st layer: 1650 – 1930 m,
- range of offsets to pick first breaks: 0 – 2000 m,
- max. depth of model used to estimate static corrections: 100 m below NAP.

The figures below present:

Fig. 11 - examples of first break picking for selected shot records,

Fig. 12 - section through near surface model. Presented model is only a part of whole one, produced for merged NAM DEEP lines. The part corresponds to EBN Test Line,

Fig. 13 - distribution of refraction statics (applied in the processing) for shot & receiver points,

Fig. 14 - values of refraction and elevation statics for shot & receiver points,

Fig. 15 - control stack with elevation statics applied,

Fig. 16 - control stack with refraction statics applied.

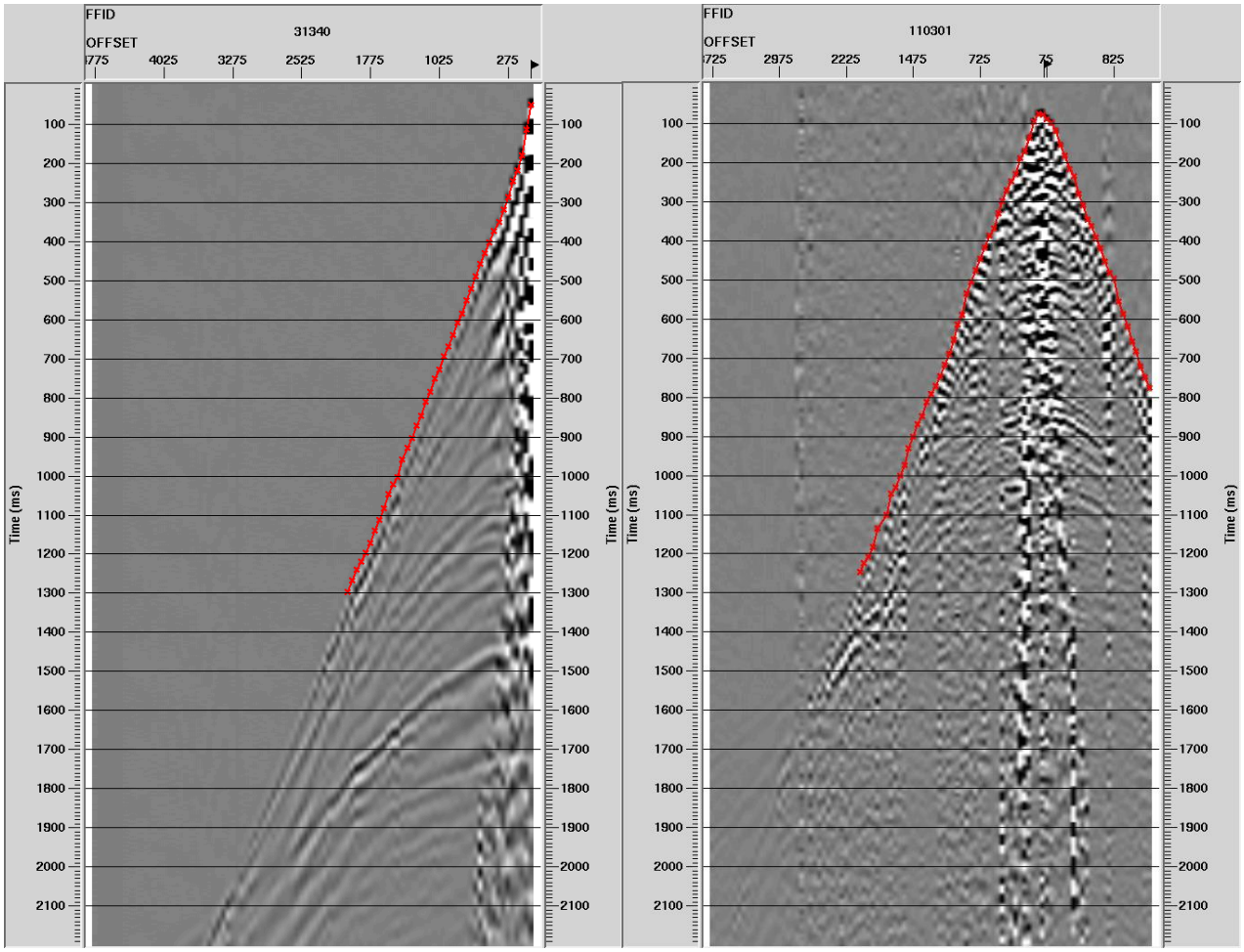

Fig. 11. Example of first break picking FFID 31340 (left), FFID 110301 (right).

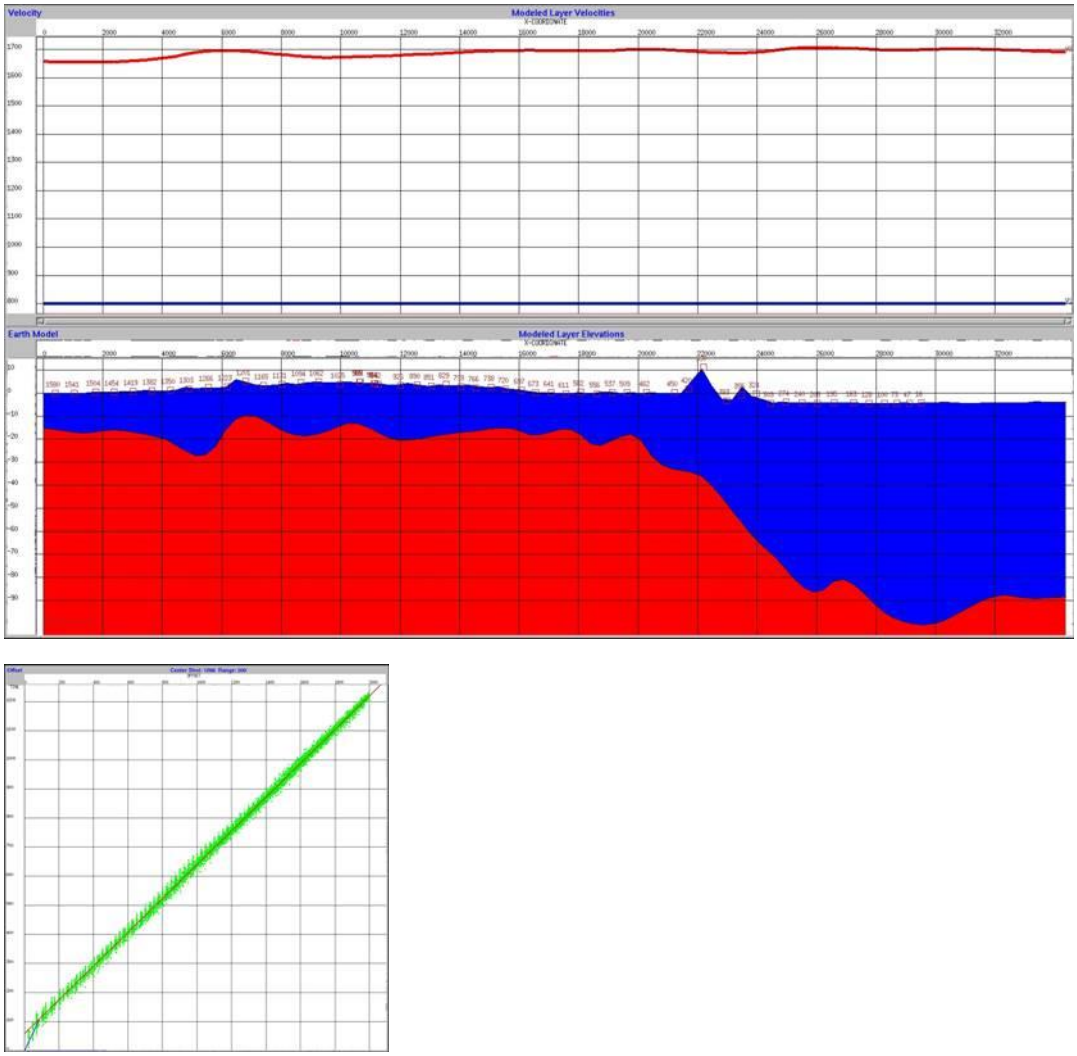

Fig. 12. Section through near surface model (top, middle) and example of first break pick.

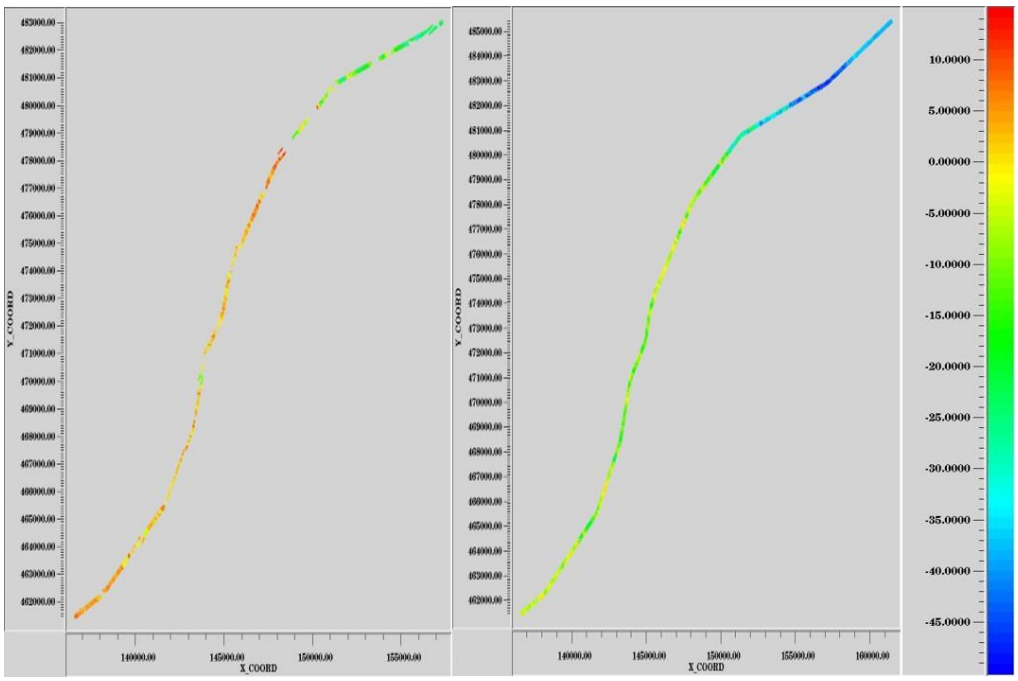

Fig. 13. Distribution of refraction static corrections for shot points (left) and receiver points (right).

Fig. 14. Comparison of static corrections calculated on basis of elevation (blue) and refraction static corrections (red) for shot points (top) and receivers (bottom).

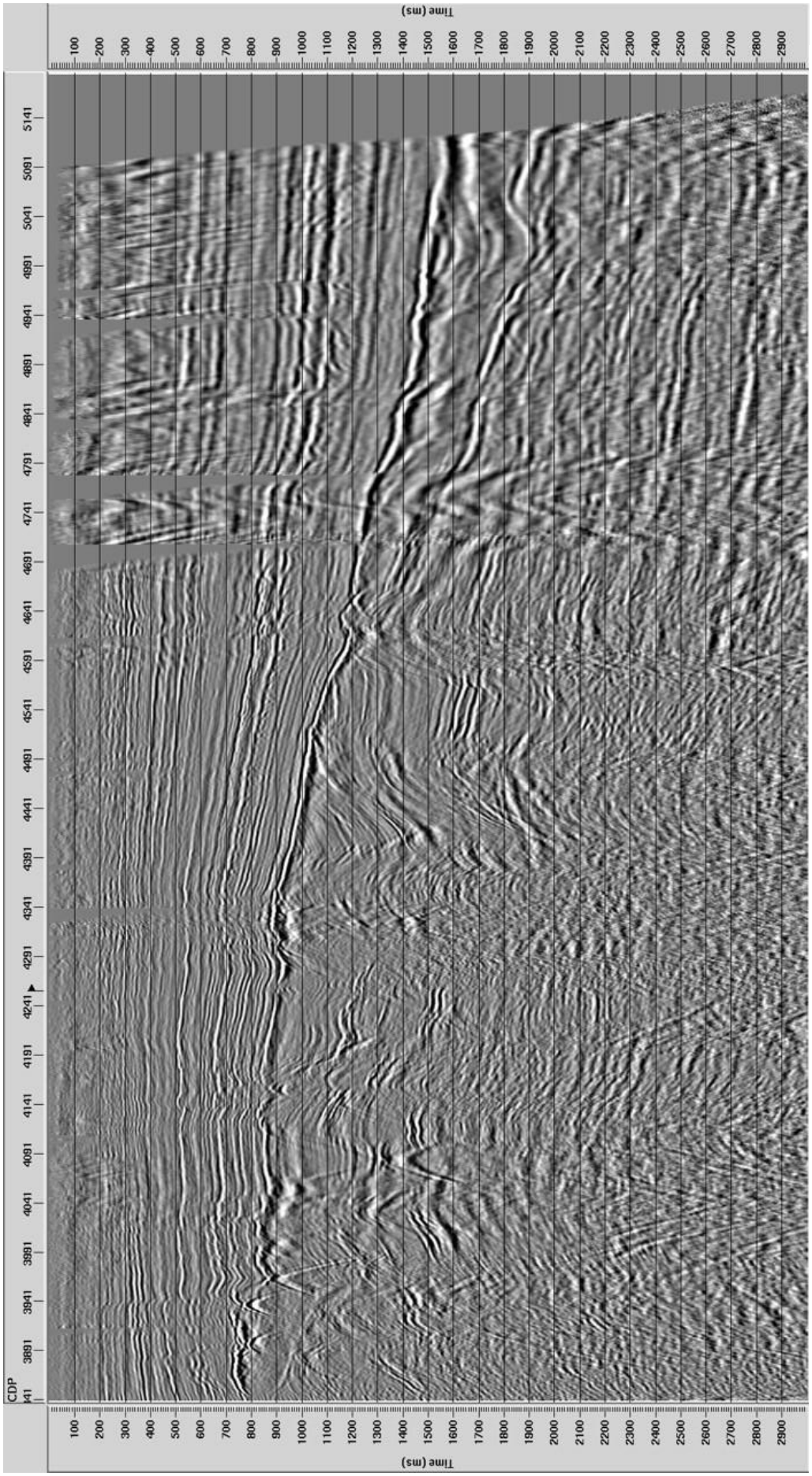

Fig. 15. Control seismic section with application of elevation statics.

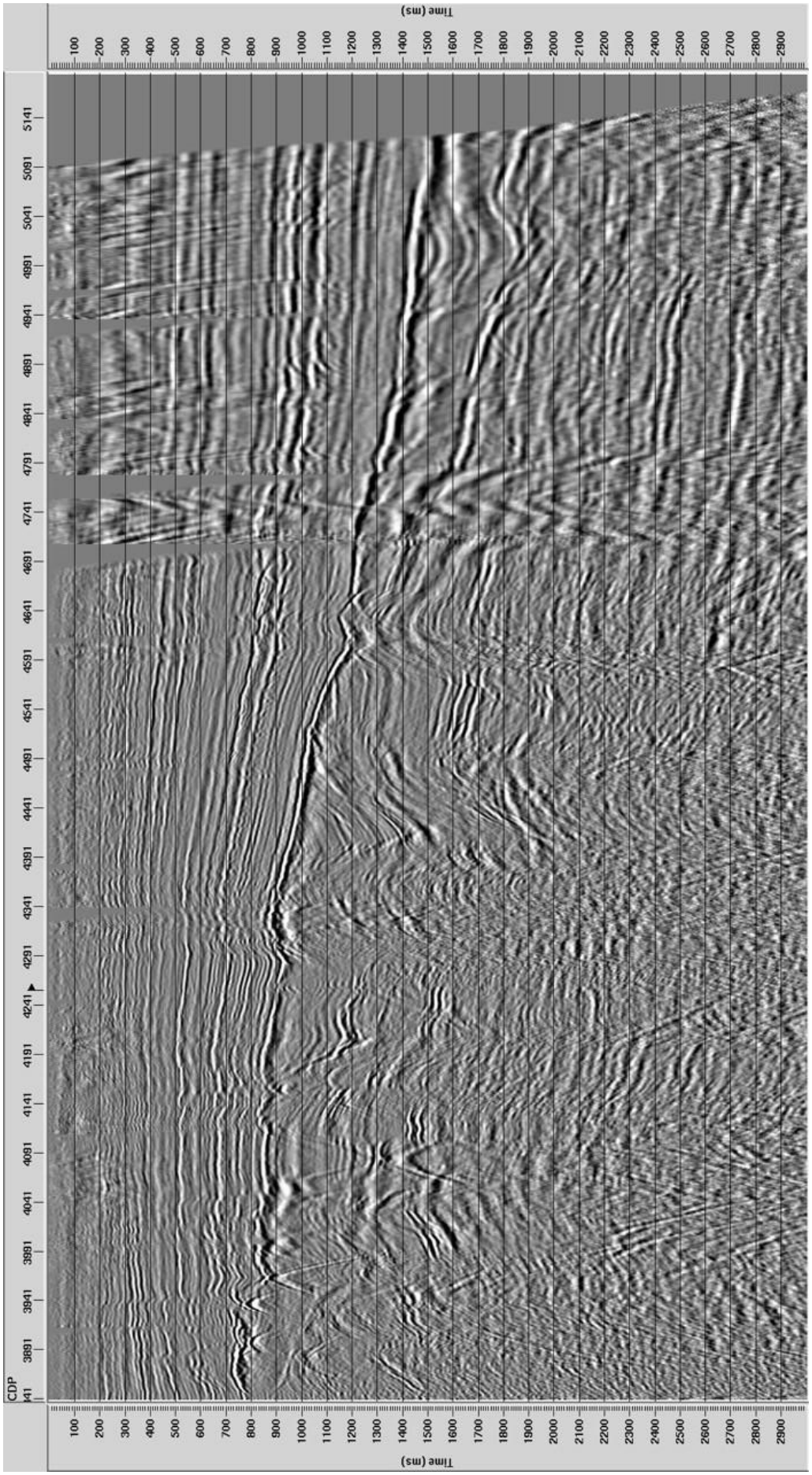

Fig. 16. Control seismic section with application of refraction statics.

8.3. Linear noise and surface wave attenuation

The input data was heavily affected by coherent noise presence. Two types of noise were identified:

- shot-related linear noise,
- surface wave (ground roll).

In order to minimalize impact of coherent noise, attenuation in shot domain was applied with use of the program:

- *Ground Roll Removal (GRR)* for surface wave attenuation.

The results of this stage are presented on Fig. 17 and Fig. 18.

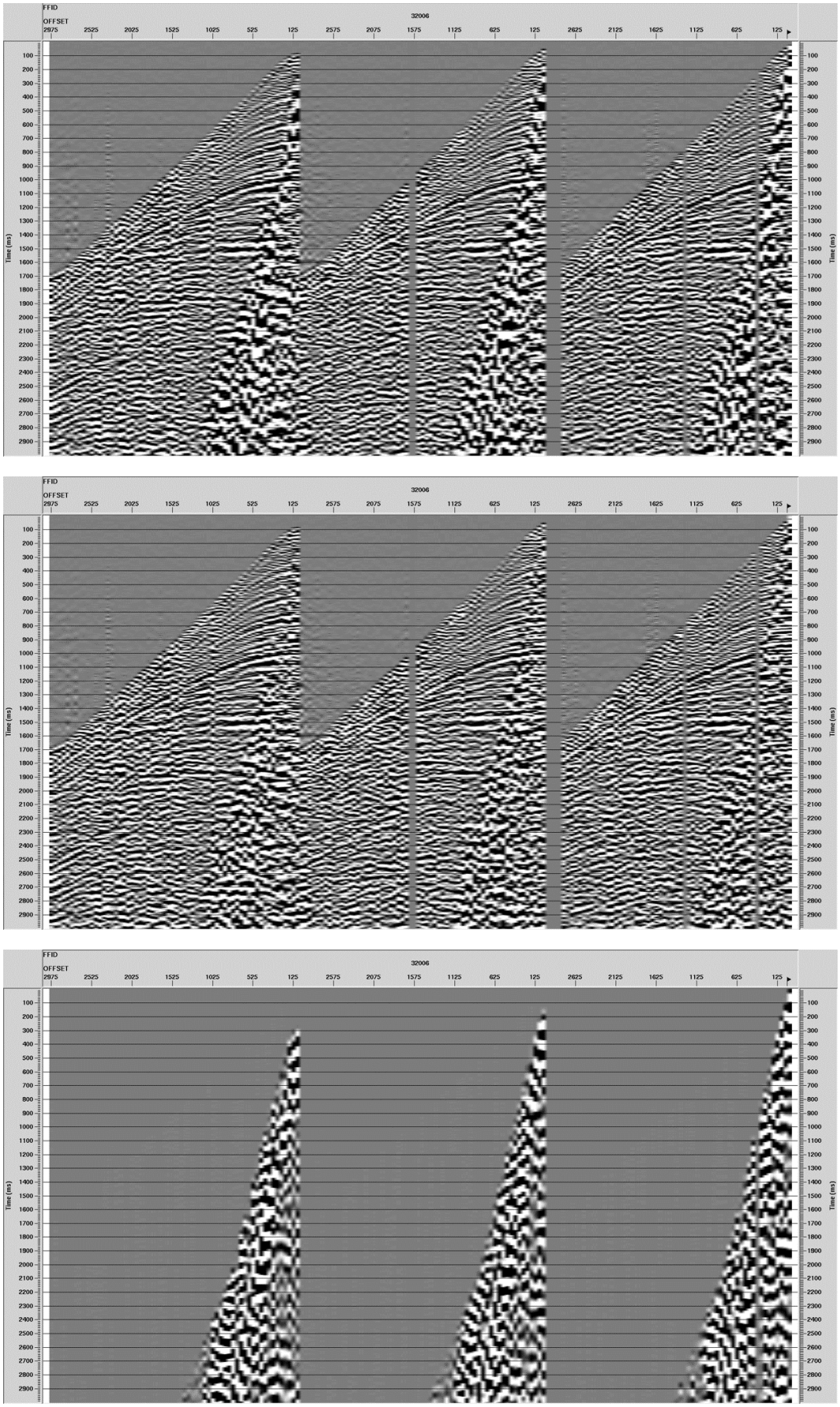

Fig. 17. Example of coherent noise attenuation on shot record (FFID 32006): before noise attenuation (top), after noise attenuation (center) and before minus after noise attenuation (bottom).

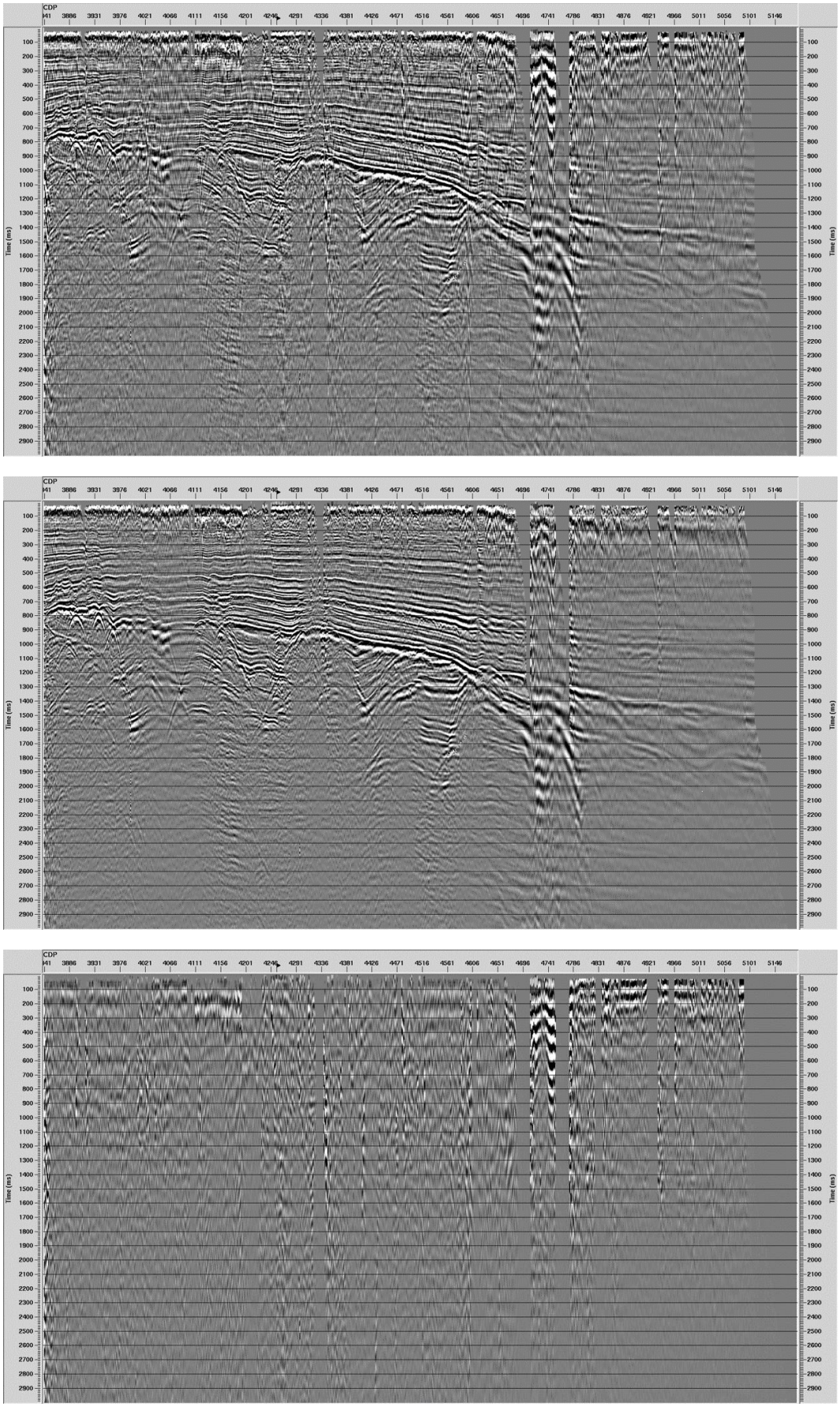

Fig. 18. Example of coherent noise attenuation on stacked section: before noise attenuation (top), after noise attenuation (center) and before minus after noise attenuation (bottom).

8.4. Random noise attenuation

In order to remove high content of random noise, the procedure *De-burst energy scaling (DBST)* in shot and then in receiver domain were applied on useable part of data i.e. from just below first breaks up to 10000 ms.

The results of this stage are presented below:

Fig. 19 shows the shot record before, after and difference noise attenuation,

Fig. 20 shows the spectra. Each spectra was calculated over the red box shown on the top of the Fig.20,

Fig. 21 shows the stacked section before, after and difference.

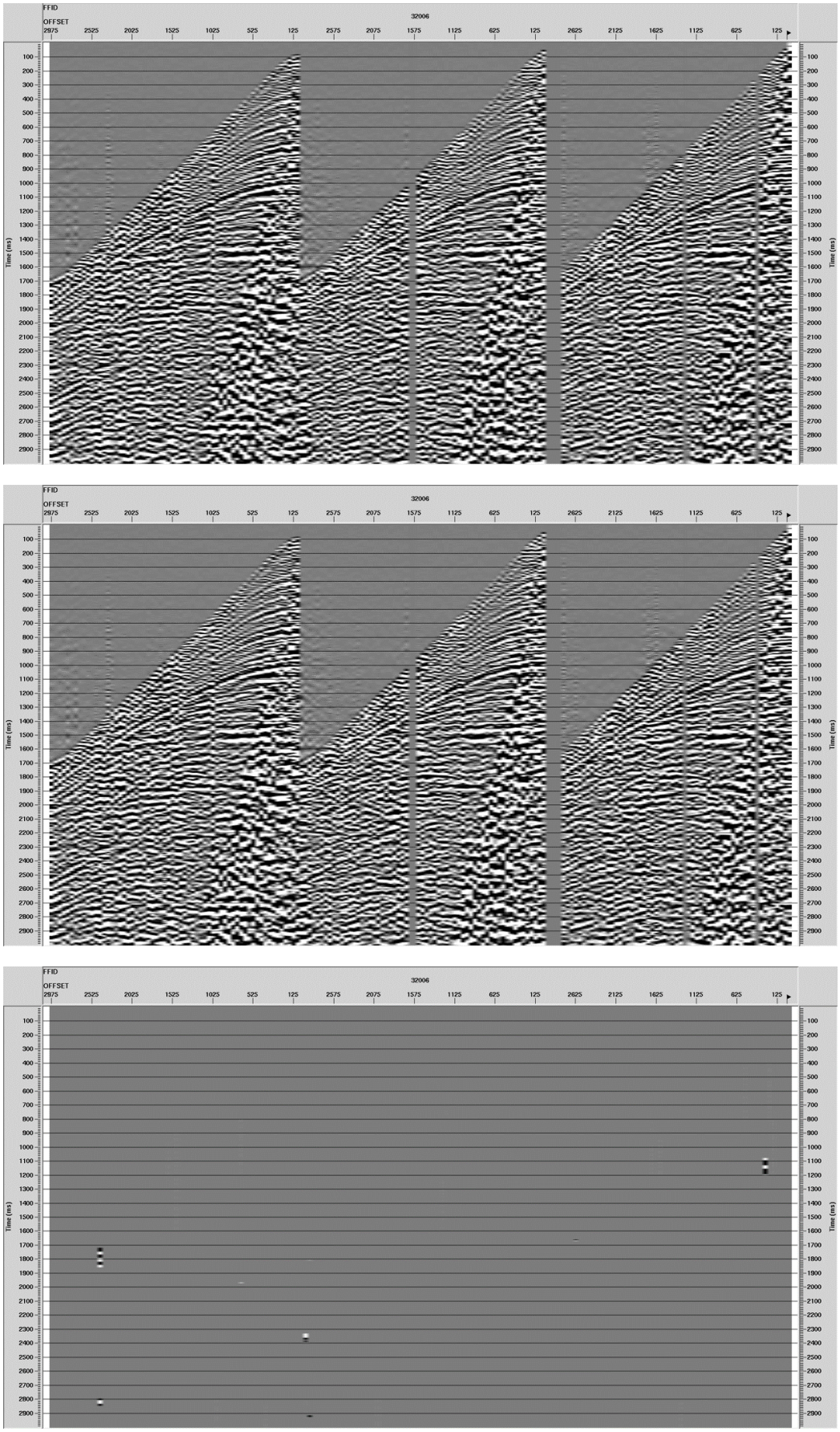

Fig. 19. Example of coherent noise attenuation on shot record (FFID 32006): after coherent noise attenuation (top), after coherent and random noise attenuation (middle) and before minus after random noise attenuation (bottom).

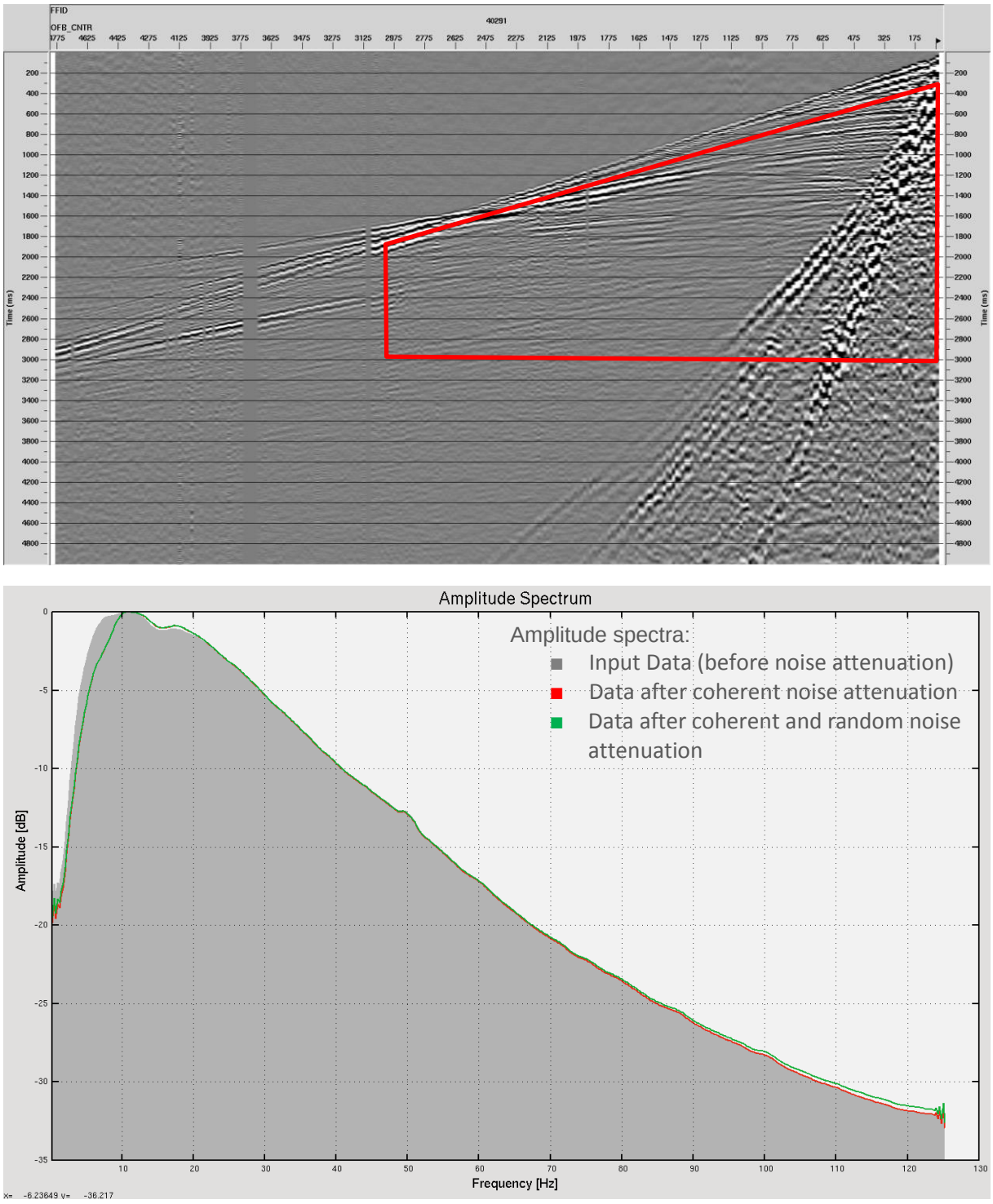

Fig. 20. Amplitude spectra for shot record before and after noise attenuation: time gate used to derive spectrum - red gate (top), and amplitude spectra (bottom).

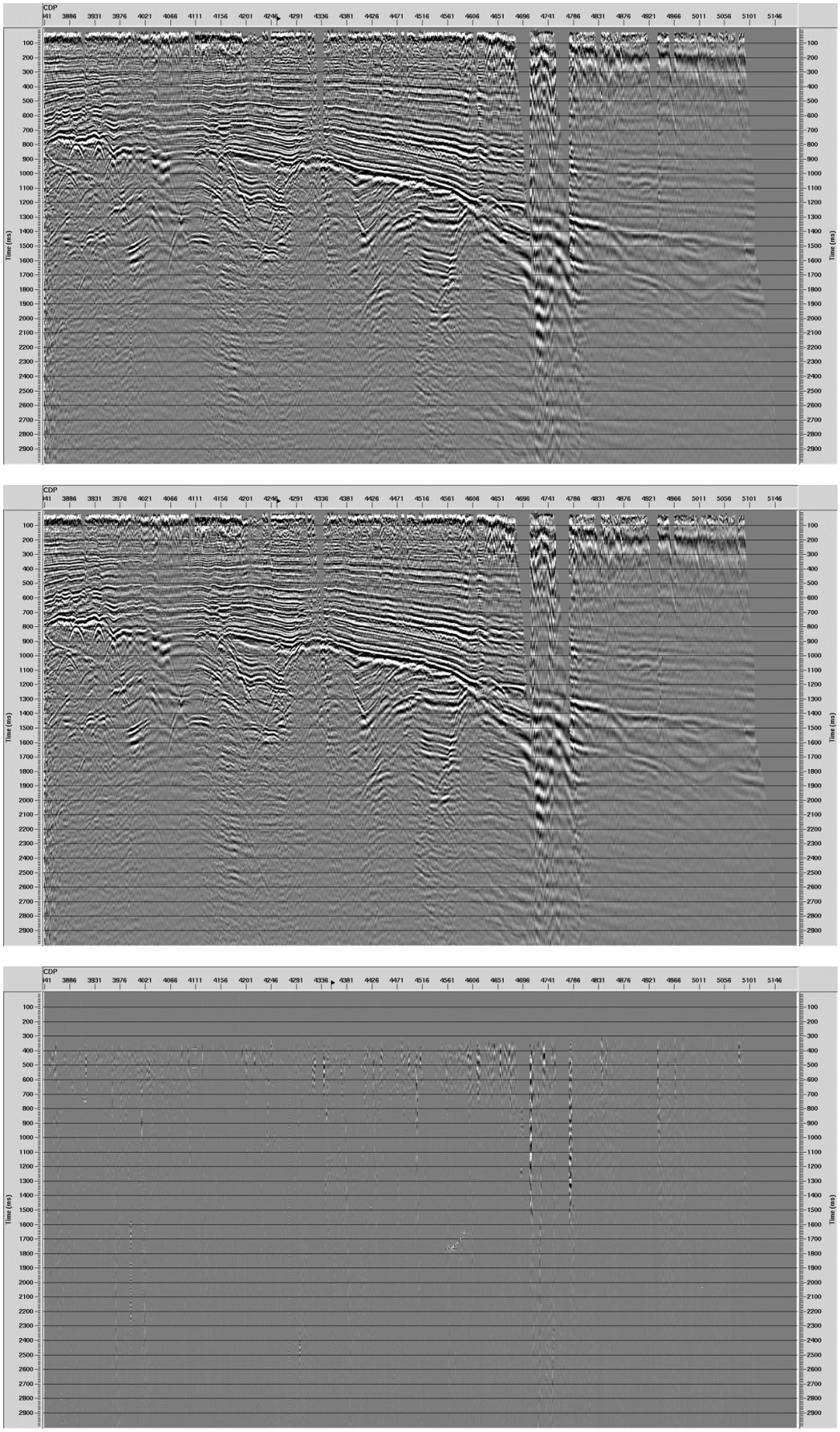

Fig. 21. Example of coherent noise attenuation on stacked section: after coherent noise attenuation (top),after coherent and random noise attenuation (middle) and before minus after random noise attenuation (bottom).

8.5. Surface-consistent amplitude scaling

Averaged amplitudes of traces being samples of seismic wavefield were analyzed in time window covering key seismic horizons. Scaling coefficients were estimated by method of separating three components, which related amplitude changes to surface conditions being functions of source, receiver and associated offset.
Amplitudes of seismic traces were corrected with coefficients estimated for sources locations, receiver locations and source-receiver offsets.

Surface-Consistent Amplitude Compensation (SCAC) was performed in two stages:

- First iteration of Surface-Consistent Amplitude Compensation (I SCAC) – scaling coefficients were computed on data before deconvolution,
- Second (residual) iteration of Surface-Consistent Amplitude Compensation (II SCAC) – scaling coefficients were computed on data after deconvolution.

Seismic sections were generated with elevation statics, preliminary velocity analyses, compensation of amplitude propagation decay, coherent and random noise attenuation, geophone dephasing. Sections for II SCAC have additionally spike deconvolution applied.

The figures below present:
Fig. 22 - distribution of average amplitudes before SCAC,
Fig. 23 - distribution of average amplitudes after I SCAC,
Fig. 24 - distribution of average amplitudes after II SCAC,
Fig. 25 - control stacks: before SCAC and after I SCAC (without deconvolution),
Fig. 26 - control stacks: after I SCAC and after II SCAC (with deconvolution).

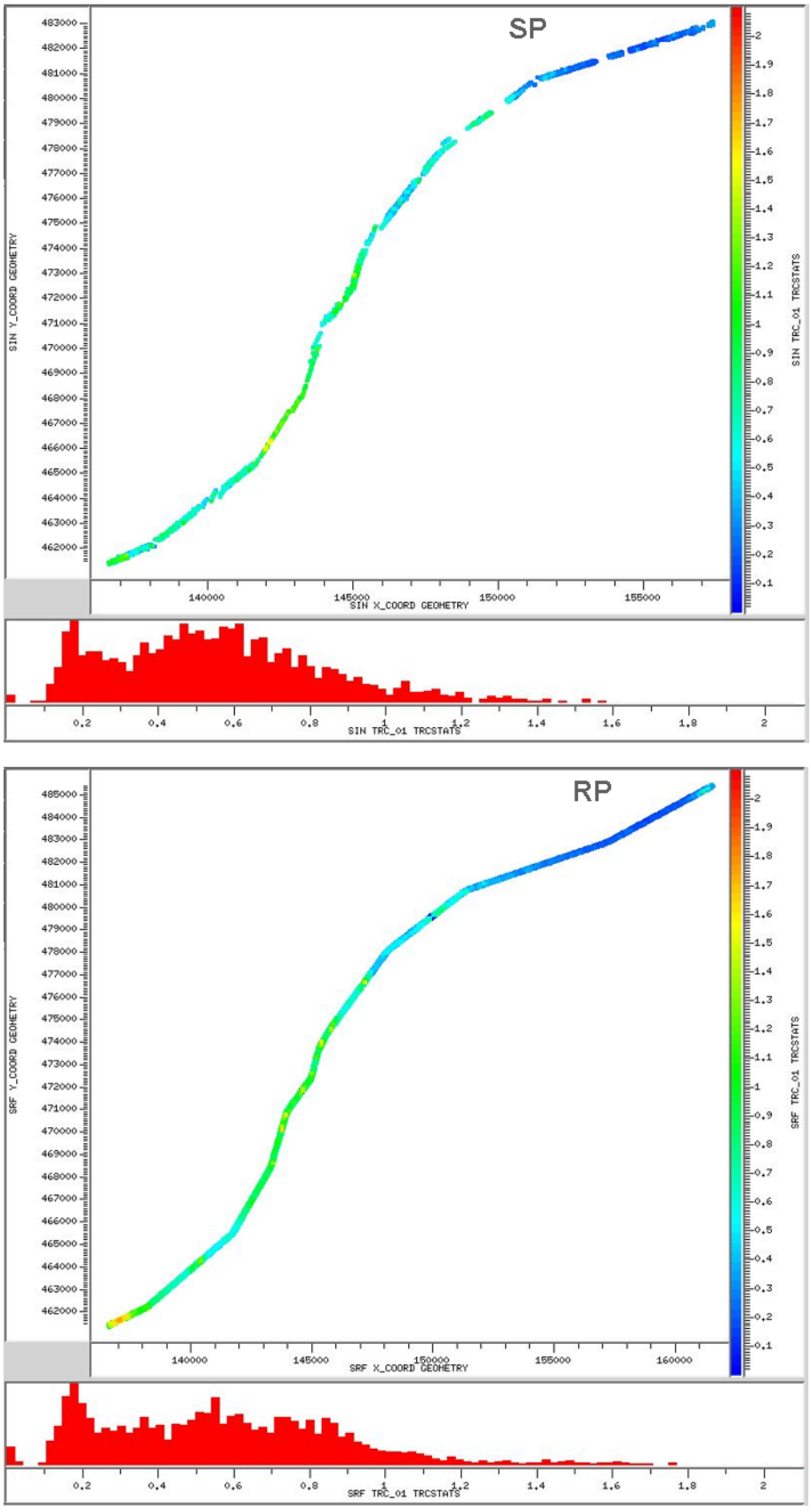

Fig. 22. Distribution of average amplitudes before Surface-Consistent Amplitude Compensation for shot points (top), and receiver points (bottom).

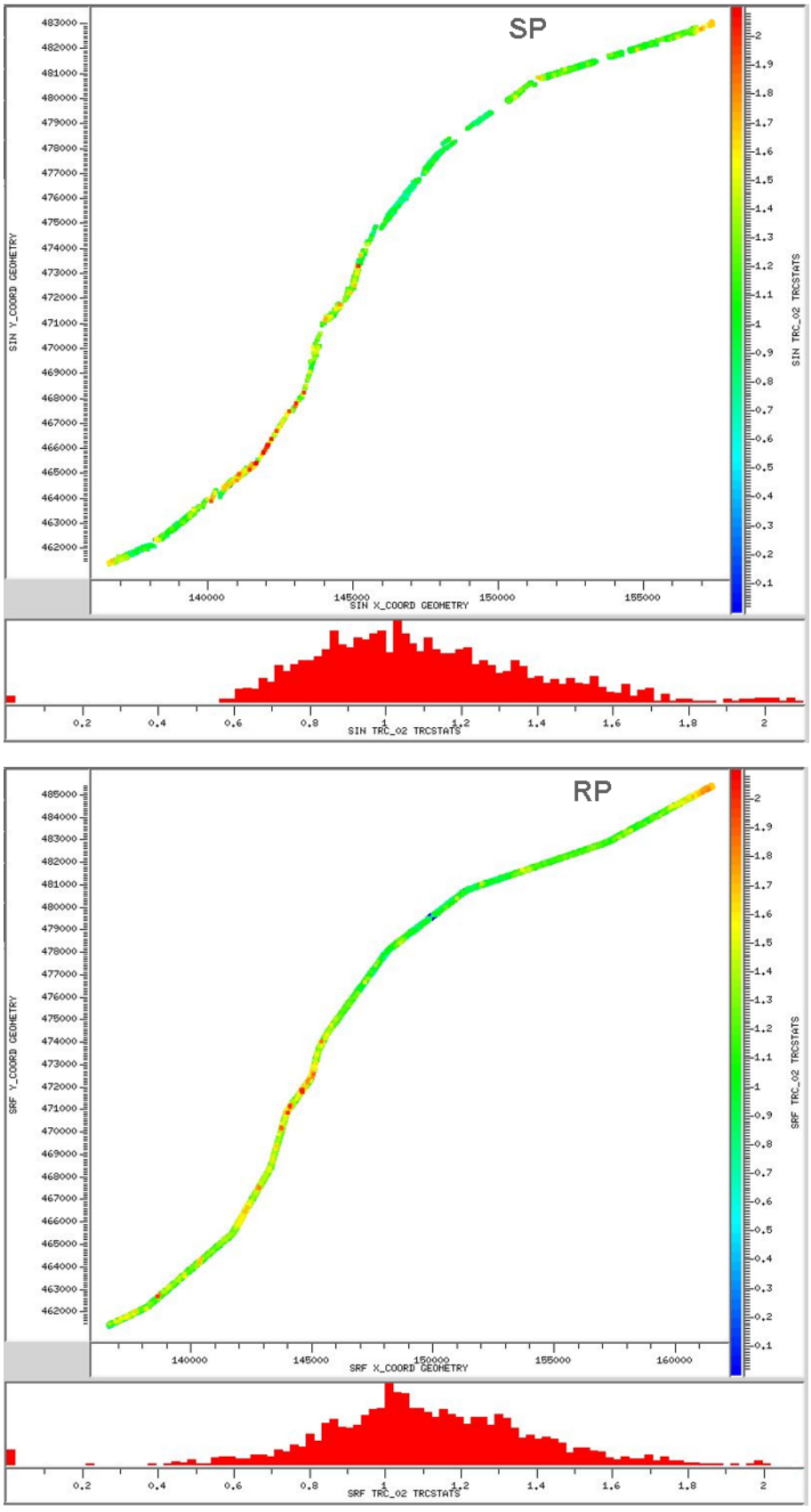

Fig. 23. Distribution of average amplitudes after first iteration of Surface-Consistent Amplitude Compensation (I SCAC) for shot points (top), and receiver points (bottom).

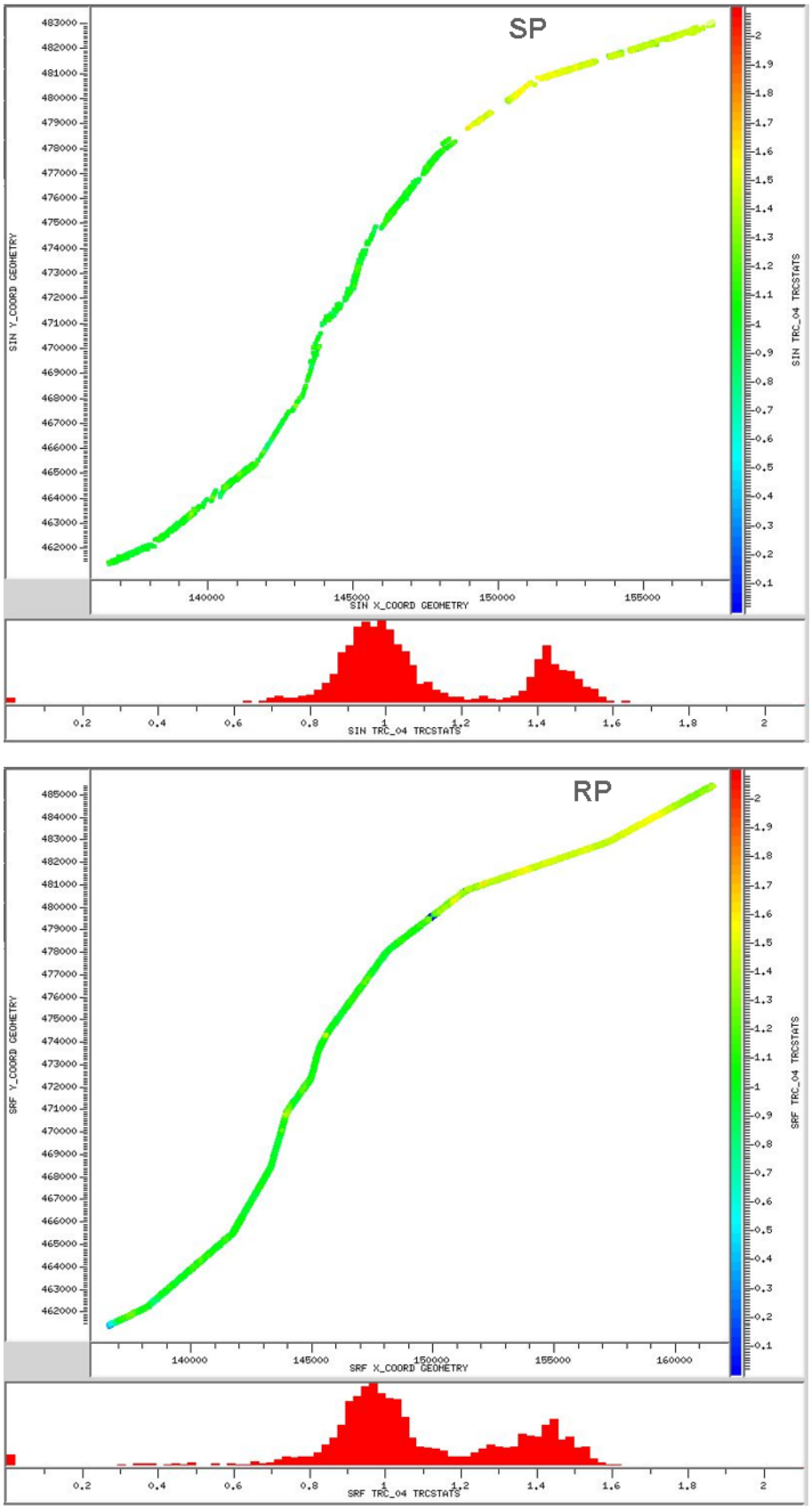

Fig. 24. Distribution of average amplitudes after second iteration of Surface-Consistent Amplitude Compensation (II SCAC) for shot points (top), and receiver points (bottom).

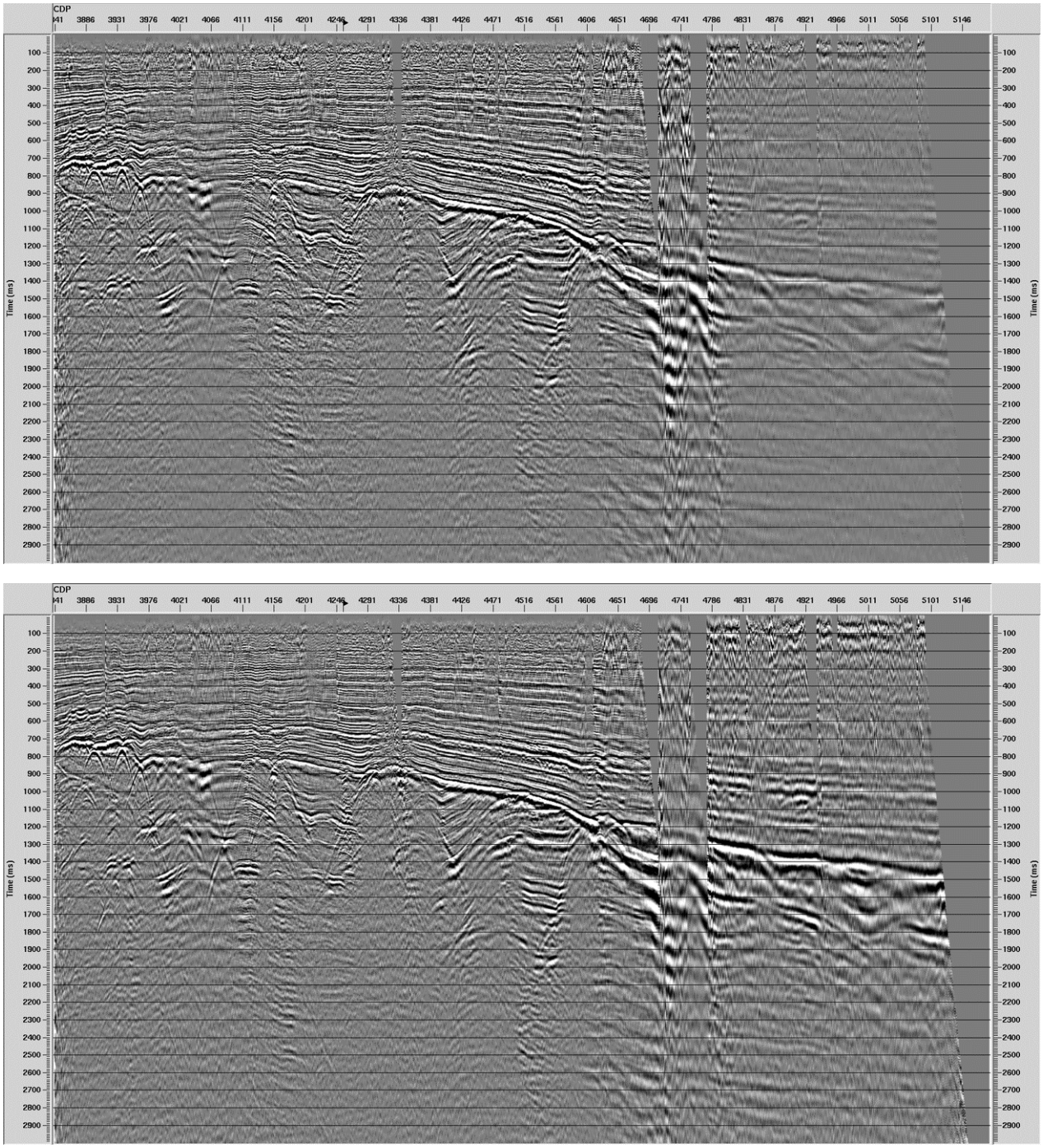

Fig. 25. Effectiveness of Surface-Consistent Amplitude Compensation (SCAC) on control sections: before first iteration of SCAC (top), and after first iteration of SCAC (bottom).

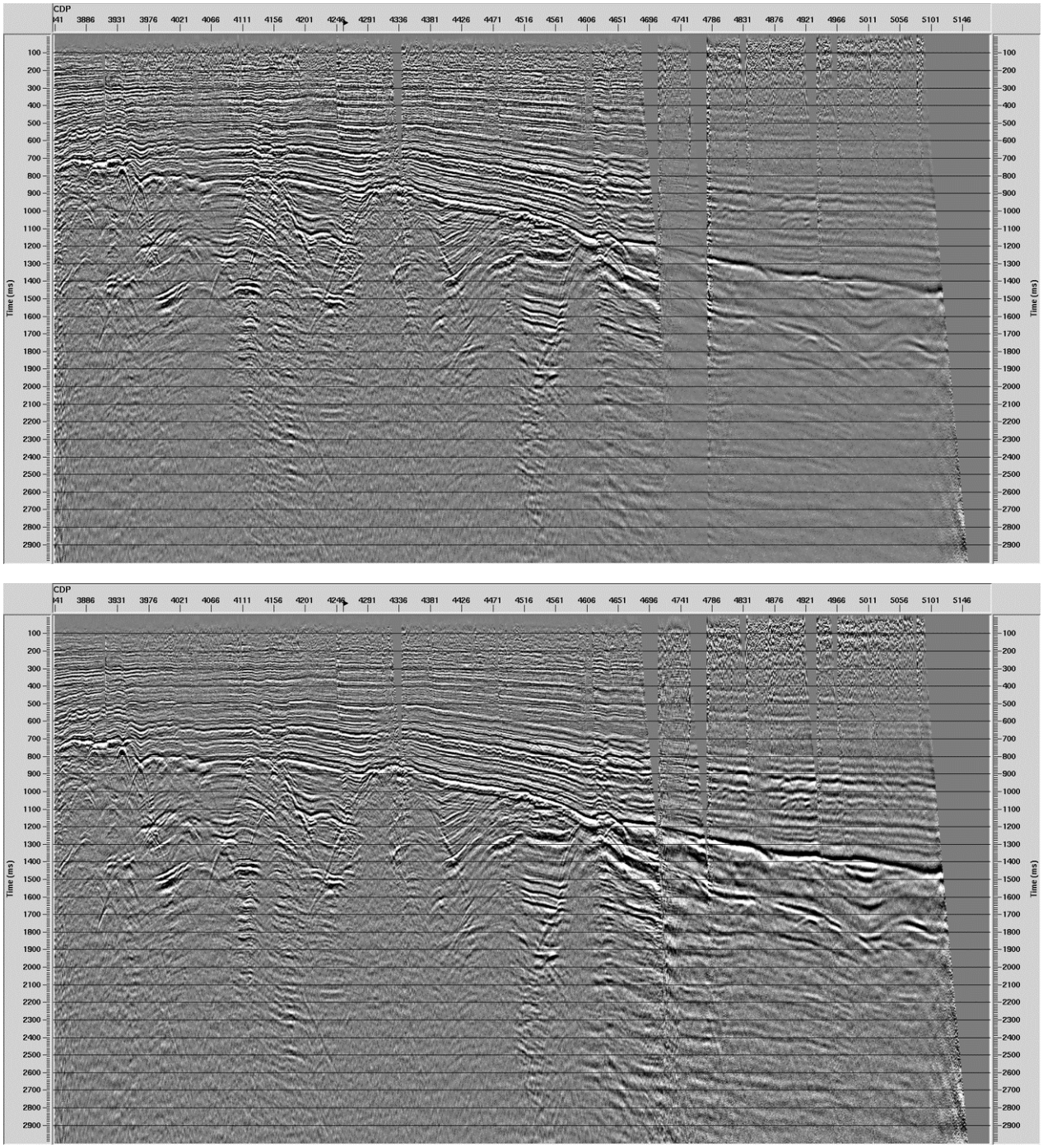

Fig. 26. Effectiveness of Surface-Consistent Amplitude Compensation (SCAC) on control sections: after first iteration of SCAC and deconvolution (top), and after first iteration of SCAC, deconvolution and second iteration of SCAC (bottom).

8.6. Inverse phase and amplitude Q-compensation

The aim of Inverse Phase and Amplitude Q-Compensation applied before deconvolution is to compensate for dispersion effects on propagating seismic wave. Expected effect is as close as possible unification of signal wavelet as well as amplitude and phase spectrum along entire data length. For proper inverse Q estimation, spectral ratio was calculated on stack section in 2 time windows of width 500 ms – see Fig. 27 (top). The Q value is estimated from a slope of natural logarithm from amplitude ratio diagram versus frequency.

Reference frequency (15 Hz) was selected on basis of spectral analysis in time gates. Maximum gain (15 dB) was selected on basis of control sections – see Fig. 27 (bottom). Final Q value (Q = 100) was selected on basis EBN Representative's choice.

Effectiveness of Q compensation is illustrated on figures Fig. 28 to Fig. 30.

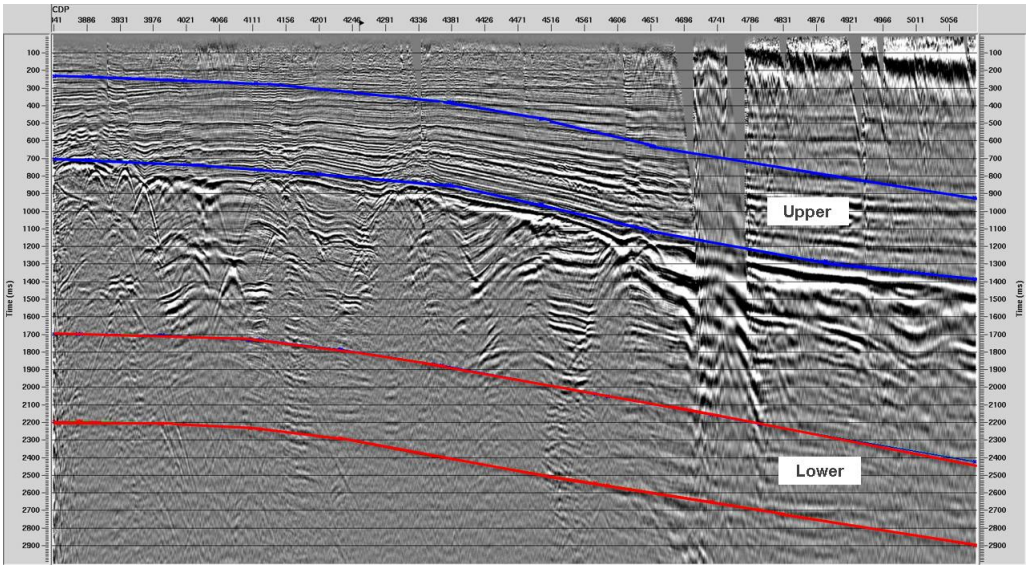

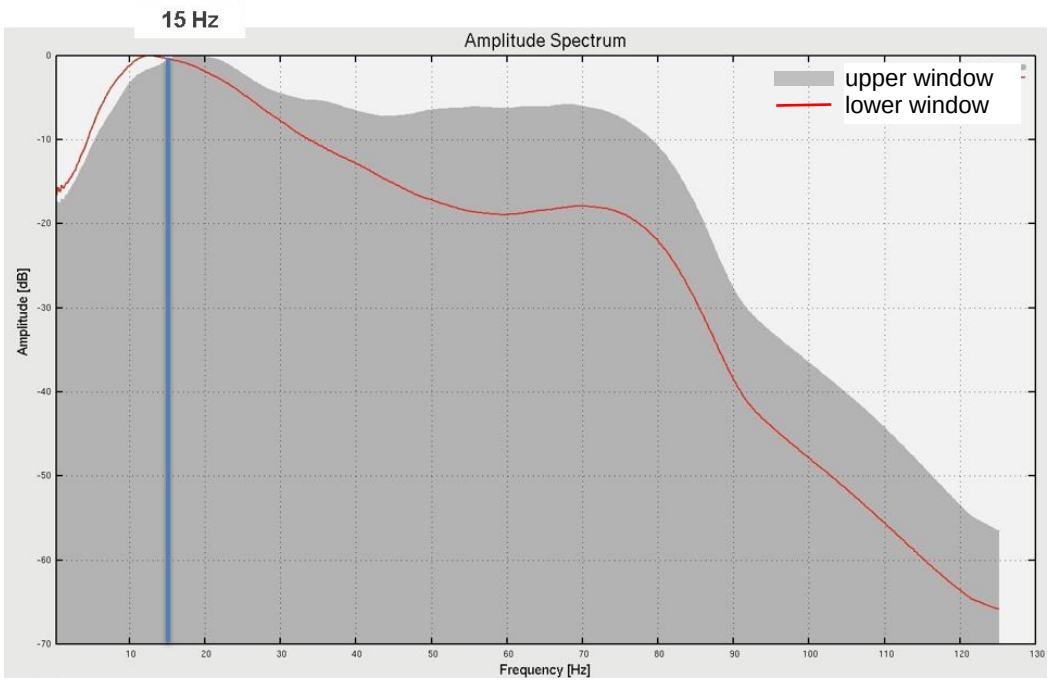

Fig. 27. Time gates for dominant frequency selection (top), selection of dominant frequency (bottom).

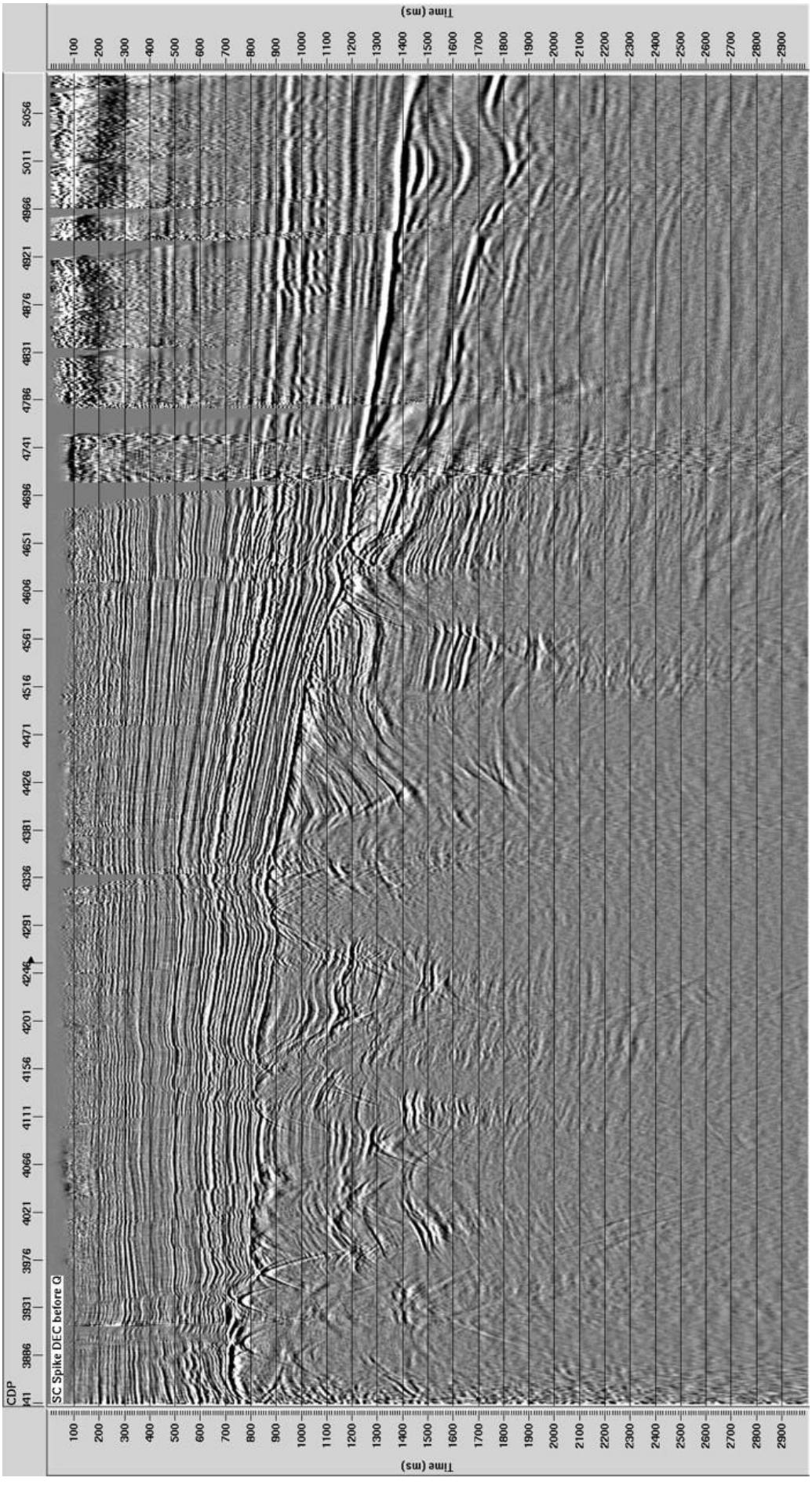

Fig. 28. Control seismic section after deconvolution with no Q-compensation applied.

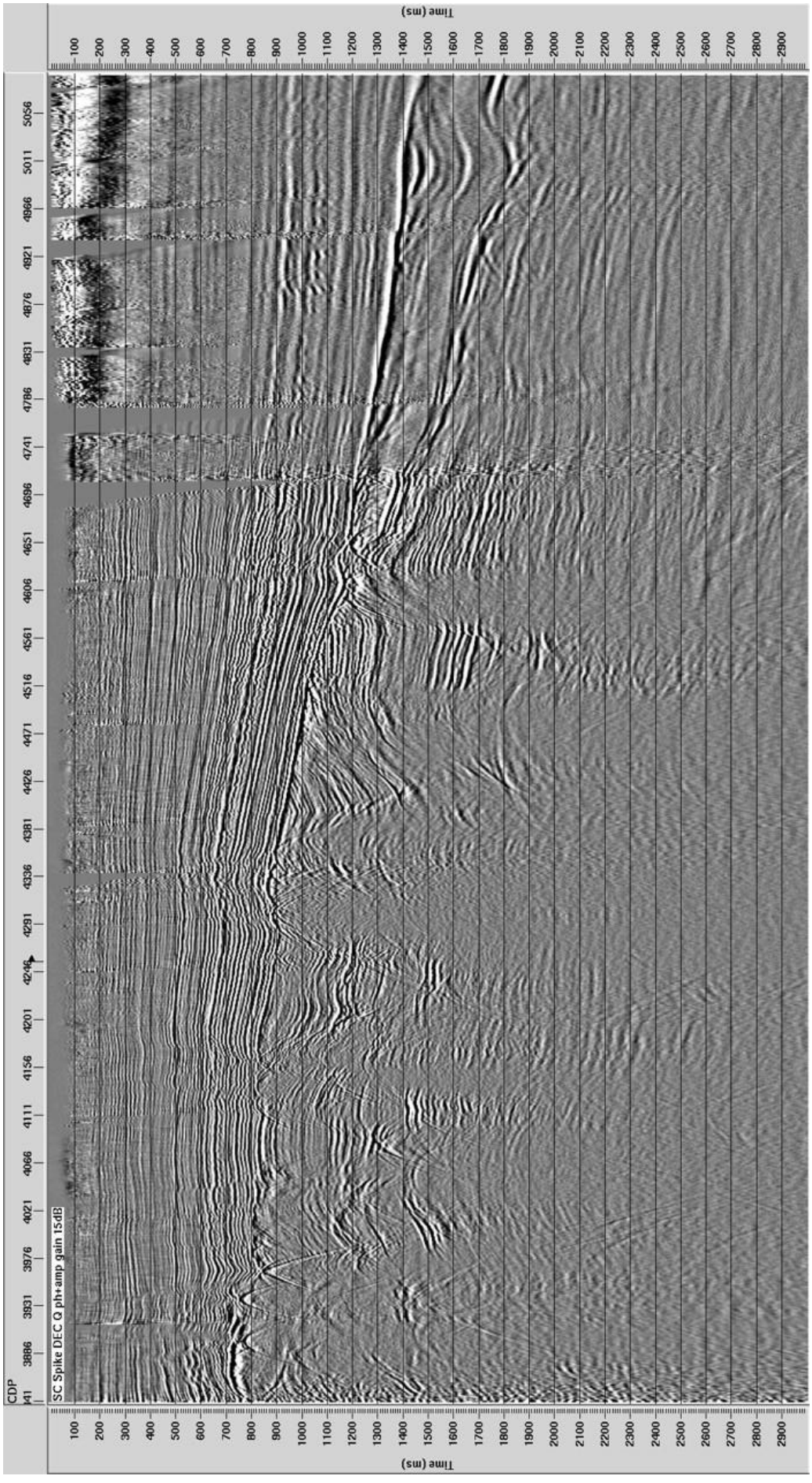

Fig. 29. Control seismic section after deconvolution with Q-compensation applied.

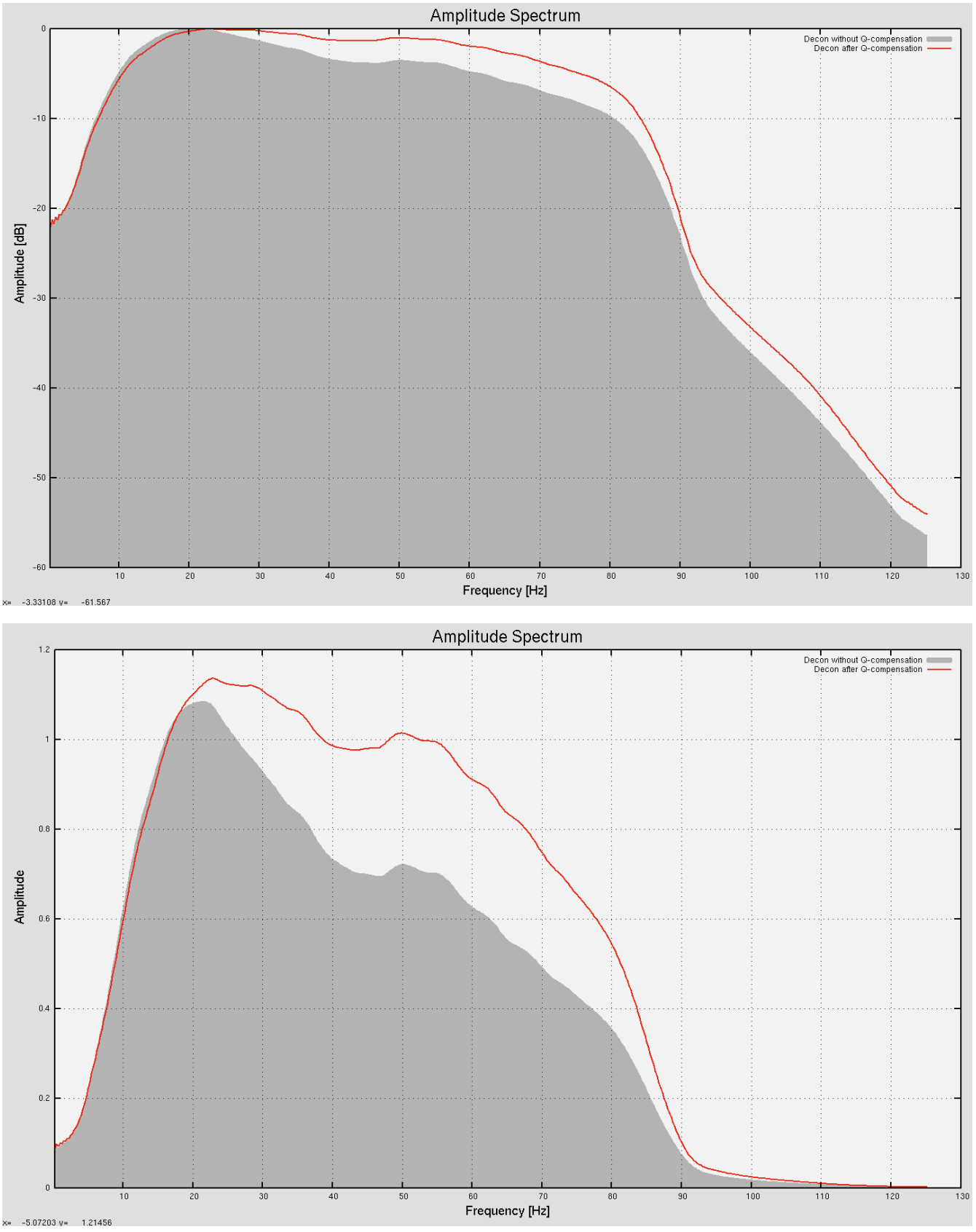

Fig. 30. Amplitude spectrum after deconvolution without Q-compensation (grey) and performed after Q-compensation (red); relative Decibel scale (top), and linear scale (bottom). Time window to derive spectra is the same as for deconvolution - see Fig. 31.

8.7. Deconvolution

This stage of wavelet shaping included correction for variable conditions on source and on receiver points. Principle of balance between vertical resolution and lateral continuity was the decisive factor of deconvolution type selection and setting of parameters. The requirement of real amplitude reconstruction forced usage of surface-consistent application. The testing included the following steps:

- deconvolution type selection (spiking, predictive or combination of both),
- time gate for deconvolution – see Fig. 31
- prediction distance (for predictive deconvolution),
- operator length,
- pre-whitening level.

Results of tests were viewed on control sections with autocorrelation (see Fig. 33 and Fig. 34), amplitude spectra and wavelets – see Fig. 32.

After testing and consultation with EBN, the following settings for above stage have been selected:

- single surface-consistent predictive deconvolution,
- prediction distance: 16 ms,
- operator length: 160 ms,
- pre-whitening level: 0.1%.

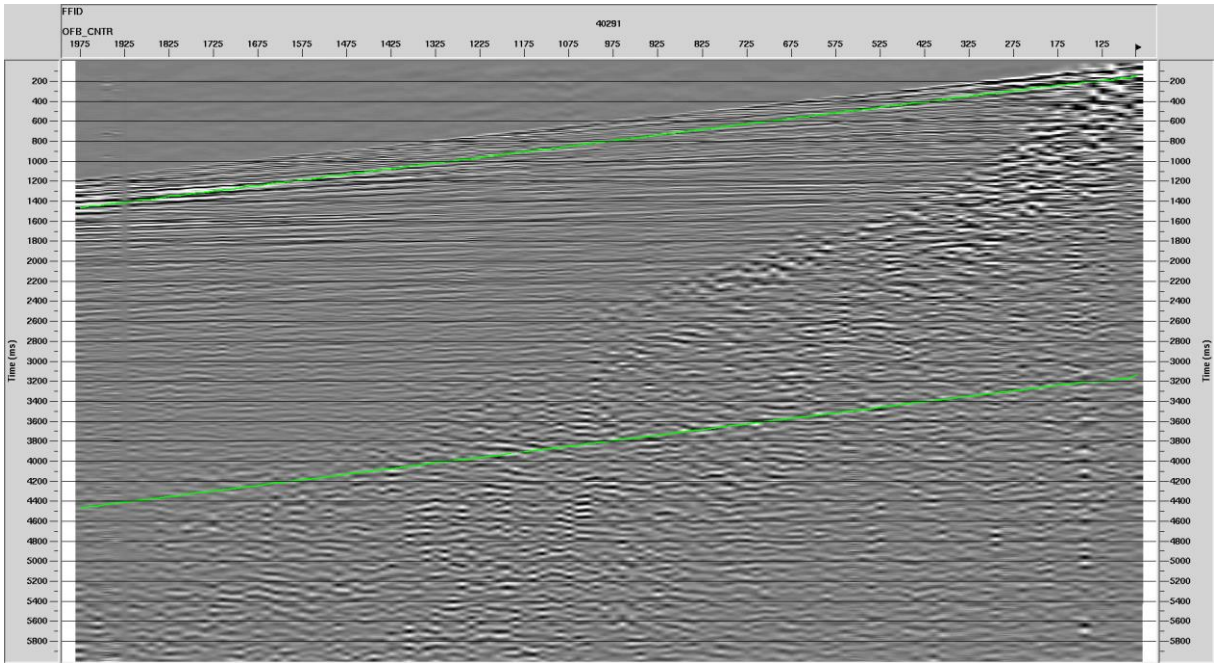

Fig. 31. Time gate for deconvolution parameter selection.

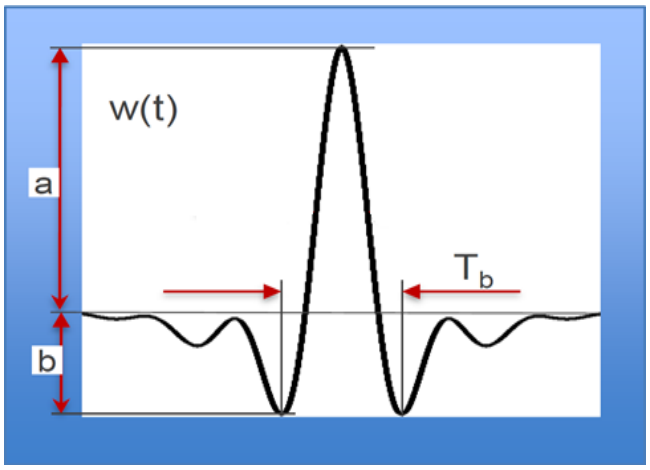

T_b (TB) – dominant period of wavelet,

b/a (B_A) – shape coefficient of wavelet, expressed in percentage.

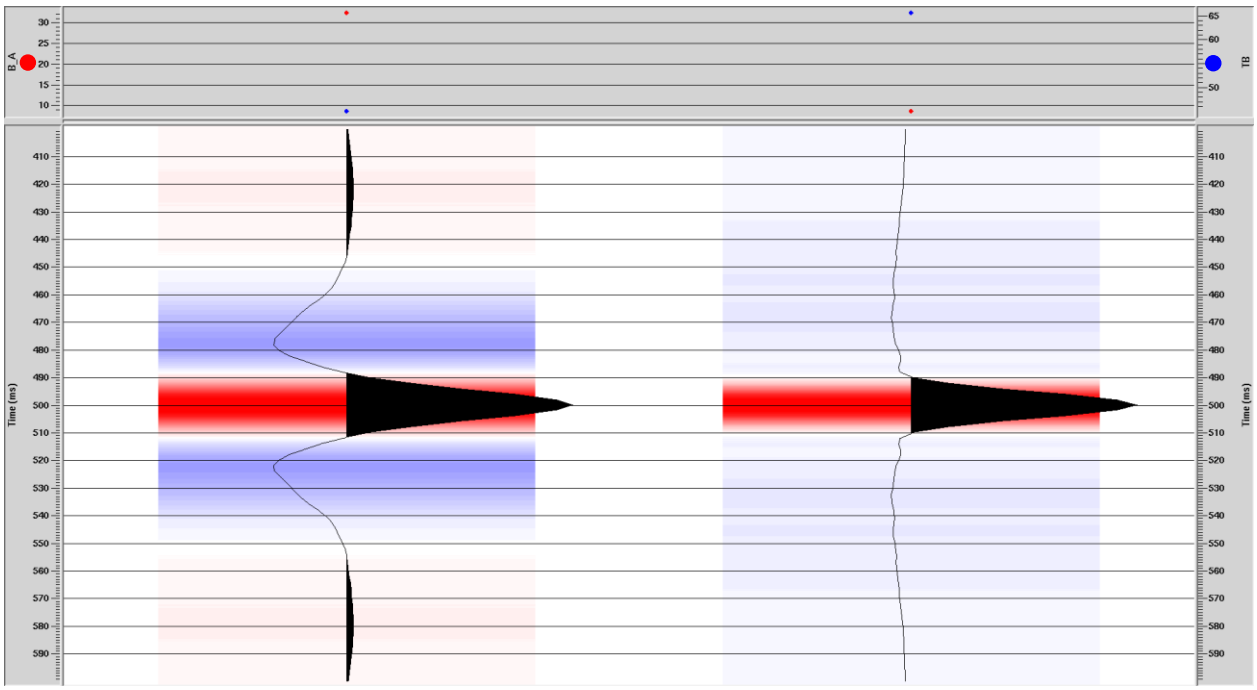

Fig. 32. Explanation of basic coefficients (top), and wavelets (bottom): before deconvolution (left) and after deconvolution (right), extracted in the window shown on Fig. 31.

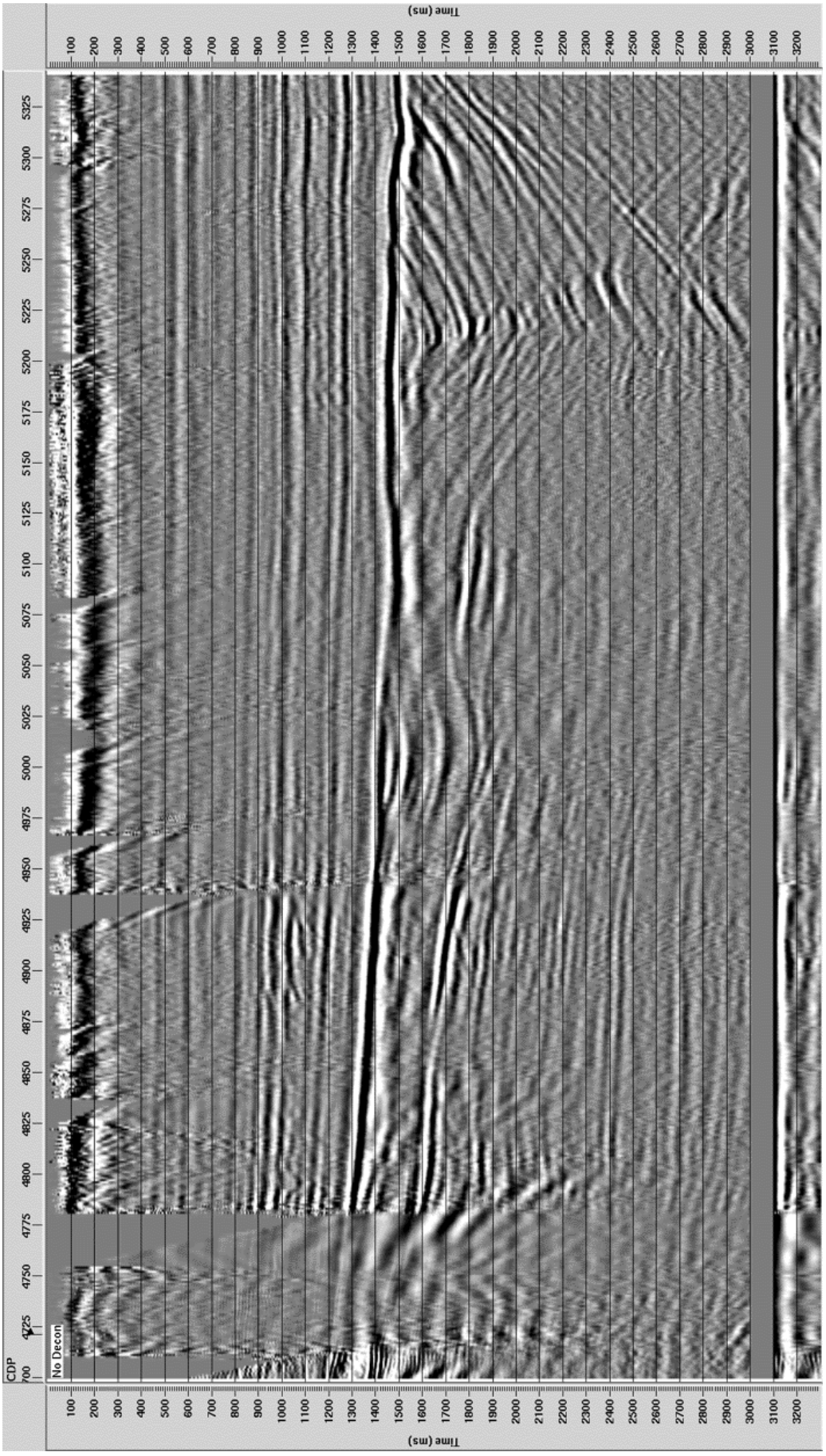

Fig. 33. Control seismic section with autocorrelation - before deconvolution. CDP range: 4700-5340

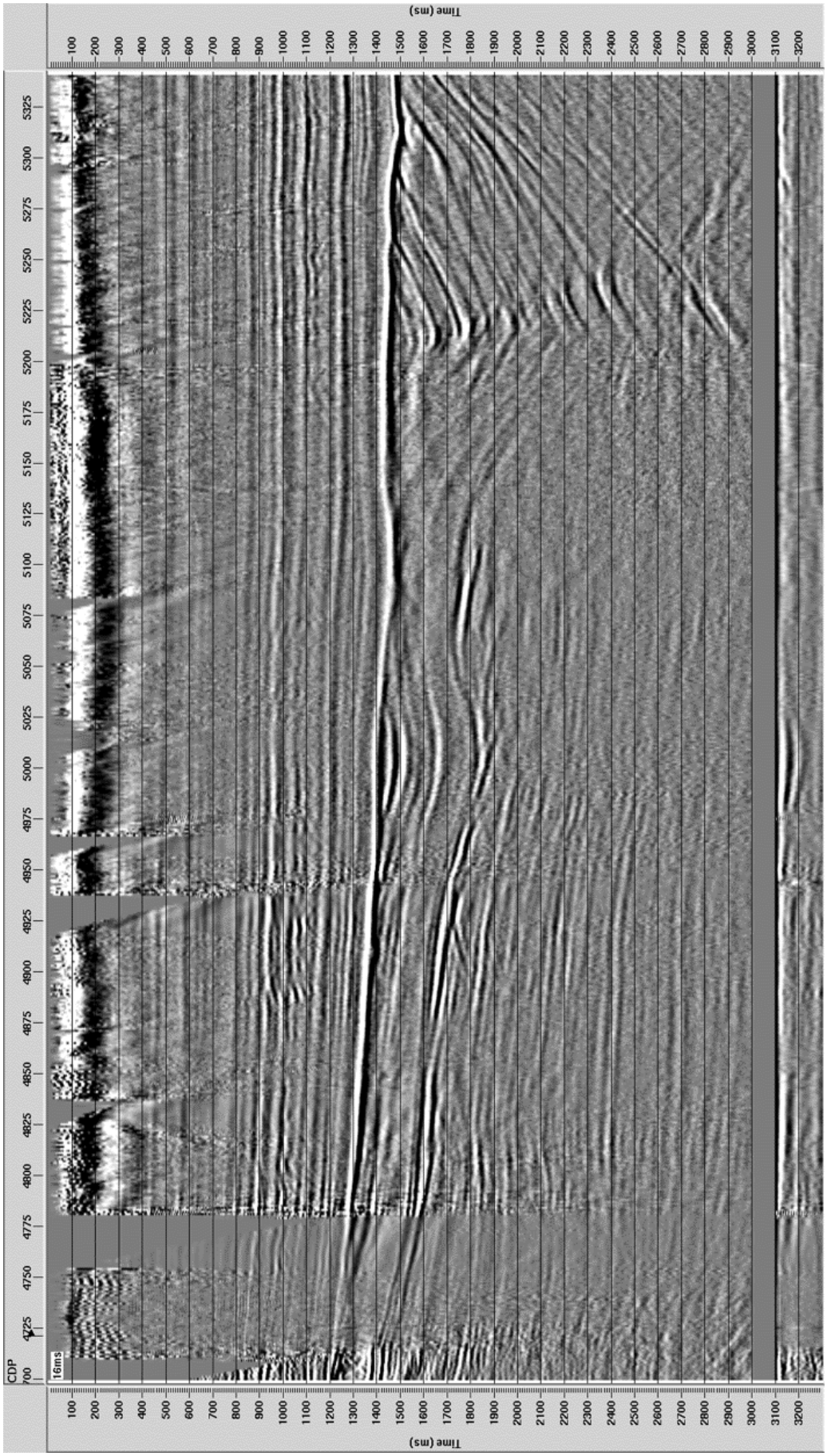

Fig. 34. Control seismic section with autocorrelation - after deconvolution. CDP range: 4700-5340

8.8. Velocity and mute analysis

Basic processing sequence before Pre-Stack Time Migration included three iterations of velocity analysis, performed interactively at floating datum – smoothed elevation. Second & third iteration was followed by residual static correction computation.

Three following iterations of velocity analysis were performed:

Initial iteration	located every 1000 m,	supergather 11 CMPs,
2nd iteration	located every 500 m,	supergather 11 CMPs,
3rd iteration	located every 500 m,	supergather 11 CMPs.

Trace muting was analyzed in the same locations as velocity analysis (VA).

The figures below present:

Fig. 35 - example of velocity and mute analysis,

Fig. 36 - velocity field after third iteration of VA & residual statics,

Fig. 37 - total residual statics applied,

Fig. 38 - control sections before residual statics and after three iterations of VA & residual statics.

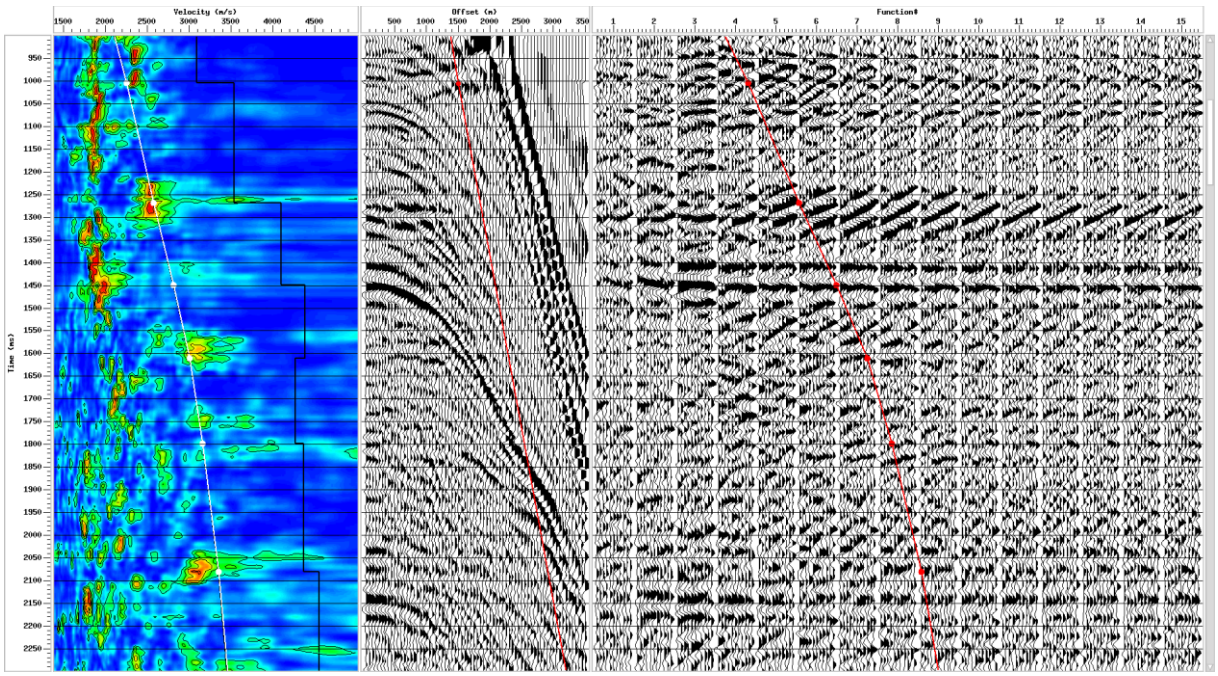

Fig. 35. Example of velocity and mute analysis. CDP 3880.

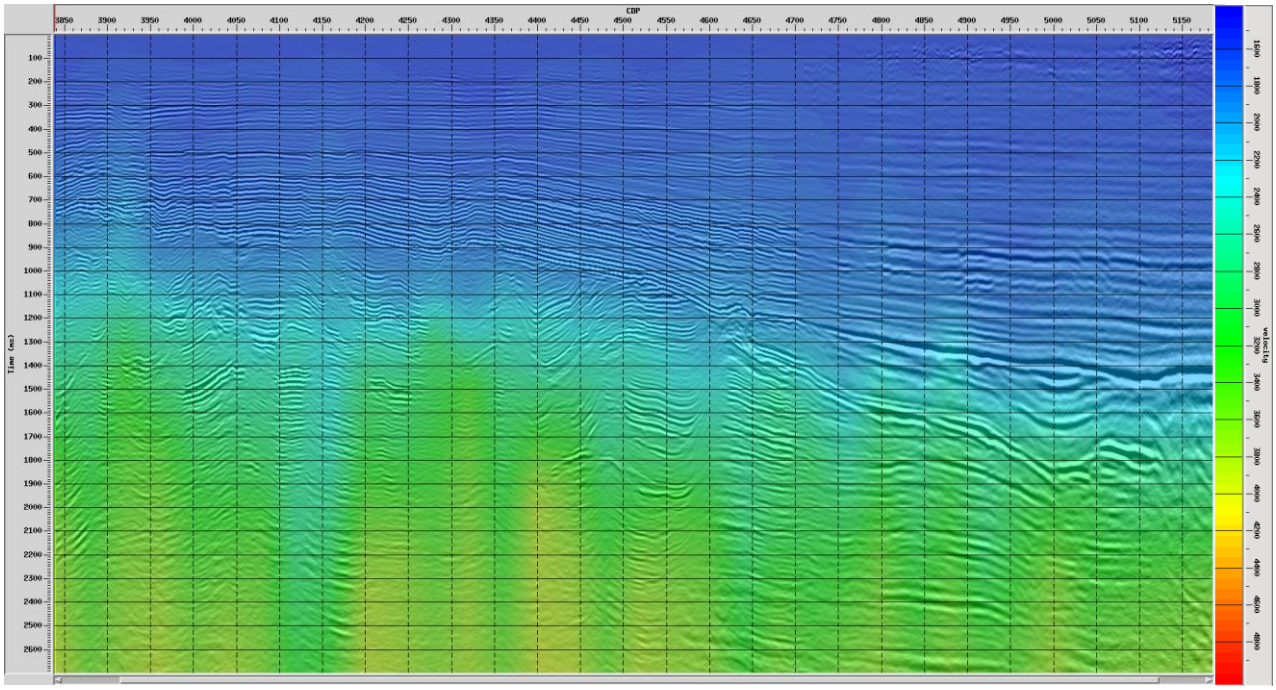

Fig. 36. Stacked section on background of velocity field.

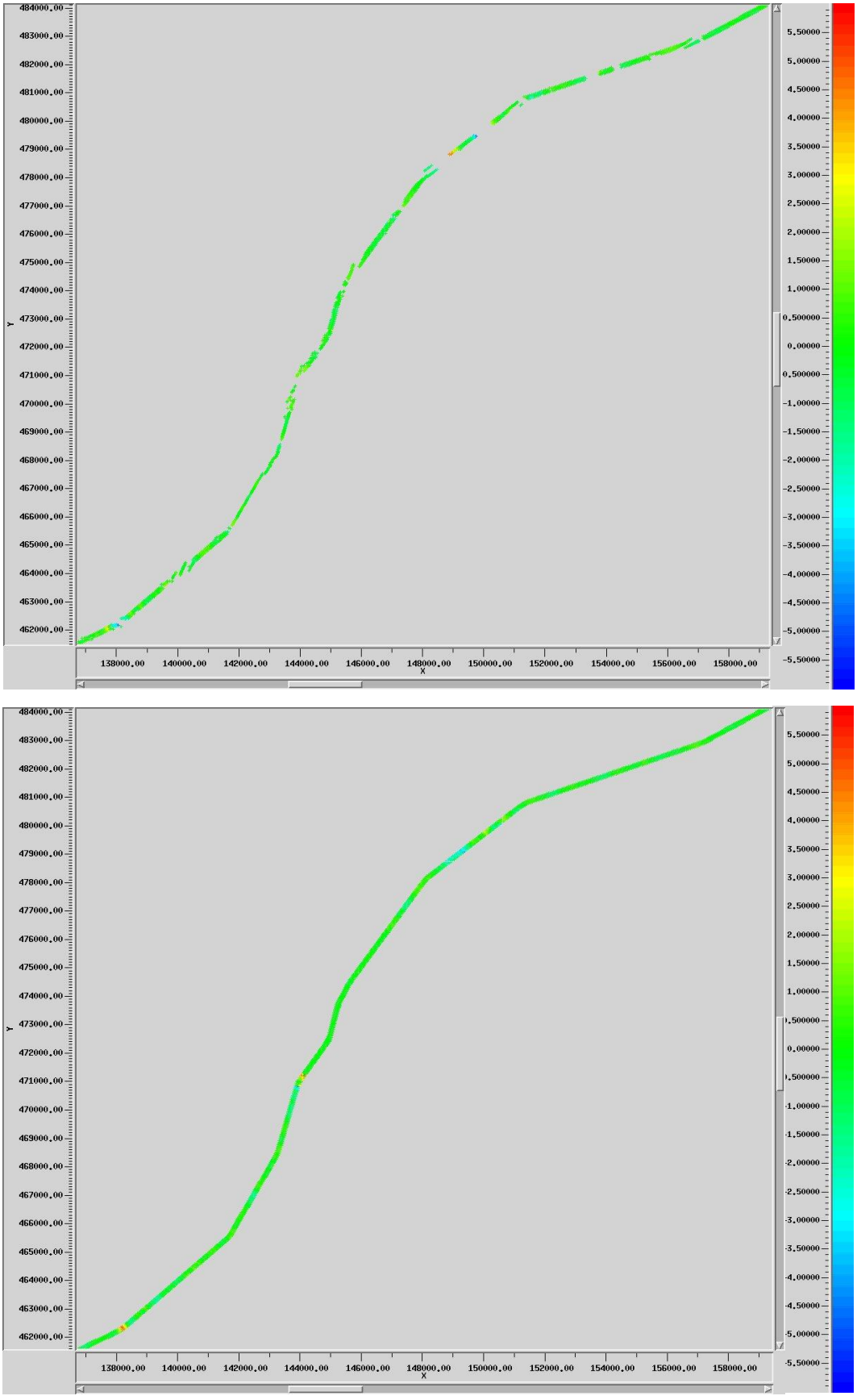

Fig. 37. Total residual static corrections for sources (top) and receivers (bottom). Part of NAM-DEEP corresponding to EBN Test line.

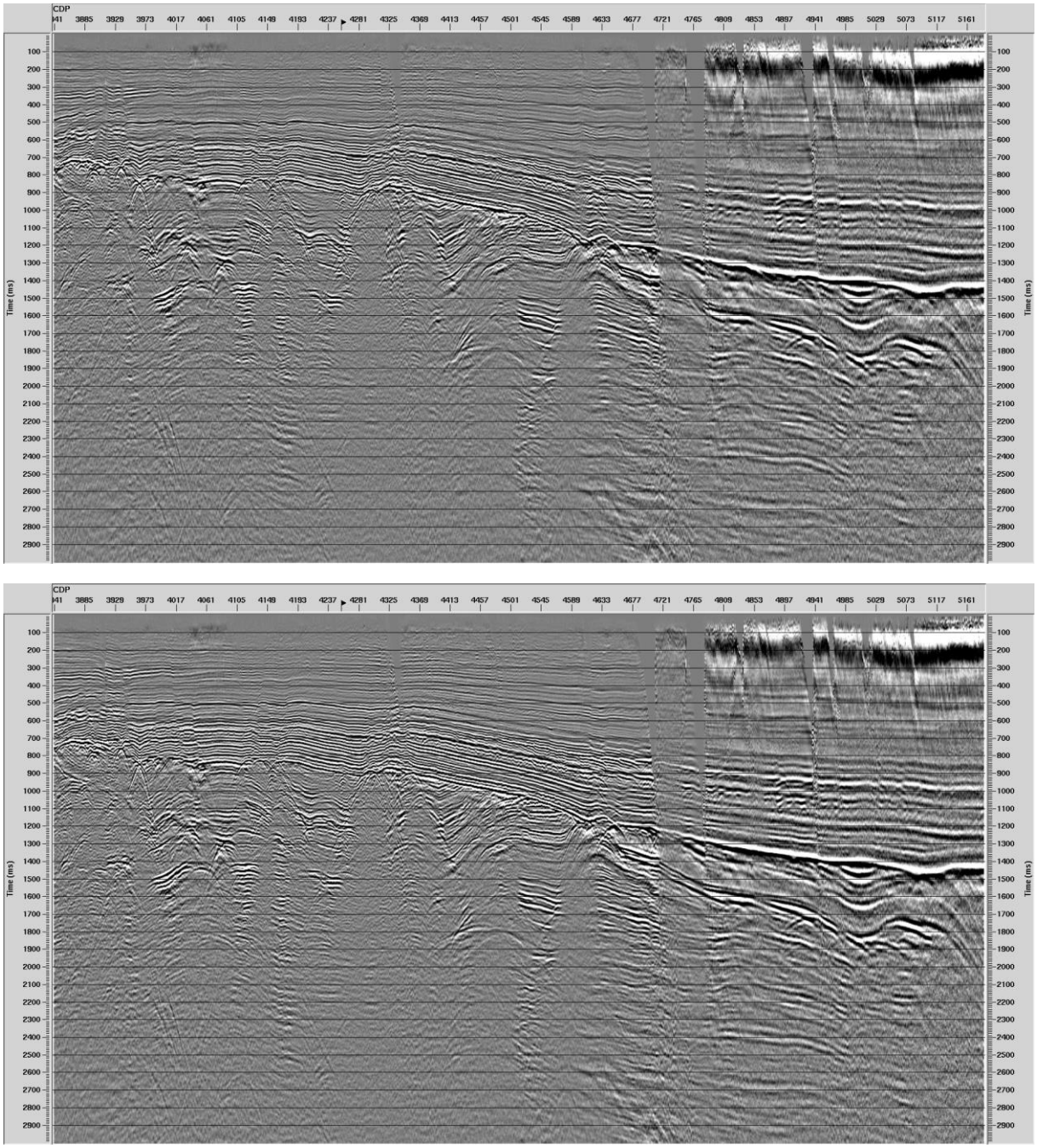

Fig. 38. Control section after preliminary iteration of velocity analysis (top), and after 3rd iteration of velocity analysis and 3rd iteration of residual statics calculation (bottom).

8.9. Multiple reflection attenuation

First approach to multiple reflection attenuation was performed before Pre-Stack Time Migration. *Radon Filter* module was used. Multiple reflections were modeled in Tau-P domain and then subtracted from data using specially designed muting– see Fig. 39

Effectiveness of multiple reflection attenuation is shown in Fig. 40 and Fig. 41.

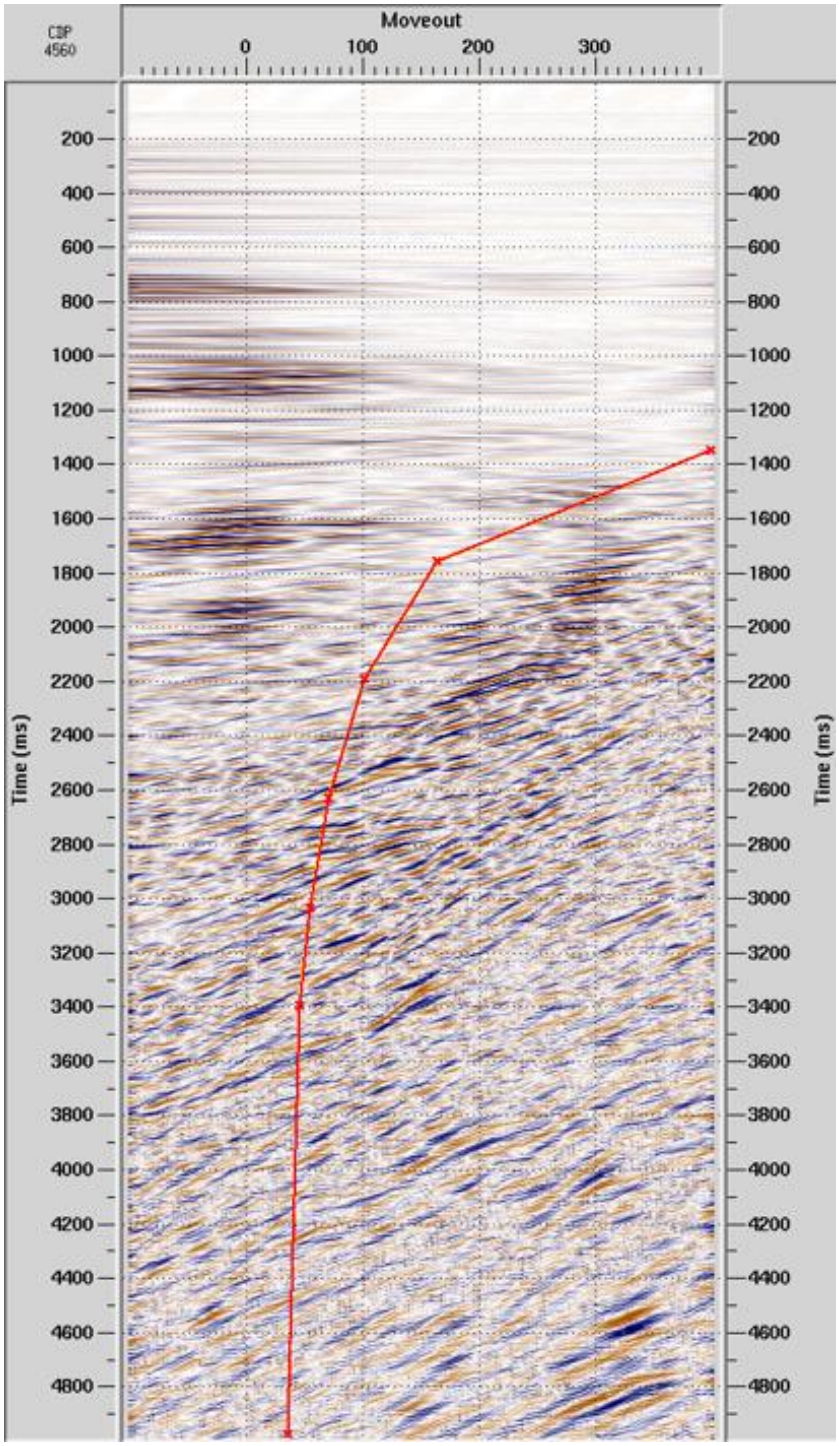

Fig. 39. Example of analysis of multiple reflections in Tau-p domain. Red line defines separation between primaries and multiples.

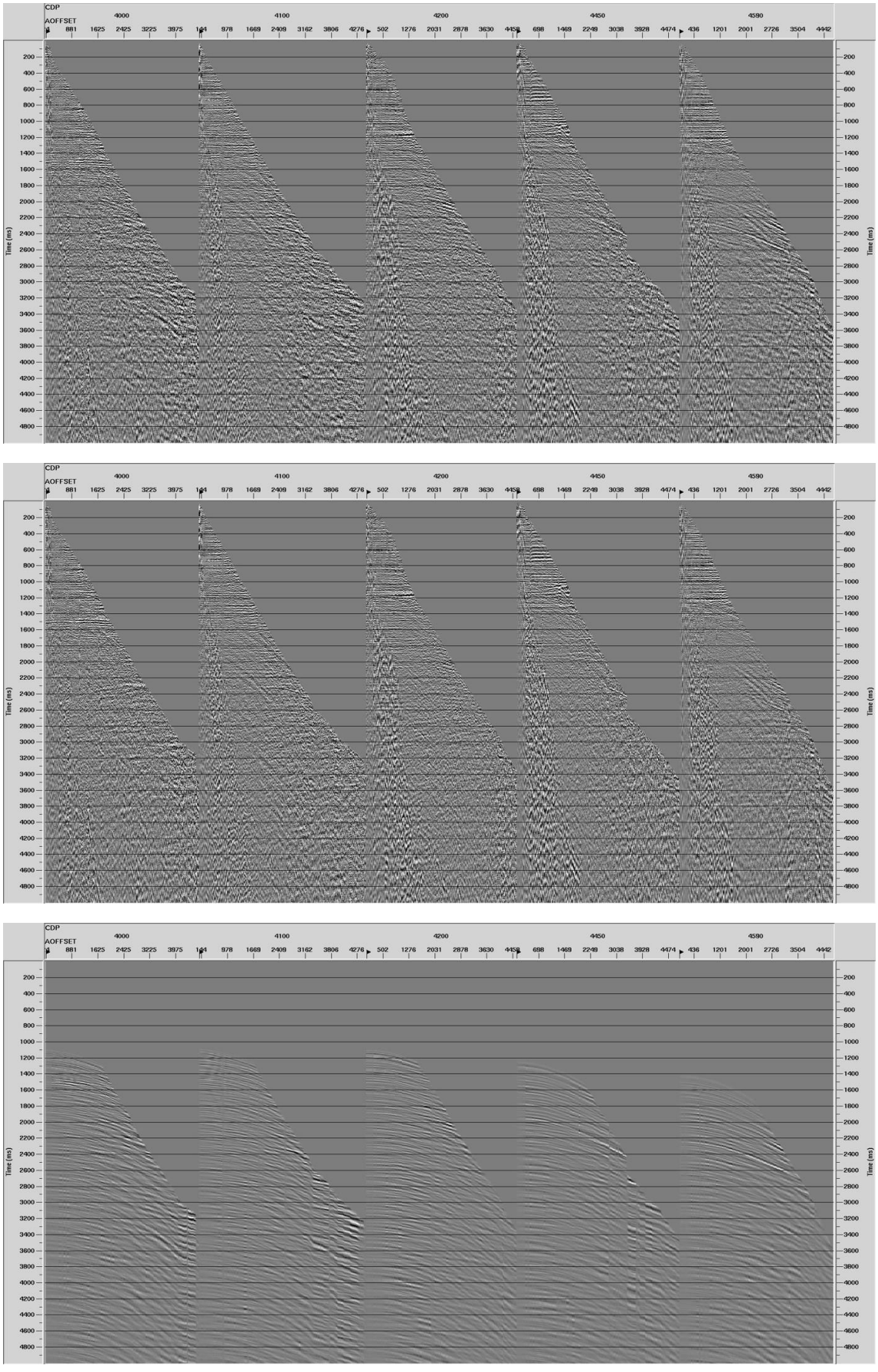

Fig. 40. Effectiveness of multiple reflection attenuation: CDP gathers before multiple reflection attenuation (top), after multiple reflection attenuation (middle), model of multiples subtracted from data (bottom).

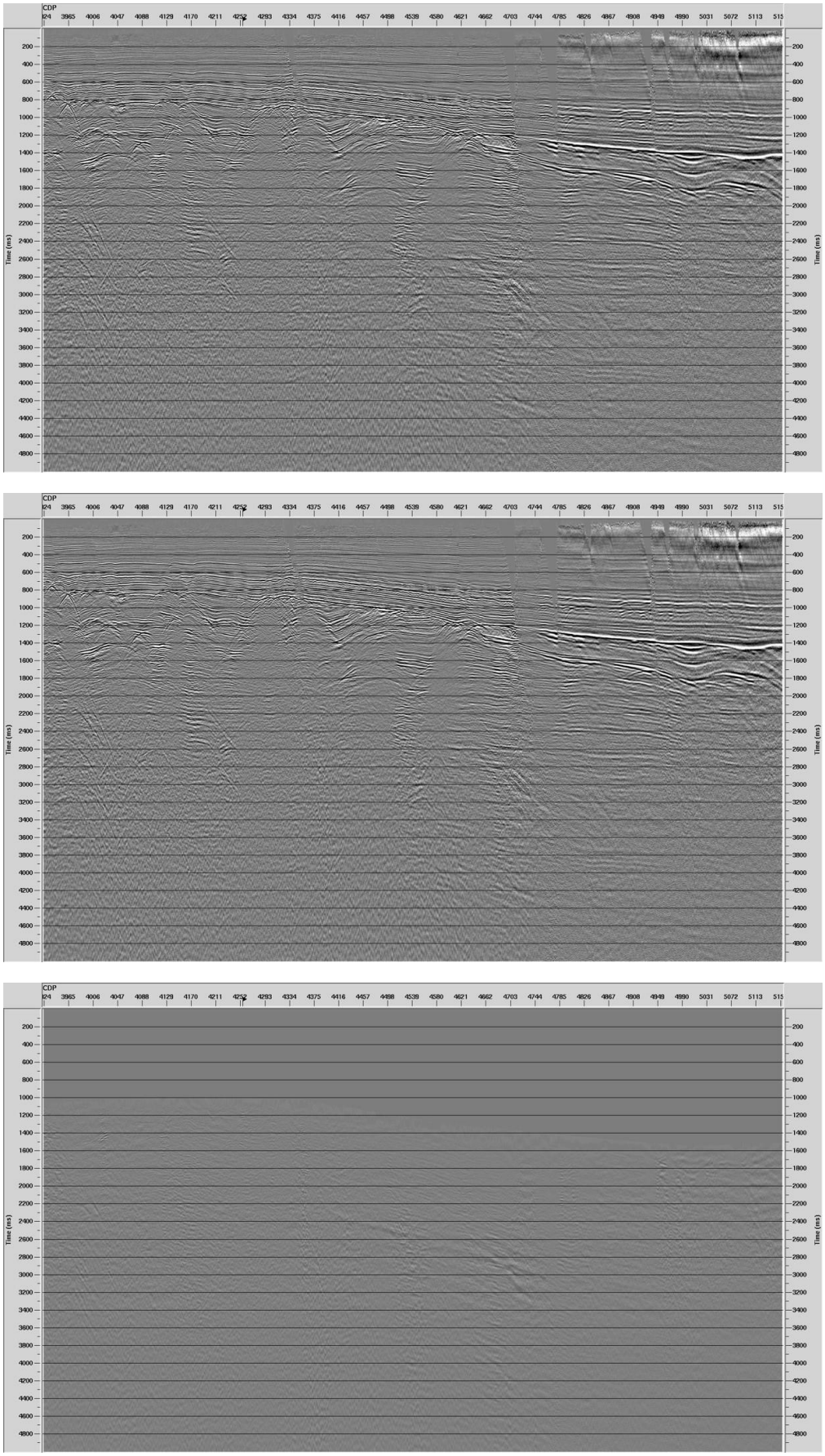

Fig. 41. Effectiveness of multiple reflection attenuation: stacked section before multiple reflection attenuation (top), after multiple reflection attenuation (middle), model of multiples subtracted from data (bottom).

8.10. Pre-Stack Time Migration (PreSTM)

2D Pre-Stack Time Migration with corresponding velocity analysis was performed using *Techco Summig PSTM* module. Kirchhoff algorithm in Techco software will be applied in three steps. The two passes of isotropic PreSTM were performed for preparing data for velocity analysis. Final PreSTM was applied as anisotropic (VTI) with final velocity field.

8.10.1. Data interpolation

Effectiveness of Pre-Stack Time Migration is highly dependent on regularity of offset distribution of input data. For the purpose of PreSTM, tests of data interpolation and regularization with use *of LSS Trace Interpolation* module were performed. Effects of this procedure were viewed on offset and CMP gathers and stacked sections before and after PreSTM.

After tests and consultations with EBN, a moderate approach to interpolation was accepted:

- interpolated traces were inserted only in locations of missing data (“gaps”),
- original traces were retained (no regularization was applied),
- no extrapolation on edges was allowed.

The following parameters of interpolation were accepted:

- maximum/minimum dip: +/- 3 ms/trace,
- gate length: 60 ms,
- max. distance for interpolation: 31 traces,

Results of interpolation are presented on Fig. 42 and Fig. 43.

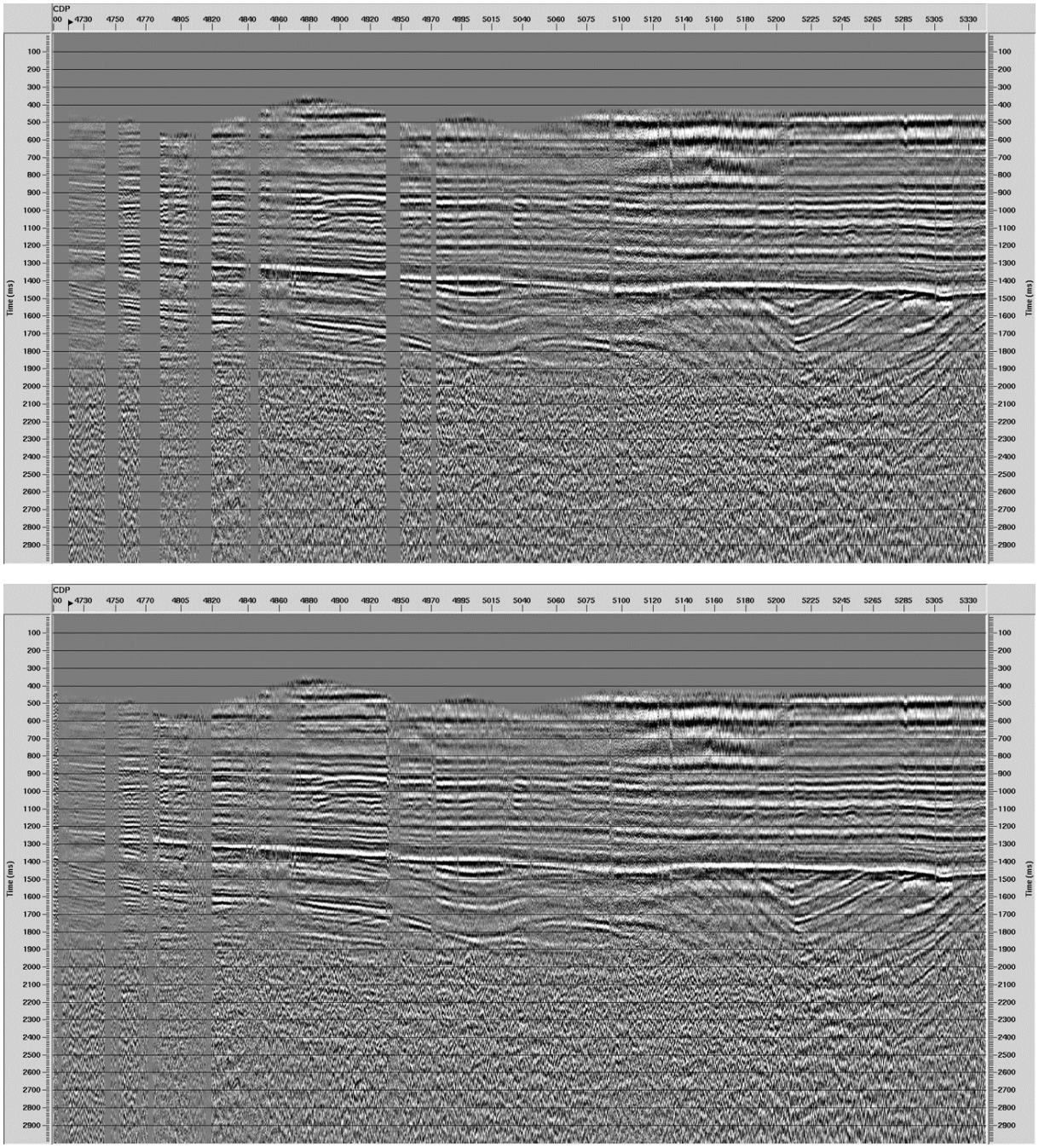

Fig. 42. Effectiveness of data interpolation: fragment of control section for offset range 650-700m before interpolation (top), and after interpolation (bottom).

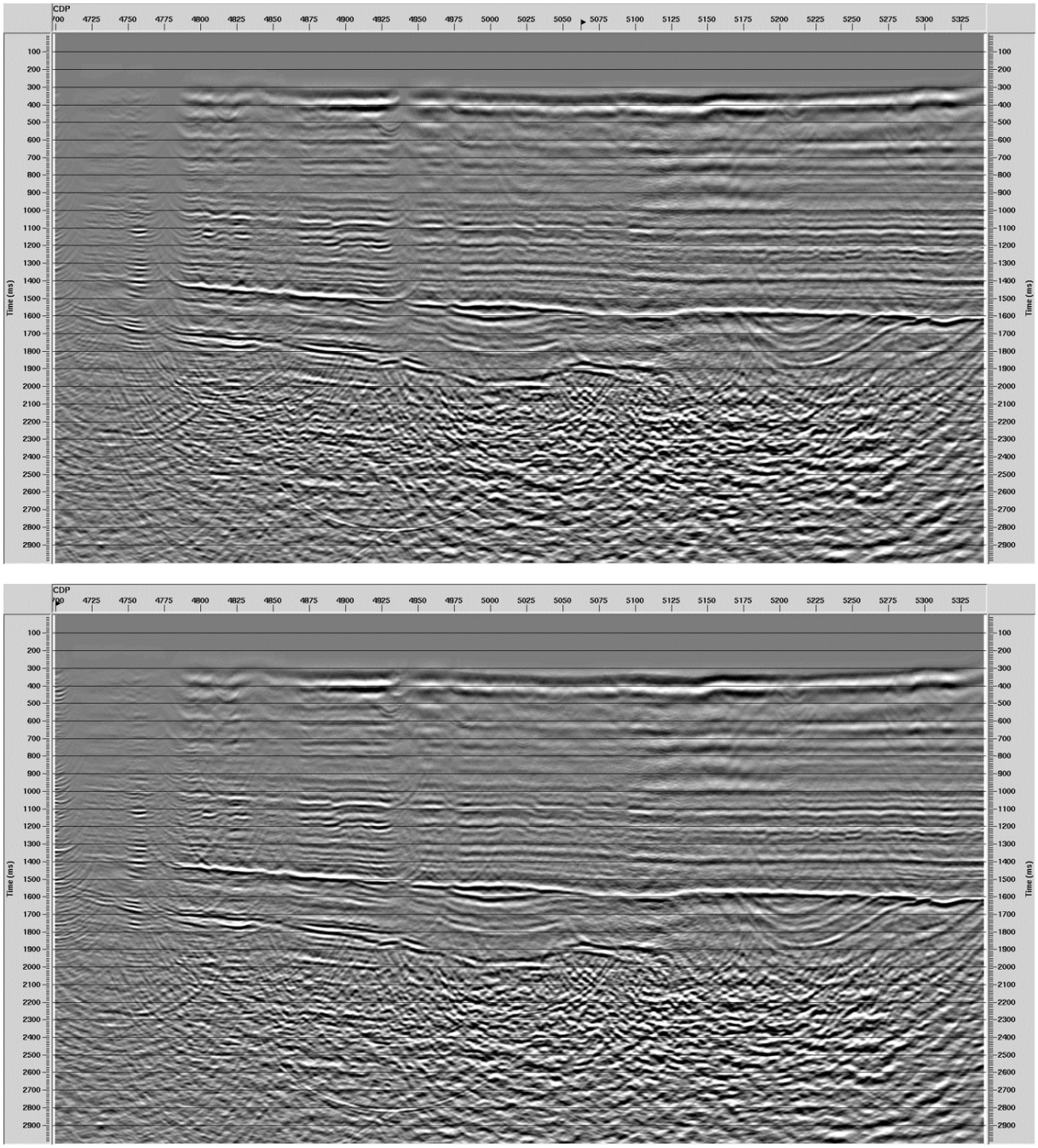

Fig. 43. Effectiveness of data interpolation: fragment of control section for offset range 675 m after Pre-Stack Time Migration without interpolation (top), and with interpolation (bottom).

8.10.2. ETA coefficient selection

Final iteration of 2D Pre-Stack Time Migration was performed as anisotropic (VTI).

Straight-ray NMO approximation, used as standard in most of time processing, is given by standard hyperbolic NMO formula:

$$T^2(X) = T_0^2 + (X / V)^2$$

Where:

T(X) – reflection time at offset X

T_0 – zero-offset reflection time

V – stacking velocity for reflection event.

In Pre-Stack Time Migration, straight-ray approximation usually offers good solution for near offsets. For moderate and far offsets arrival times in CDP gather may differ from results of hyperbolic formula due to stratifying of media. This phenomenon may be observed on CDP gather as “hockey stick” distortion on reflection event.

Above effect may be eliminated by application of mute, what causes loss of data. In order to compensate for non-hyperbolic effects, Vertical Transverse Isotropy (VTI) model was introduced. In this model, the actual velocity for given reflection event is considered to be offset-dependent. NMO formula according to Harlan (1995) transfers to:

$$T^2(X) = T_0^2 + (X / V(X))^2$$

Where:

$$V^2(X) = V_0^2 / [1 – 2 * ETA * (X^2 / (X^2 + V_0^2 * T_0^2))]$$

V_0 – zero-offset reflection velocity (stacking velocity).

In practical application of VTI PreSTM in data processing, the crucial step is to find proper ETA parameter value. The analysis is performed as a panel test of a range of ETA values for a set of selected CDP gathers. Final ETA field is given as space- and time-variant.

Selected ETA field and results of PreSTM are presented on Fig. 44 and Fig.45.

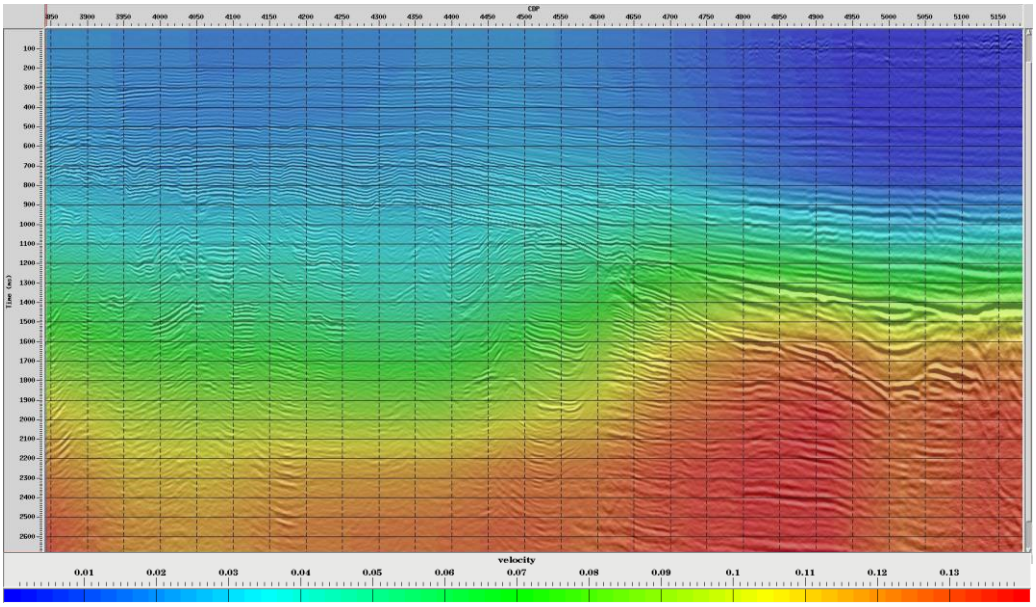

Fig. 44. Selected ETA field on background of control section.

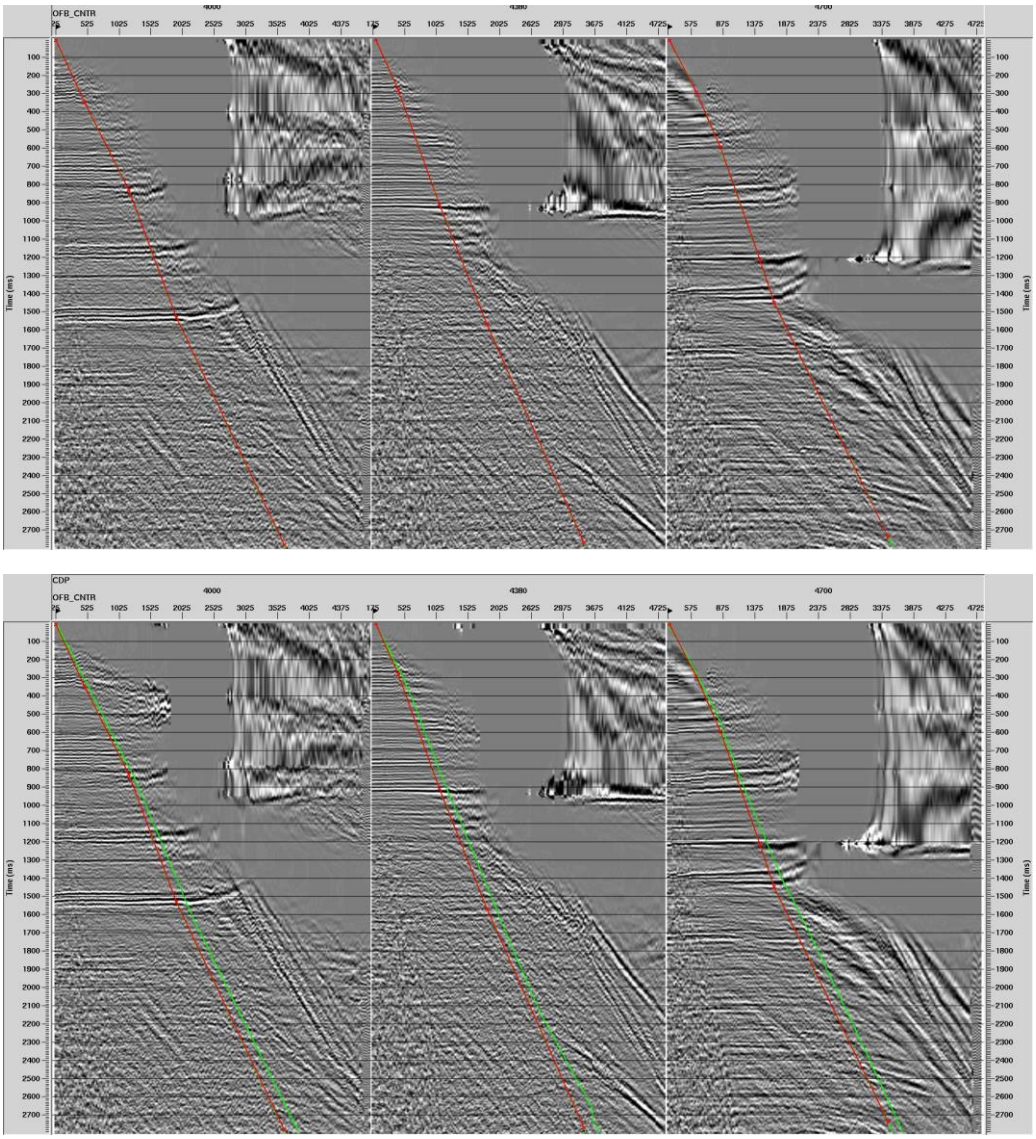

Fig. 45. CDP gathers after isotropic PreSTM, red line – mute (top), and after VTI PreSTM, red line - mute. for isotropic version, green line – mute for VTI version.

8.10.3. Final Pre-Stack Time Migration

For final iteration of 2D Pre-Stack Time Migration (PreSTM) the following parameters were selected:

- maximum aperture half-radius: 3000 m,
- migration max. dip angle: 30 degrees,
- stretch mute cutoff: 0,7,
- minimum offset: 0 m,
- maximum offset: 6000 m,
- offset bin size in CDP: 25 m.

Basic processing included requirement of real amplitude reconstruction (RAP). For better structural imaging, an additional version with AGC scaling after PreSTM was created.

8.11. Post-migration velocity and mute analysis

Final velocity and mute analysis included the following steps:

- final offset range for stacking selection,
- final mute selection,
- final velocity analysis

For the final mute selection, a set of four sections was prepared:

- “Full” for 100% of production mute
- “Near” for 33,3% of mute offset
- “Mid” for mute offset between 33,3% and 66,7%
- “Far” for mute offset between 66,7% and 100%.

Final mute was selected on basis partial mute analysis.

Final velocity analysis was performed with distance of 250 m between analysis points, in supergathers of 5 CDPs.

Partial mutes were presented on Fig. 46. An example of final velocity analysis after PreSTM was shown in Fig. 47. Final velocity field was presented on Fig. 48.

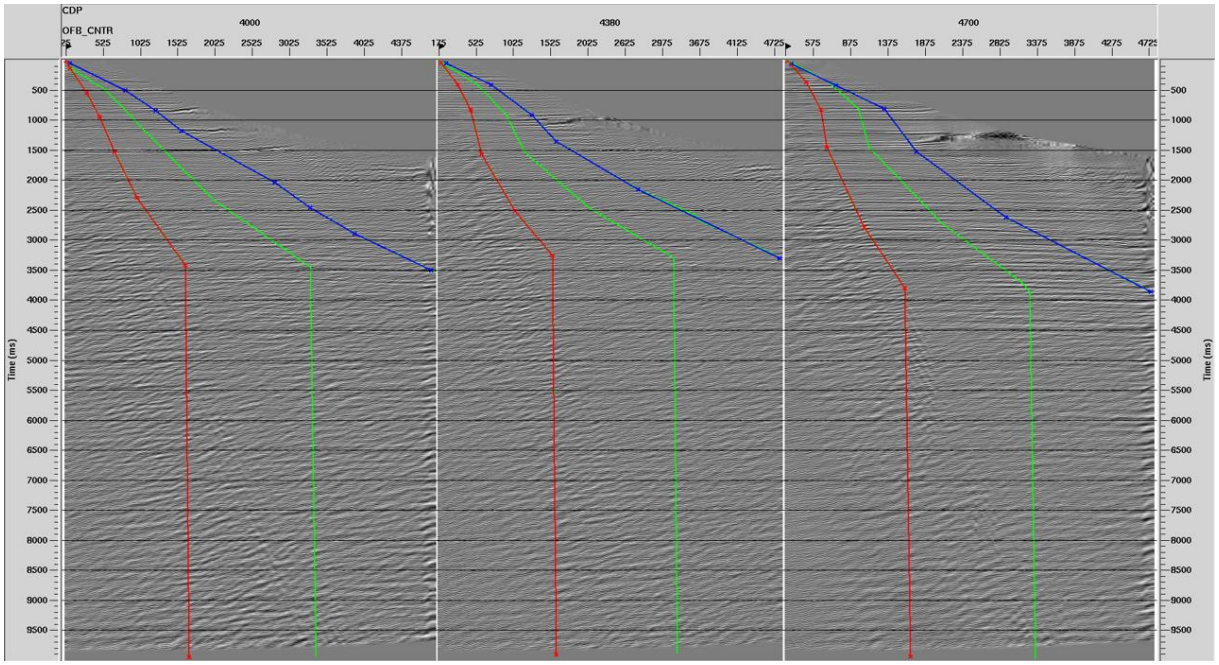

Fig. 46. CDP gathers with percentage mutes indicated: 100% of mute – blue, 66,7% of mute – green, 33,3% of mute – red.

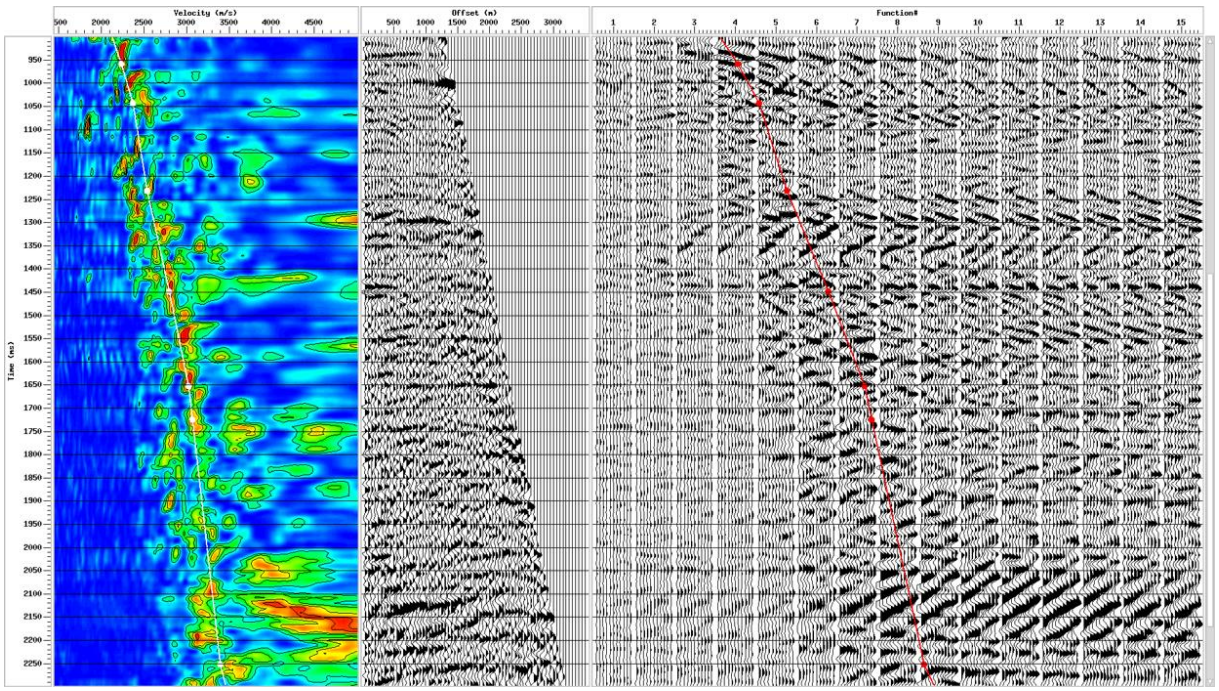

Fig. 47. Example of final velocity analysis after PreSTM. CDP 3880

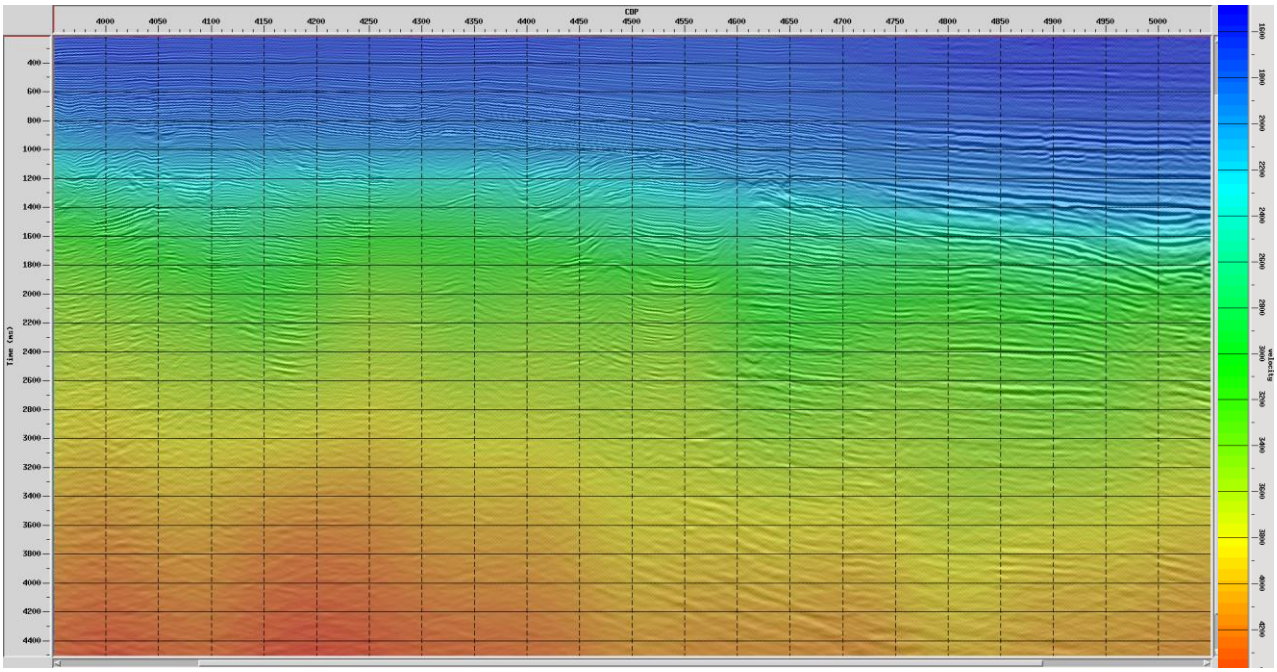

Fig. 48. Final velocity field on background of control section after PreSTM.

8.12. Final multiple reflection and linear noise attenuation

Pre-stack processing sequence after final VTI PreSTM included the following stages:

- final (residual) multiple reflection attenuation to attenuate multiple reflections remaining after first iteration of de-multiple performed prior to PreSTM,
- final (residual) linear noise attenuation.

Final approach to multiple reflection attenuation was performed on data after final VTI Pre-Stack Time Migration. *Radon Filter* module was used. Multiple reflections were modeled in Tau-P domain and then subtracted from data using specially designed muting – see Fig. 49.

For the tau-p transformation, and for the *Radon Filter* module for multiple reflection attenuation, the following parameters were used:

- reference offset: 1500 m,
- range of kinematic corrections: -100 ms / +400 ms,
- transform option: parabolic.

Effectiveness of multiple reflection attenuation is shown in Fig.50 and Fig. 51.

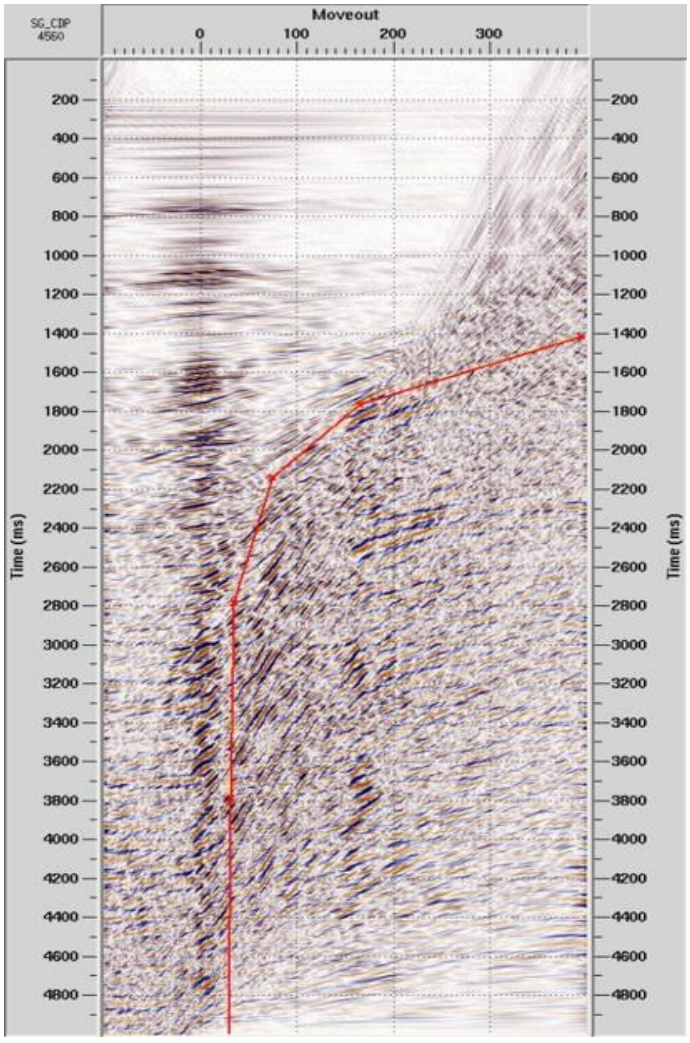

Fig. 49. Example of analysis of multiple reflections in Tau-p domain after final VTI PreSTM. Red line defines separation between primaries and multiples.

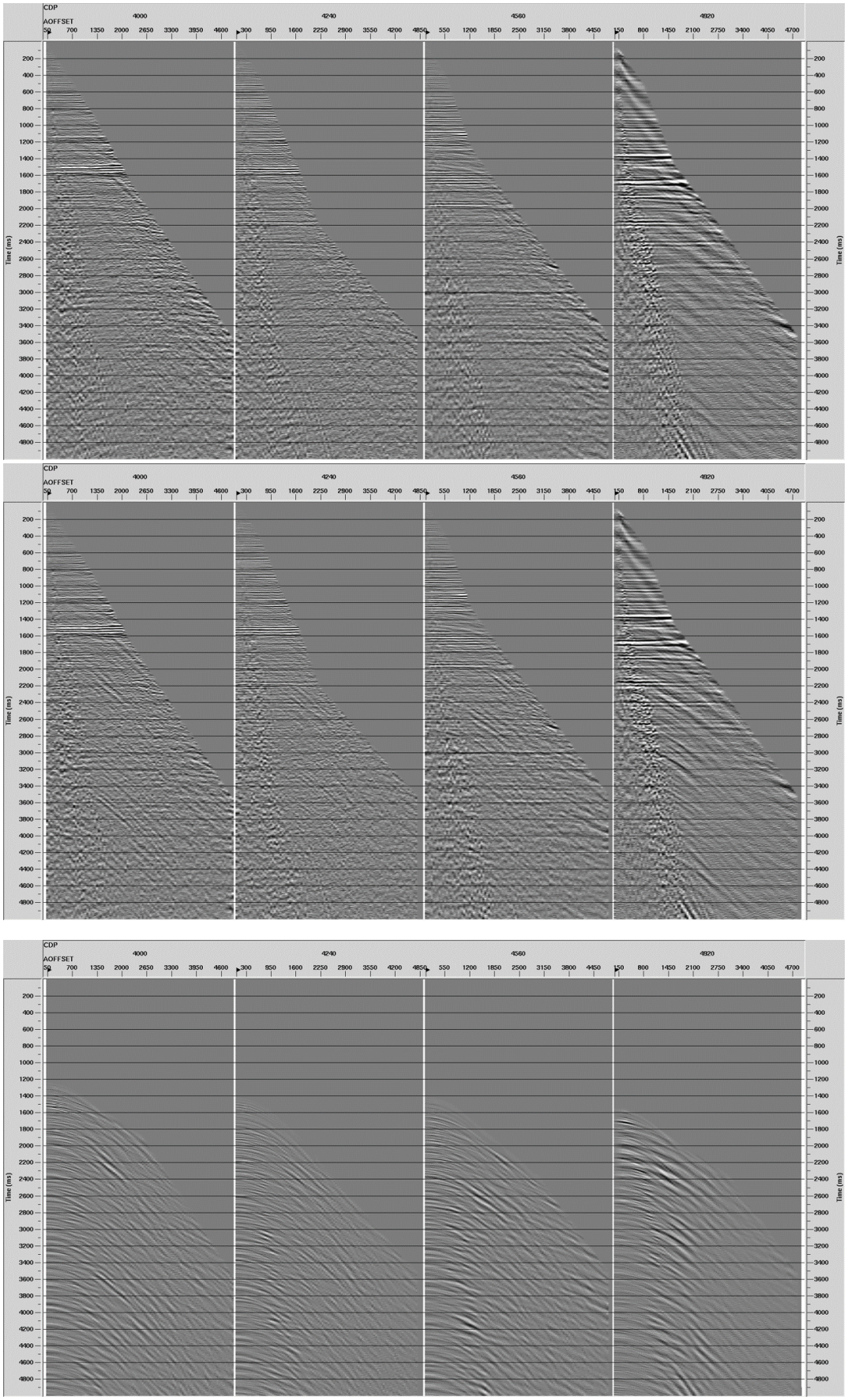

Fig. 50. Effectiveness of multiple reflection attenuation after PreSTM: CDP gathers before final multiple reflection attenuation (top), after multiple attenuation (middle), model of multiples (bottom).

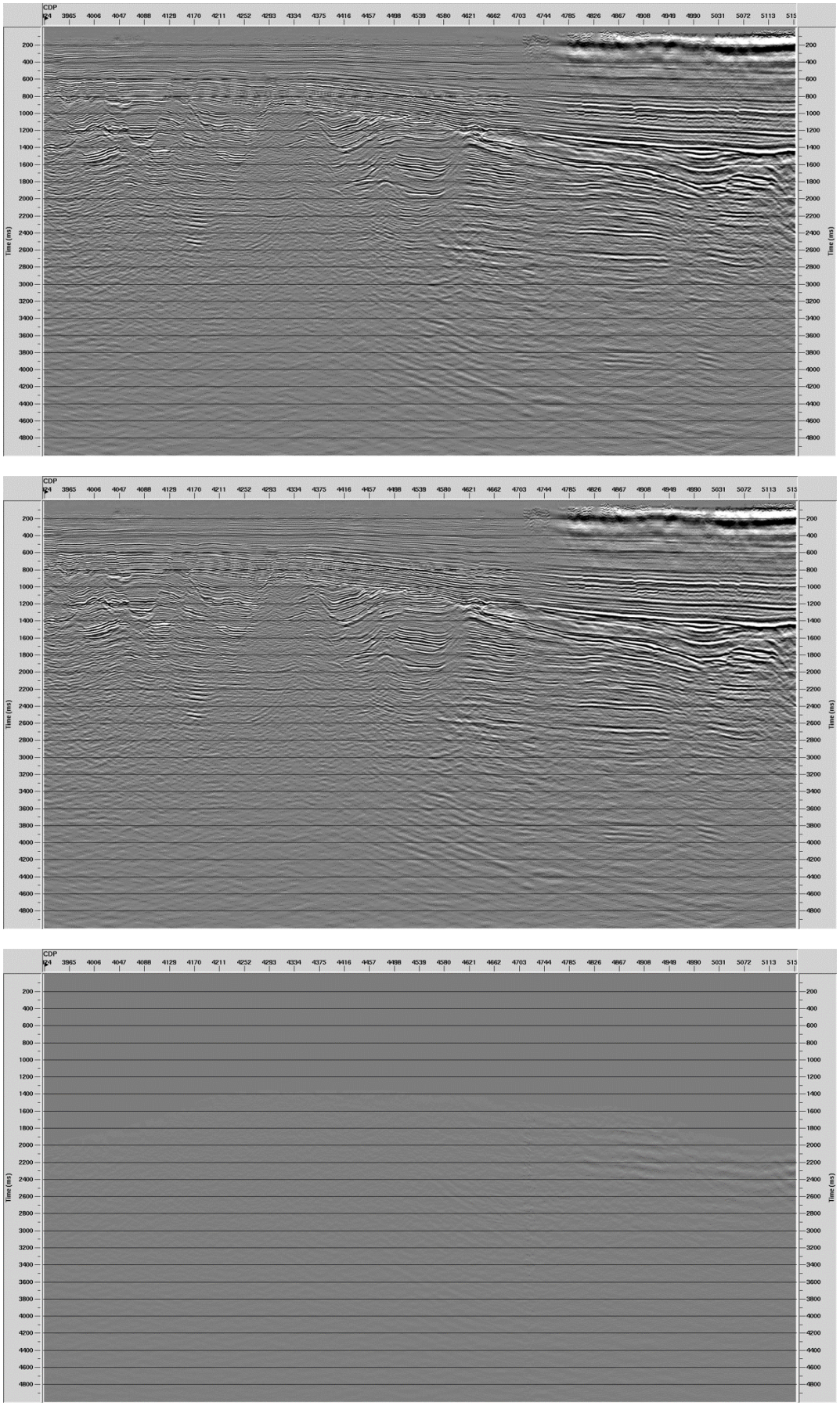

Fig. 51. Control seismic section after final VTI PreSTM before final multiple reflection attenuation (top), after multiple attenuation (middle), differential section with amplitudes enhanced (bottom).

For final linear noise attenuation *Linear Radon* module in cascade option was used. Coherent artifacts were modeled in Tau-P domain and then subtracted from data.

For the 1st iteration of linear noise attenuation for tau-p transformation, and for the *Radon Filter* module, the following parameters were used:

- number of P-values; 1201,
- range of P-values: 250 – 4000 ms,
- reference offset: 3000 m,
- range of frequency: 0 – 25 Hz,
- transform option: linear.

For the 2nd iteration the following parameters were used:

- number of P-values; 1201,
- range of P-values: 200 – 5500 ms,
- reference offset: 3000 m,
- range of frequency: 0 – 20 Hz,
- transform option: linear.

Effectiveness of linear noise attenuation is shown in Fig.52 and Fig. 53.

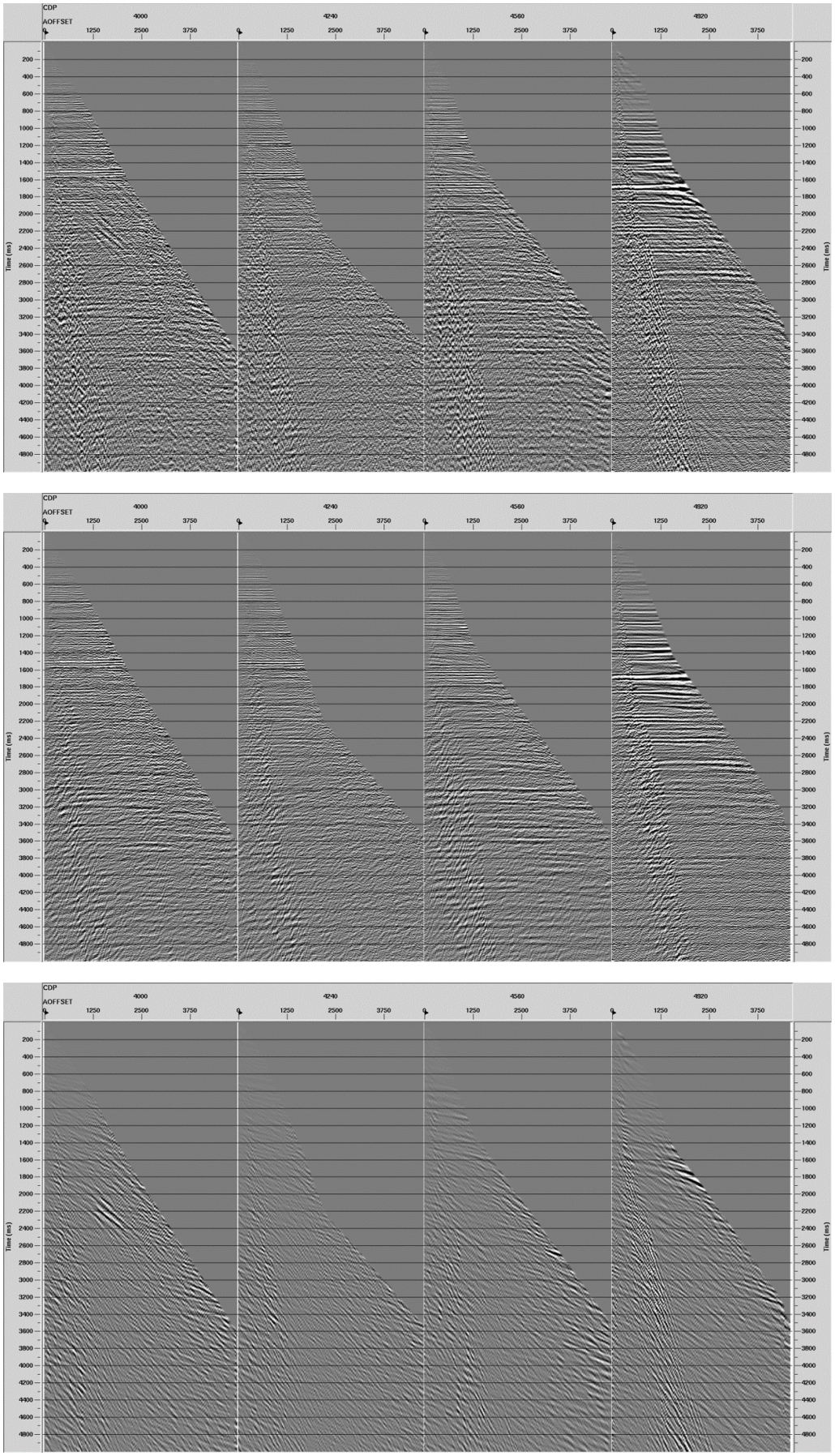

Fig. 52. CDP gathers before linear noise attenuation (top), after linear noise attenuation (center), model of multiples (bottom).

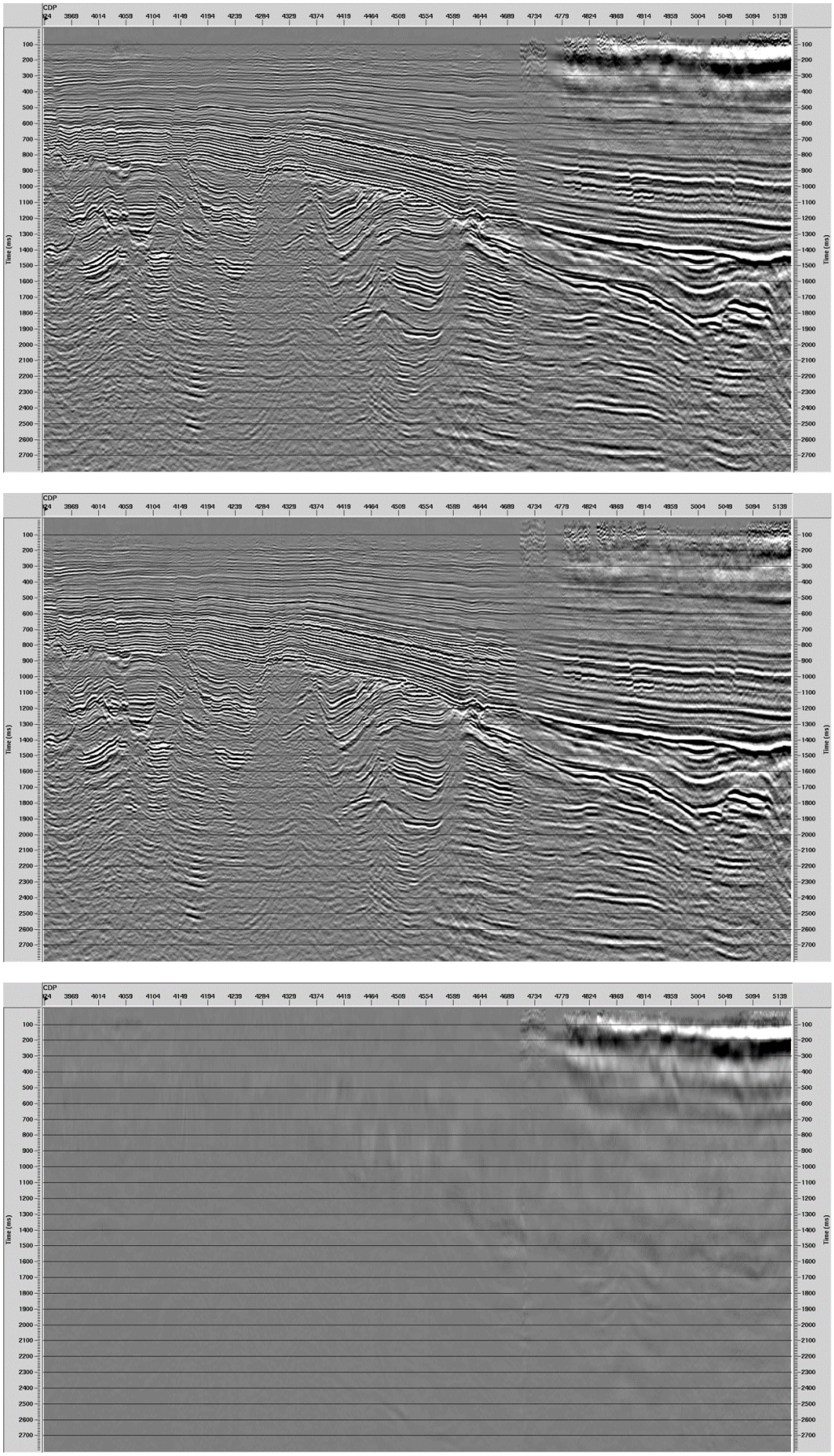

Fig. 53. Control seismic section after final VTI PreSTM before final linear attenuation (top), after linear noise attenuation (middle), differential section (bottom).

8.13. Stacking and post-processing

Preparation of data for final stack included automatic residual trimming of events alignment within CDP gathers. The External Trim Statics module was used for that purpose. Stacked section after PreSTM, multiple reflection attenuation and linear noise attenuation was used as a model. Maximum allowable time shift of 4 ms was used after consultation with EBN Representative.

At this stage the basic stacked section was generated, processed with regard to real amplitude preservation requirement (RAP), stacked with root power scalar for stack normalization equal to 1.0

Post-processing sequence included the following steps, performed after consultation with EBN Representative:

- Post-Stack S/N Enhancement (Dip Scan Stack)

aperture size	5 traces
dip range (min/max)	+/-12ms

- spectral balancing performed with use of *Spectral Shaping* module. The following frequency-amplitude (Hz – dB) pairs were applied: 2-0, 6-8, 10-5, 30-3, 60-8, 90-0
- final post-stack filtering in 6 time windows (*Bandpass Filter*):

Time window:	Filter frequency values:
0 – 1000 ms	4-8-90-130 Hz,
1000 – 2000 ms	4-6-85-110 Hz,
2000 – 3000 ms	4-6-64-76 Hz,
3000 – 5000 ms	4-6-32-44 Hz,
5000 – 7000 ms	4-6-28-36 Hz,
7000 – 10000 ms	4-6-24-32 Hz,

- Final post-stack dynamic scaling – only for additional version with S/N ratio enhancement (*Automatic Gain Control*) with operator length 500 ms,
- Polarity reverse in order to correspond to European SEG Standard.

Effectiveness of spectral balancing was presented on Fig. 54 and Fig. 55.

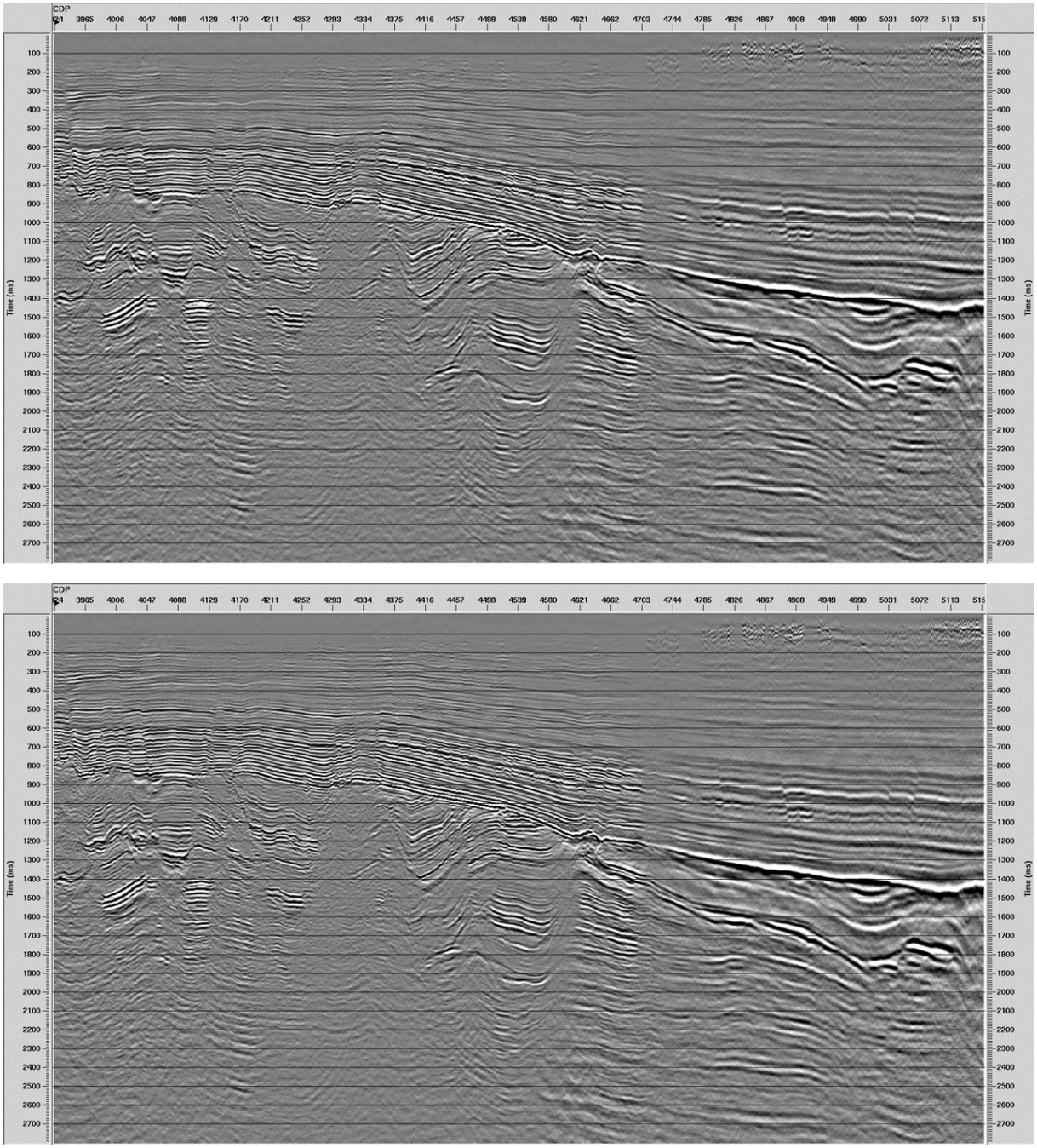

Fig. 54. Control seismic section after final VTI PreSTM before spectral balancing (top) and after spectral balancing (bottom).

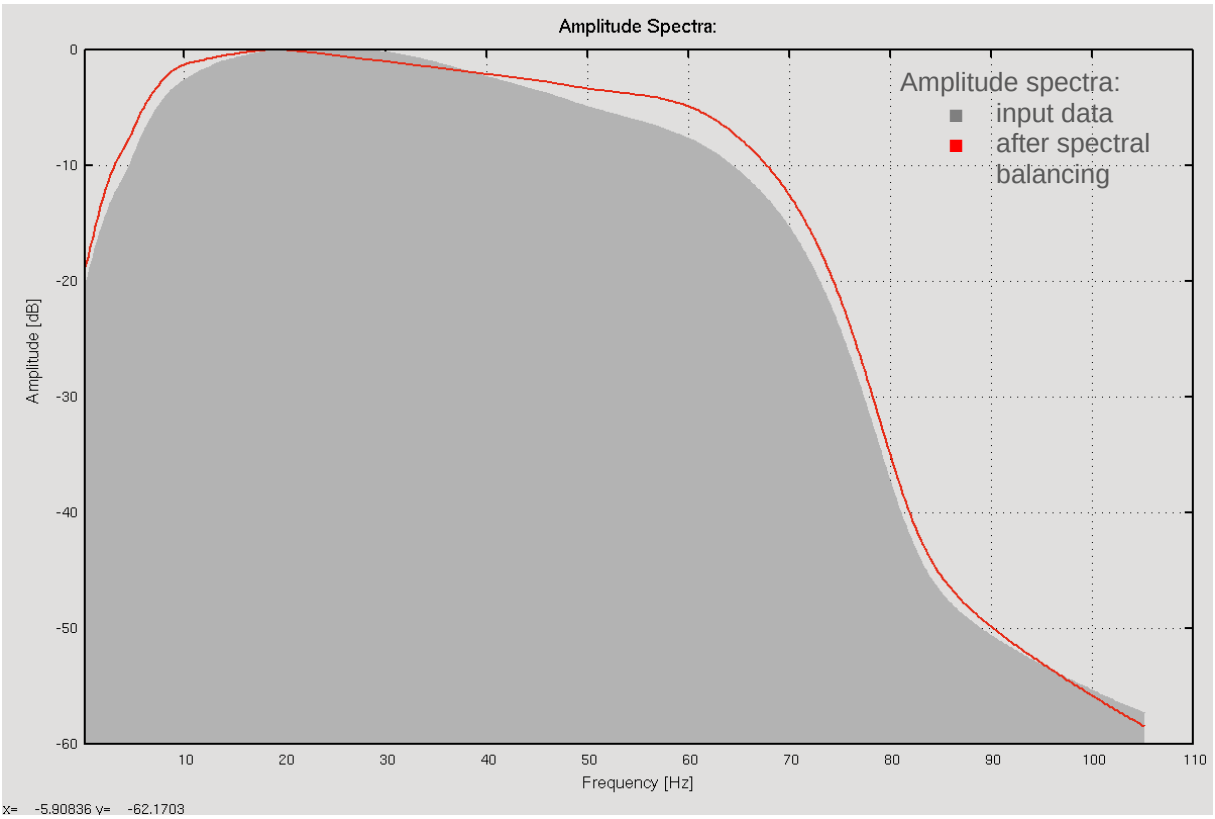

Fig. 55. Amplitude spectra before and after spectral balancing. Time window for spectrum generation: 0 – 3000 ms

9. Zero-phasing and seismic-to-well calibration

9.1. Introduction

As a part of the project, seismic-to-well correlation was performed at several, major processing steps including deconvolution and migration.

The investigation was carried out on the basis of 4 wells: BLA-01-S1, DRO-01, WGD-01, GRL-01, located in the vicinity of re-processed NAM_DEEP_Line (Fig. 56).

The study was conducted by utilizing CGG Hampson-Russell software HRS-9. The required polarity convention of the final processed data (i.e. European Convention, Positive Peak = decrease in impedance), was in opposition to the convention utilized in the software. Therefore, prior to the seismic-to-well tie process, the statistically-derived zero-phase wavelets were rotated by 180º to match the above requirement.

The phase of the seismic data was controlled against available sonic and density logs, however the final conclusions were also drawn by the careful examination of the sign, side lobe values and amplitude relations of the major seismic reflections (Aalburg formation, Zechstein anhydrite groups and Top of Rotliegend series). For that reason, the final solution is a trade-off between the applied methods.

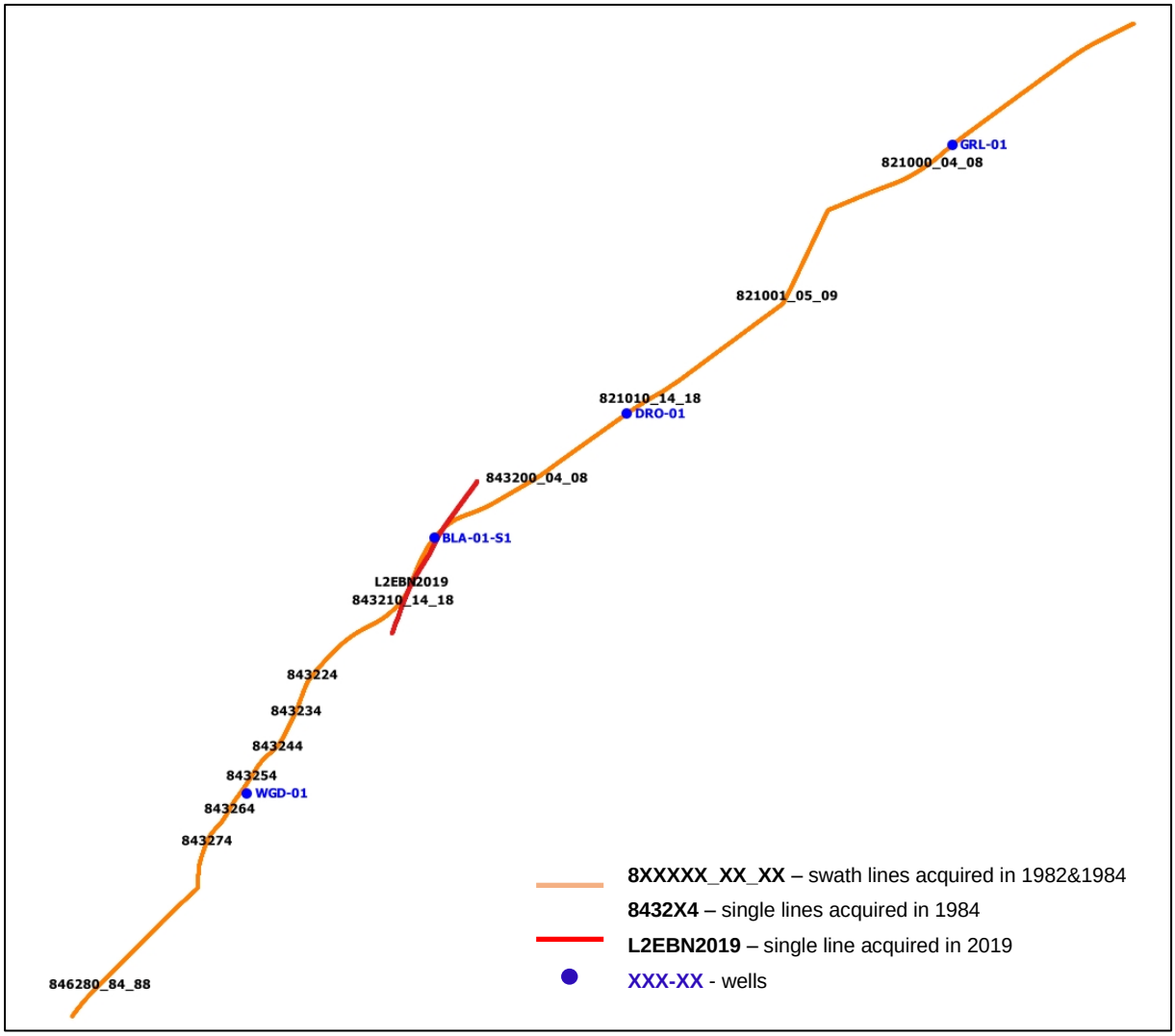

Fig. 56. Seismic lines and wells locations: blue – wells, red – EBN_Test_line (L2EBN2019), brown – NAM DEEP lines

9.2. Comments on the QC of well data

BLA-01/BLA-01-S1

Two key issues need to be taken into account while evaluating the described results of seismic-to-well correlation. First of all, the BLA-01/BLA-01-S1 trajectory is highly deviated in the perpendicular direction to the seismic line. The tops and log values are then projected onto the line. Having regard to close position of faulting, present in the upper part of the section, and also the structural complexity of the Zechstein and underlying sediments, the projection (and the well-tie) is considered an approximate solution. Furthermore, the available acoustic log consists of two separate runs, measured in different well paths. Deeper section of the log, measured in the sidetrack, had to be matched and merged with the vertical one, which can introduce some subjectivity and errors.

In addition, careful investigation of the available check shot survey revealed that there was a large discrepancy between the sonic and VSP-derived velocities, which might be caused by non-vertical propagation of the wave (from the shot point to sidetrack-placed receivers).
During the initial QC of the data it was found that even if any further attempts to obtain the match between the seismic and well log data are attempted, this borehole is generally not recommended to be used in determination of the exact phase characteristics of the data.

DRO-01

Well DRO-01 is located only several meters away from the NAM_DEEP_Line, and the frequency content of seismic data at this location is satisfactory, but the seismic-to-well tie process is ambiguous. In the shallow interval (0 - 700 ms), a lack of strong impedance contrasts causes the synthetic seismogram to be considerably weaker than the real seismic data. Due to the high complexity of the geological structure, there is limited number of usable seismic energy below 900 ms. As a result, the time window within which the synthetic seismograms could be reliably compared to measured seismic response, is not wide enough to compute a realistic cross-correlation value.
The check-shot correction gives satisfactory result only in the depth range 0-900 m, but in fact its usage is very problematic and is not recommended. The described borehole could only be used for determination of generalized time-depth table and structural seismic interpretation purposes, but not for detailed QC of the processing sequence and its parameters, or determination of phase characteristics.

WGD-01

Well WGD-01 is located 1100 m away from the seismic re-processed line, which makes the proper event matching difficult, especially by taking into account the complexity of the structure for the deeper part of the geological medium.
Additionally, the acoustic log velocity values differ considerably before and after check-shot correction. Once more, assuming the correctness of the check shot curve, no consistency between synthetic response and seismic data exists. After a detailed analysis, it was concluded that the check shot calibration should be avoided in the seismic-to-well tie process. The acoustic log starts at some 700 ms, therefore the computed cross-correlation window includes complex, dipping formations only. Due to a large distance from the 2D line, the well data (synthetic) need to be adjusted to obtain a satisfactory match in the deeper part of the section. It could only be achieved by significant squeezing and stretching of the modeled data. After the above adjustments, the resulting cross-correlation might be satisfactory.

GRL-01

Well GRL-01 is located 90 m away from the NAM_DEEP_Line. Frequency content of seismic data at this location is reasonable. The useful, high-amplitude and continuous seismic events are present to approx. 2300 ms, with good S/N ratio. The check-shot correction gives realistic results here. Seismic reflections within time window from the Base Lower North Sea Group to Base Zechstein Group can be consistently matched to those of the synthetic seismogram. It should be noted that due to deficiencies of the original density curve, a synthetic one from Gardner's equation was used in this case.

For the above reasons, a reliable synthetic seismogram can be computed at this location, which in turn leads to an approximate estimation of the phase of seismic data.

To summarize, a fully reliable synthetic seismogram could be computed only for well GRL-01. Additionally, some more conclusions could be drawn from WGD-01 well (after proper synthetic adjustments). Synthetic seismograms for other boreholes can be computed too, but their usability is questionable.

9.3. Seismic-to-well correlation using the final processing results

The attached figures (Fig. 57 to Fig. 64) show the results of seismic-to-well correlation process performed by utilizing final processed data NAM_DEEP_Line (VTI PreSTM with real amplitude preservation RAP, after post-processing). The AGC-scaled version of the data was used only in case of DRO-01 borehole to improve the interpretability of the deep seismic reflections. It was caused by the fact that on RAP version almost no seismic energy was present in this fragment of the section.
To perform the correlation, the statistical wavelet was derived from representative number of seismic reflections, in the vicinity of the wells. The wavelet was assumed to be zero-phase. As stated in the first paragraph, the 180º phase rotation was applied to the wavelet to match the required SEG convention.

The analysis revealed that the best overall match and highest cross-correlation coefficients were obtained after applying the phase rotation of +90º to the PreSTM data set. The result is clear at GRL-01 well (and to some extent at WGD-01), where the rotated versions shown a very good match with the synthetic data. In addition to overall consistency of the modeled and measured seismic data, the shape of cross-correlation function was symmetrical and resembled the shape of the zero-phase wavelet. Therefore, the phase rotated (+90º) version was considered a good approximation of the zero-phase seismic data.

The well-based results were further proved by the observations made on the individual geological boundaries, especially on the erosional one, marked by ATAL top at the location of BLA-01-S1 well.
The response of the mentioned seismic reflection changes considerably along the line. Due to the erosional character of the boundary, tuning effects and signal interference, its phase response for the whole line is changeable and unpredictable. However, for some local parts of the line (CDP 4700-5350), the boundary could be regarded as single interface separating two half spaces with considerably different velocities. Therefore, it was expected to observe a single, low-frequency, negative seismic reflection, with symmetrical side lobes on both sides. Such response can be noticed for +90º phase rotated data.

To summarize, both well-based computation of the cross-correlation between the synthetic and seismic data, and geological observations on individual seismic boundaries, revealed that after the proposed and applied phase rotation the wavelet present within the final seismic data can be considered a very good approximation of the zero-phase one.

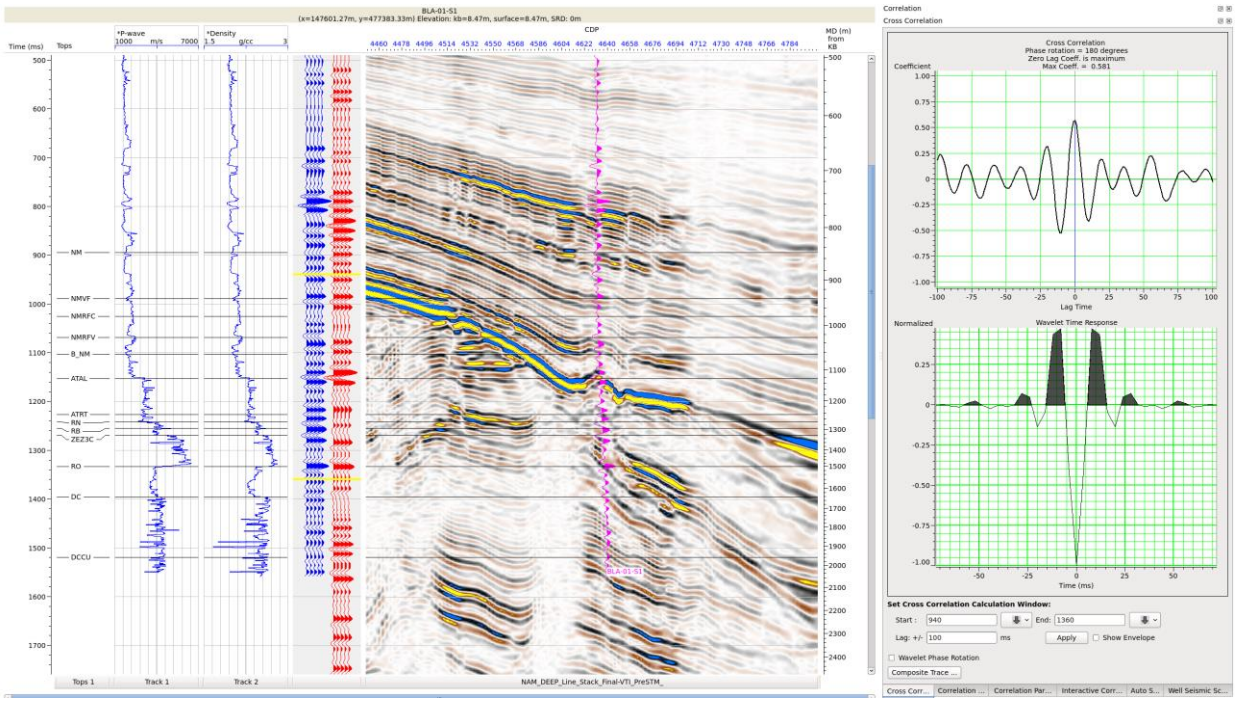

Fig. 57. Well-to-seismic correlation at the well BLA-01-S1 using final PreSTM data (phase rotation = +0°) NAM_DEEP_Line and statistically computed zero-phase wavelet. The match between the synthetic (blue) and the extracted trace (red) is expressed by cross-correlation (upper right). Cross-correlation window is marked by yellow lines. The synthetic trace was superimposed on seismic 2D line (purple).

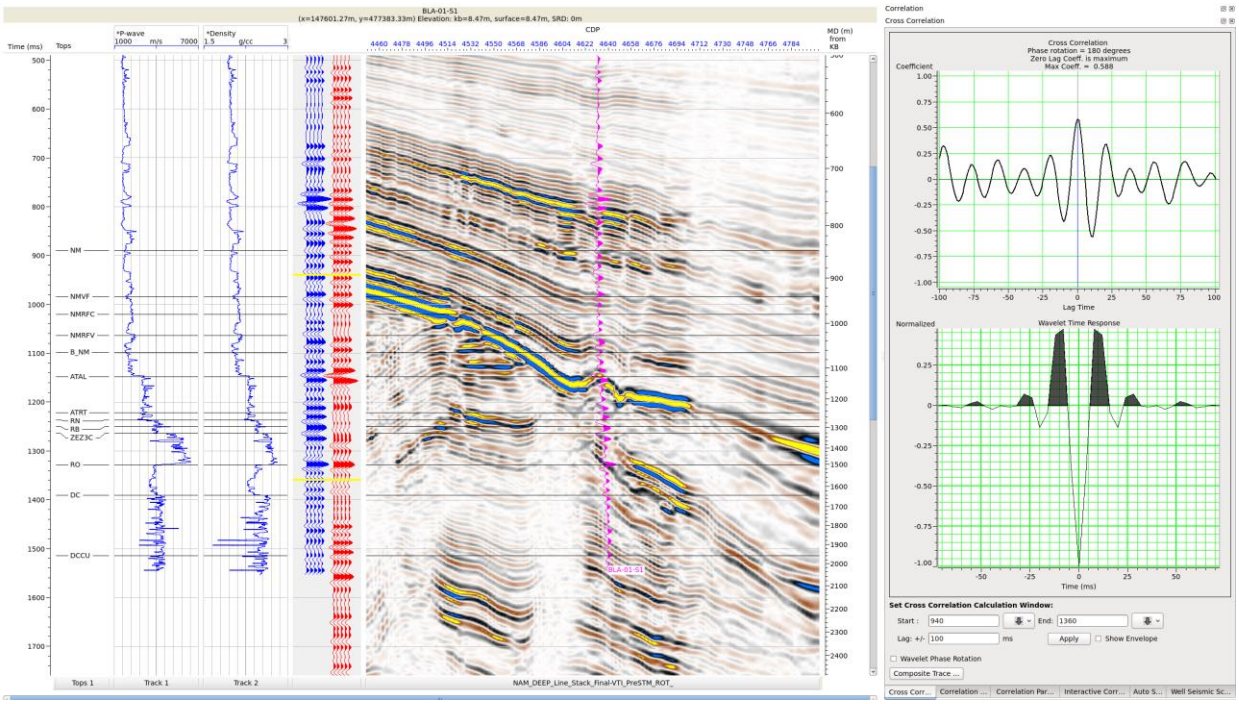

Fig. 58. Well-to-seismic correlation at the well BLA-01-S1 using final PreSTM data (phase rotation = +90°) NAM_DEEP_Line and statistically computed zero-phase wavelet. The match between the synthetic (blue) and the extracted trace (red) is expressed by cross-correlation (upper right). Cross-correlation window is marked by yellow lines. The synthetic trace was superimposed on seismic 2D line (purple).

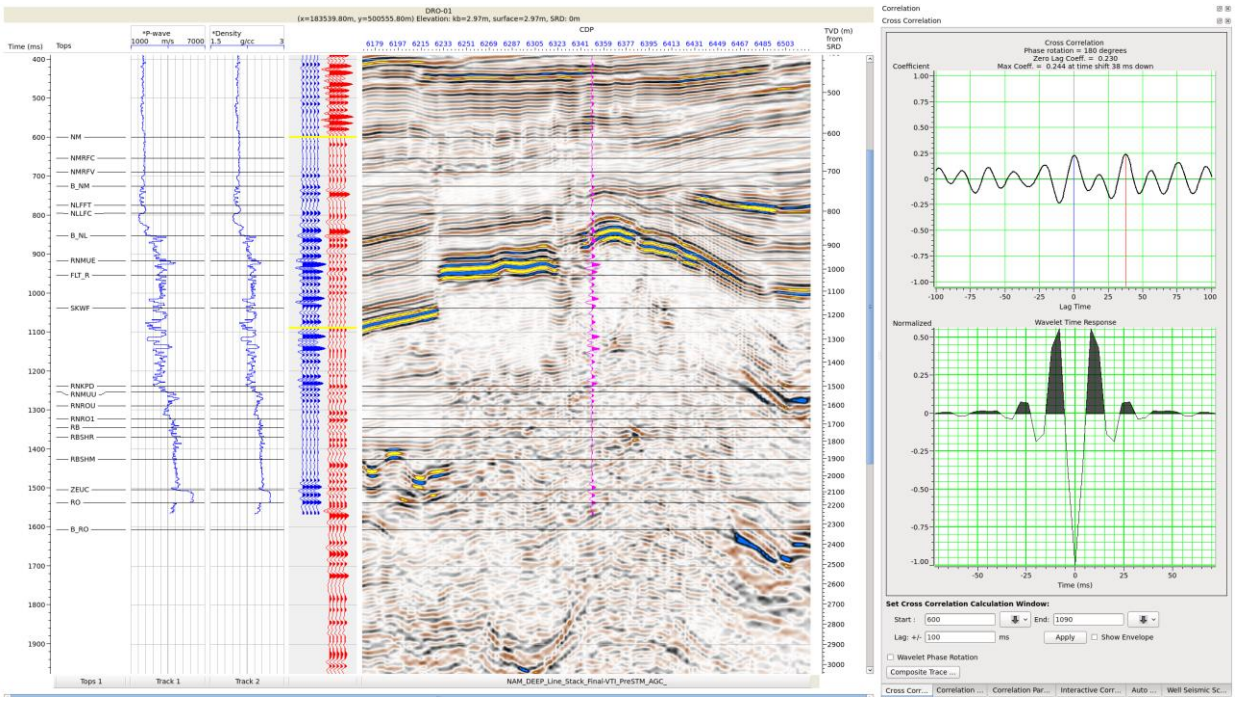

Fig. 59. Well-to-seismic correlation at the well DRO-01 using final PreSTM data (phase rotation = +0°) NAM_DEEP_Line and statistically computed zero-phase wavelet. The match between the synthetic (blue) and the extracted trace (red) is expressed by cross-correlation (upper right). Cross-correlation window is marked by yellow lines. The synthetic trace was superimposed on seismic 2D line (purple).

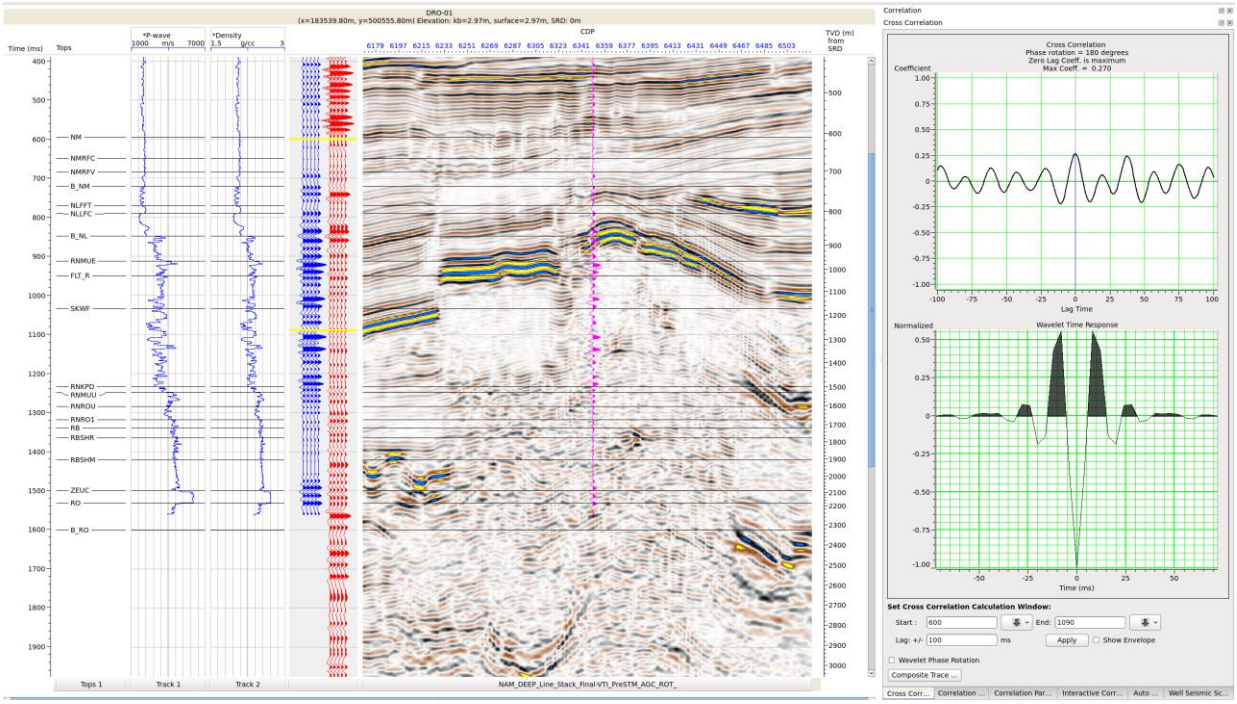

Fig. 60. Well-to-seismic correlation at the well DRO-01 using final PreSTM data (phase rotation = +90°) NAM_DEEP_Line and statistically computed zero-phase wavelet. The match between the synthetic (blue) and the extracted trace (red) is expressed by cross-correlation (upper right). Cross-correlation window is marked by yellow lines. The synthetic trace was superimposed on seismic 2D line (purple).

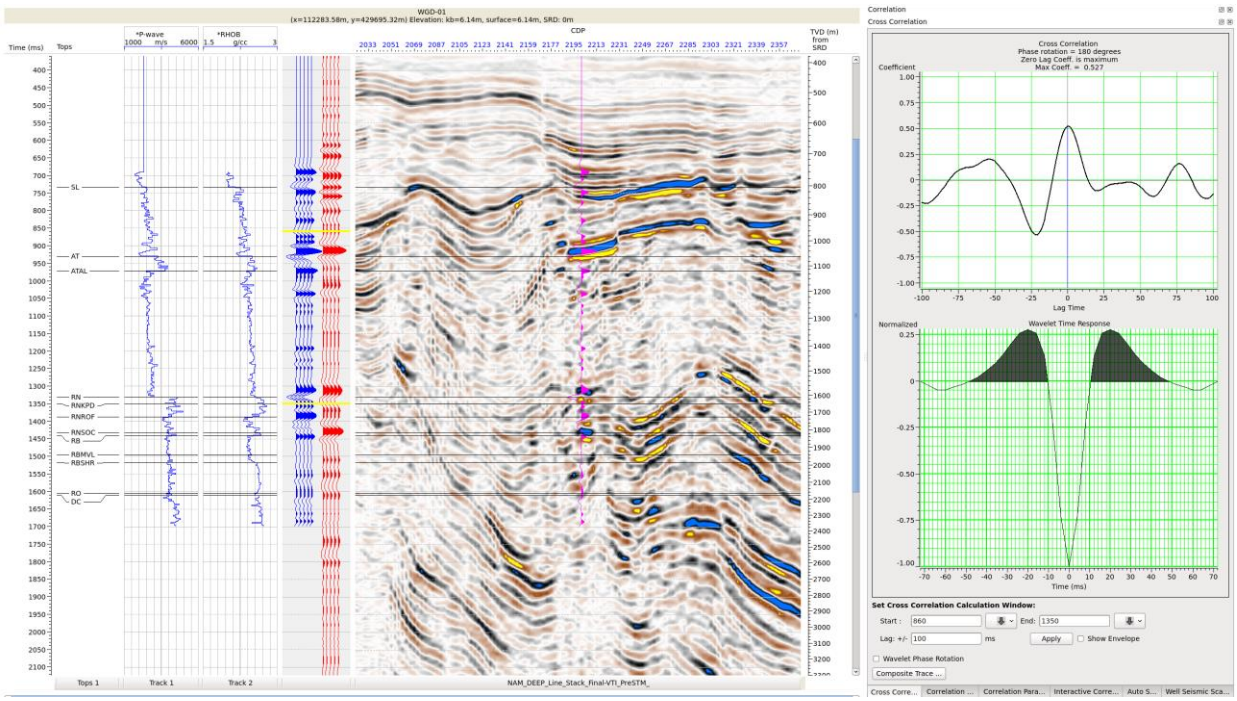

Fig. 61. Well-to-seismic correlation at the well WGD-01 using final PreSTM data (phase rotation = +0°) NAM_DEEP_Line and statistically computed zero-phase wavelet. The match between the synthetic (blue) and the extracted trace (red) is expressed by cross-correlation (upper right). Cross-correlation window is marked by yellow lines. The synthetic trace was superimposed on seismic 2D line (purple).

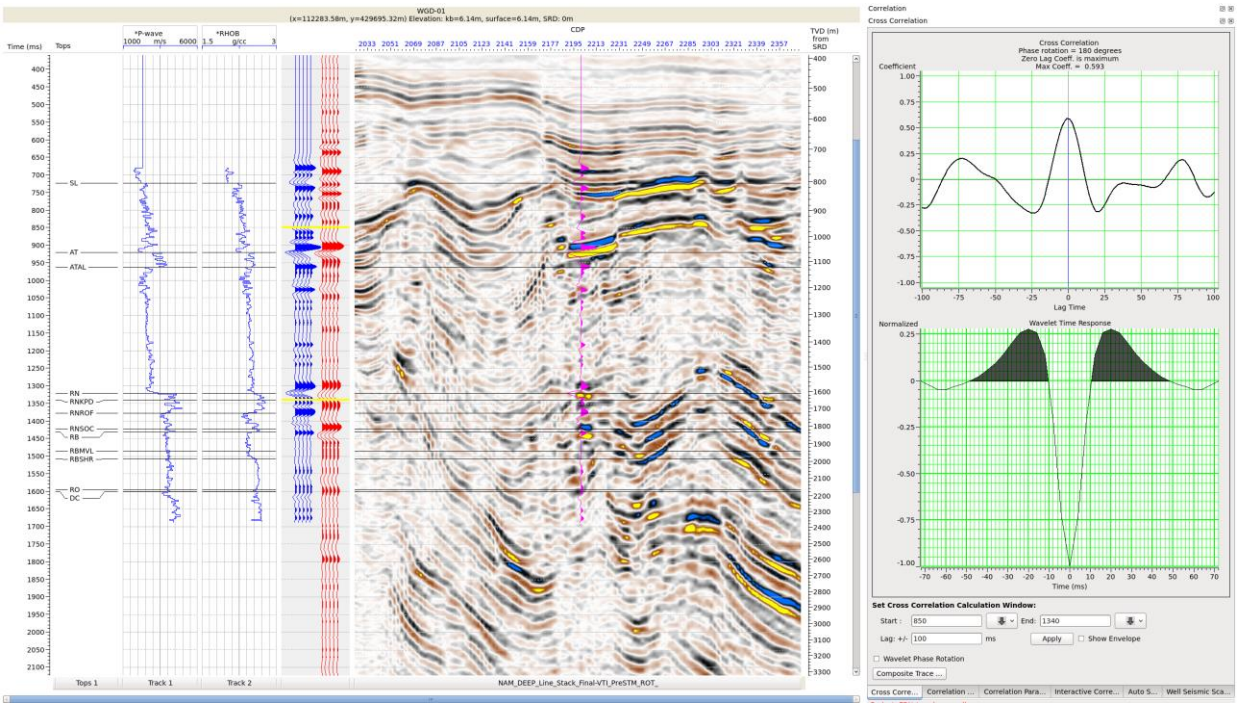

Fig. 62. Well-to-seismic correlation at the well WGD-01 using final PreSTM data (phase rotation = +90°) NAM_DEEP_Line and statistically computed zero-phase wavelet. The match between the synthetic (blue) and the extracted trace (red) is expressed by cross-correlation (upper right). Cross-correlation window is marked by yellow lines. The synthetic trace was superimposed on seismic 2D line (purple).

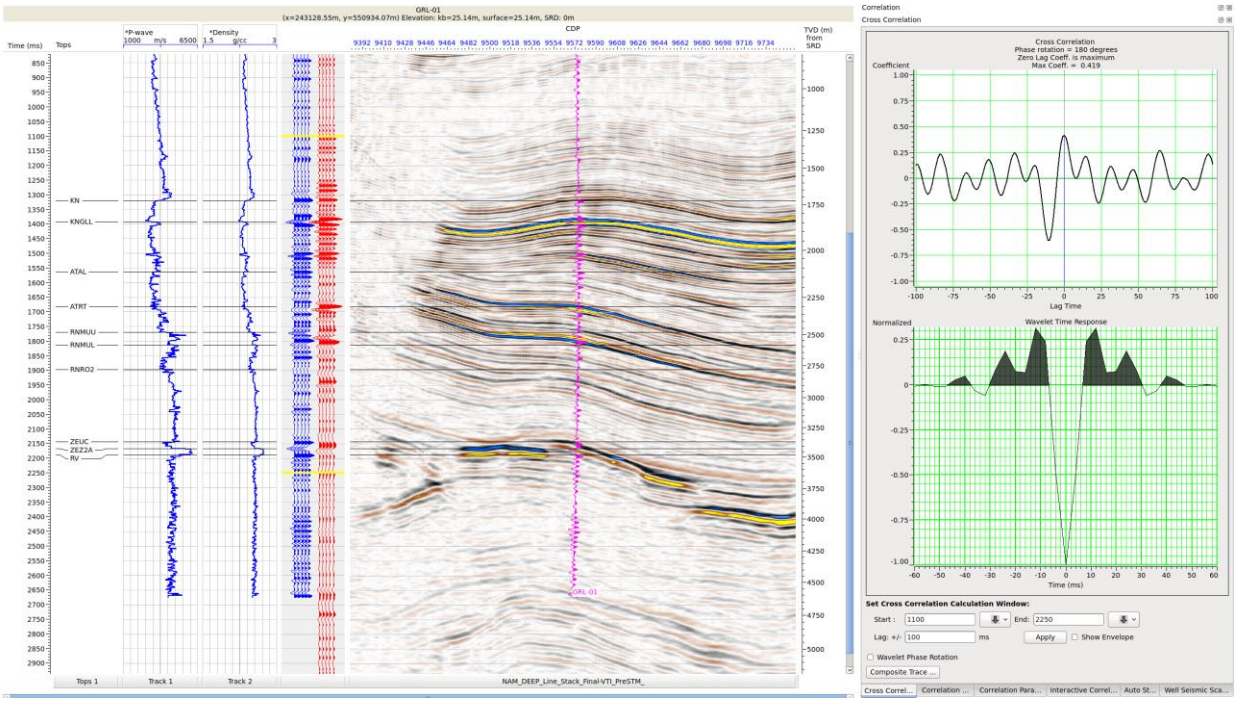

Fig. 63. Well-to-seismic correlation at the well GRL-01 using final PreSTM data (phase rotation = +0°) NAM_DEEP_Line and statistically computed zero-phase wavelet. The match between the synthetic (blue) and the extracted trace (red) is expressed by cross-correlation (upper right). Cross-correlation window is marked by yellow lines. The synthetic trace was superimposed on seismic 2D line (purple).

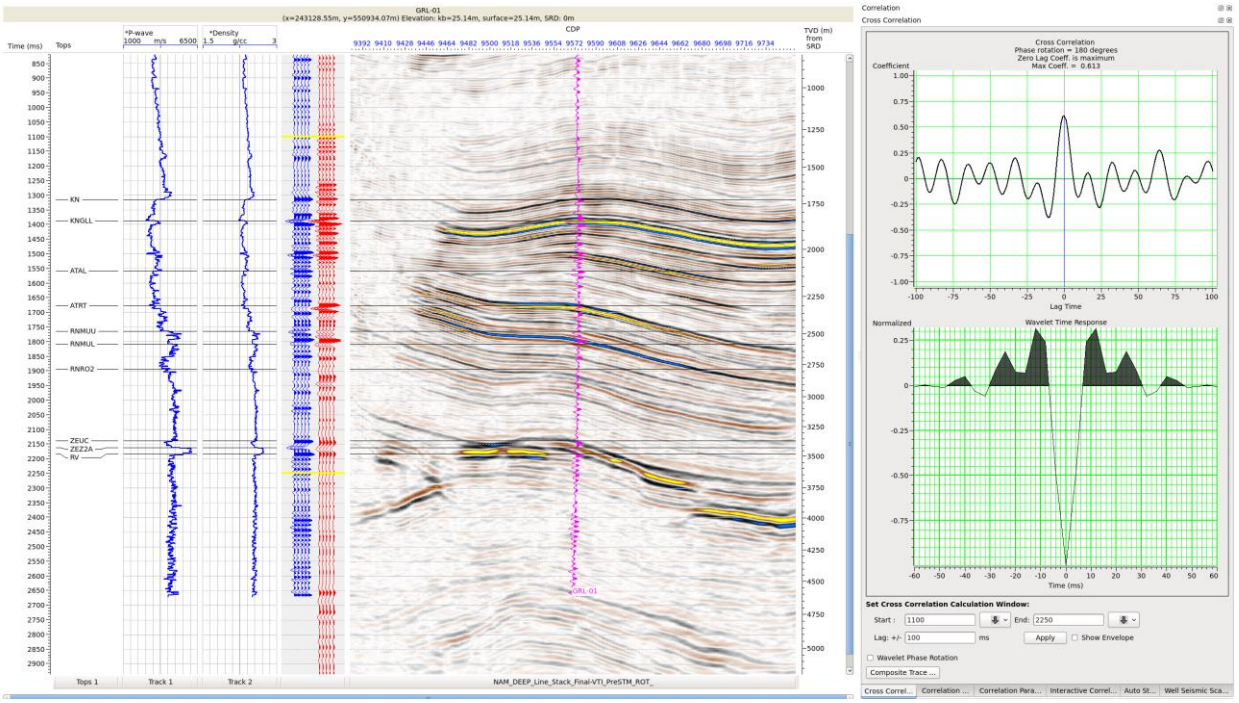

Fig. 64. Well-to-seismic correlation at the well GRL-01 using final PreSTM data (phase rotation = +90°) NAM_DEEP_Line and statistically computed zero-phase wavelet. The match between the synthetic (blue) and the extracted trace (red) is expressed by cross-correlation (upper right). Cross-correlation window is marked by yellow lines. The synthetic trace was superimposed on seismic 2D line (purple).

10. Illustration of processing results

Figures 65 - 67 illustrate Basic Processing results, whereas Fig. 68 shows of the NAM-DEEP vintage data.

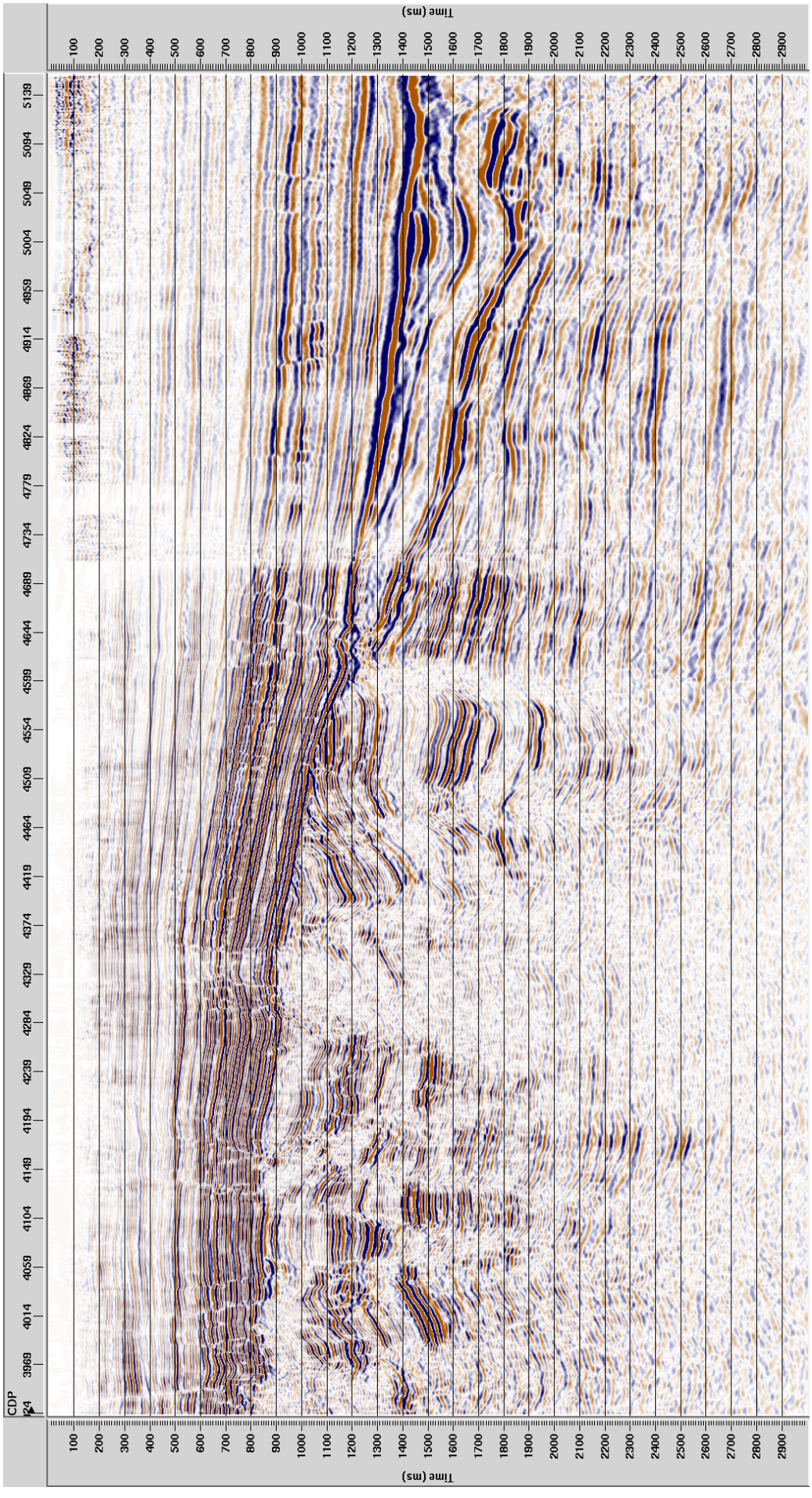

Fig. 65. Final seismic section after VTI PreSTM with real amplitude preservation (RAP) before post-processing.

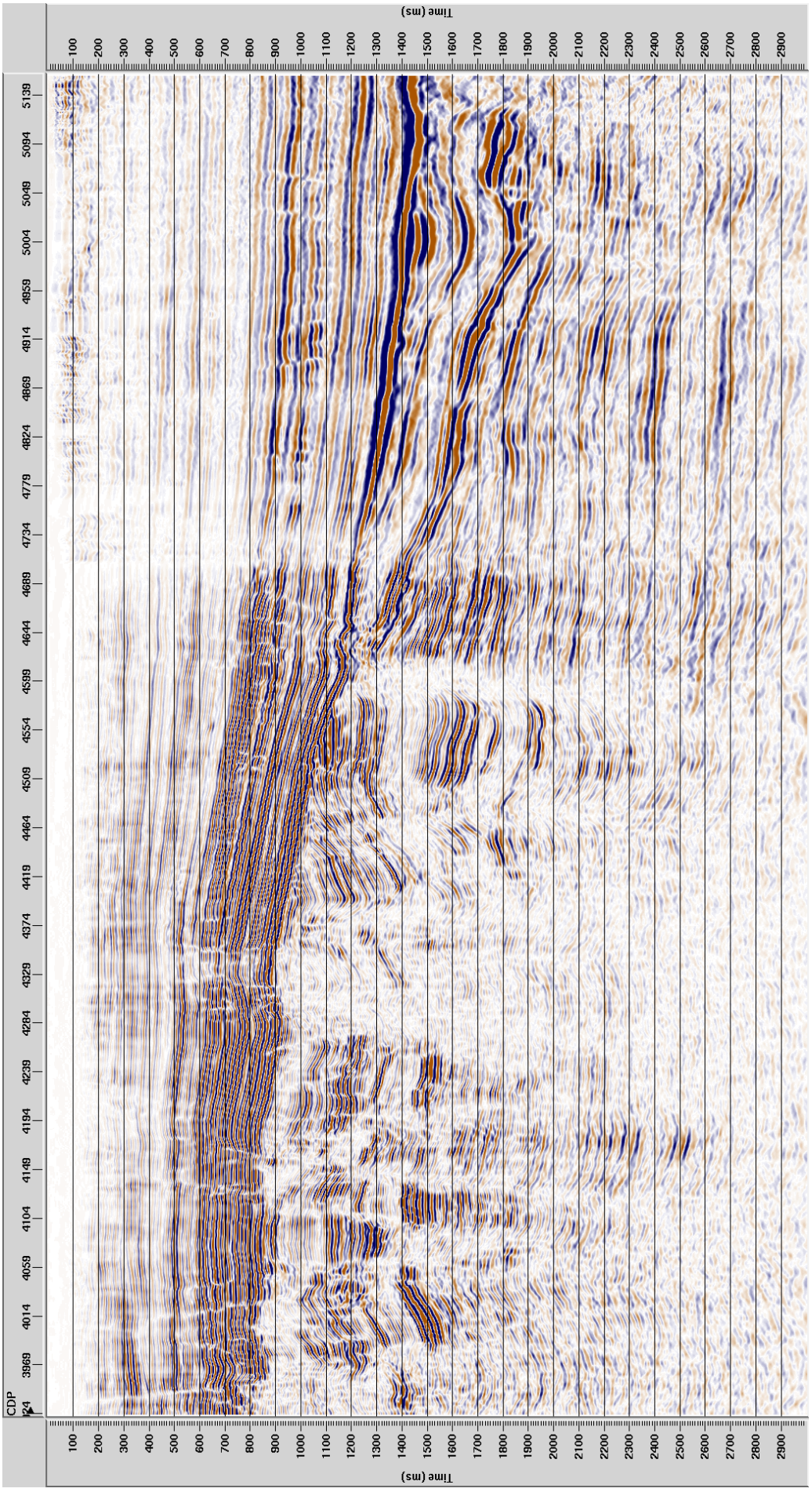

Fig. 66. Final seismic section after VTI PreSTM with real amplitude preservation (RAP) after post-processing.

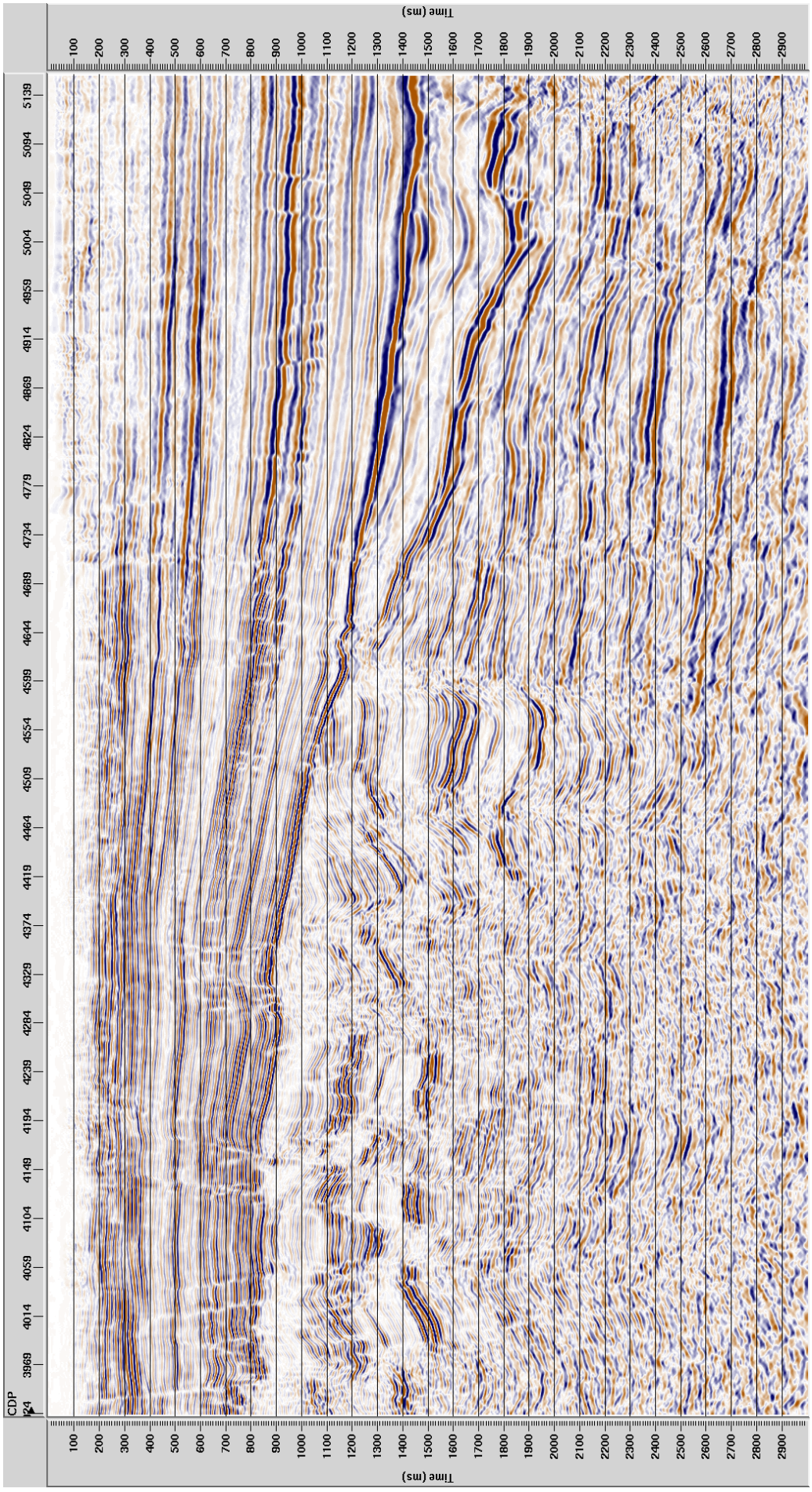

Fig. 67 Final seismic section after VTI PreSTM with dynamic scaling (AGC) applied post-stack, after post-processing.

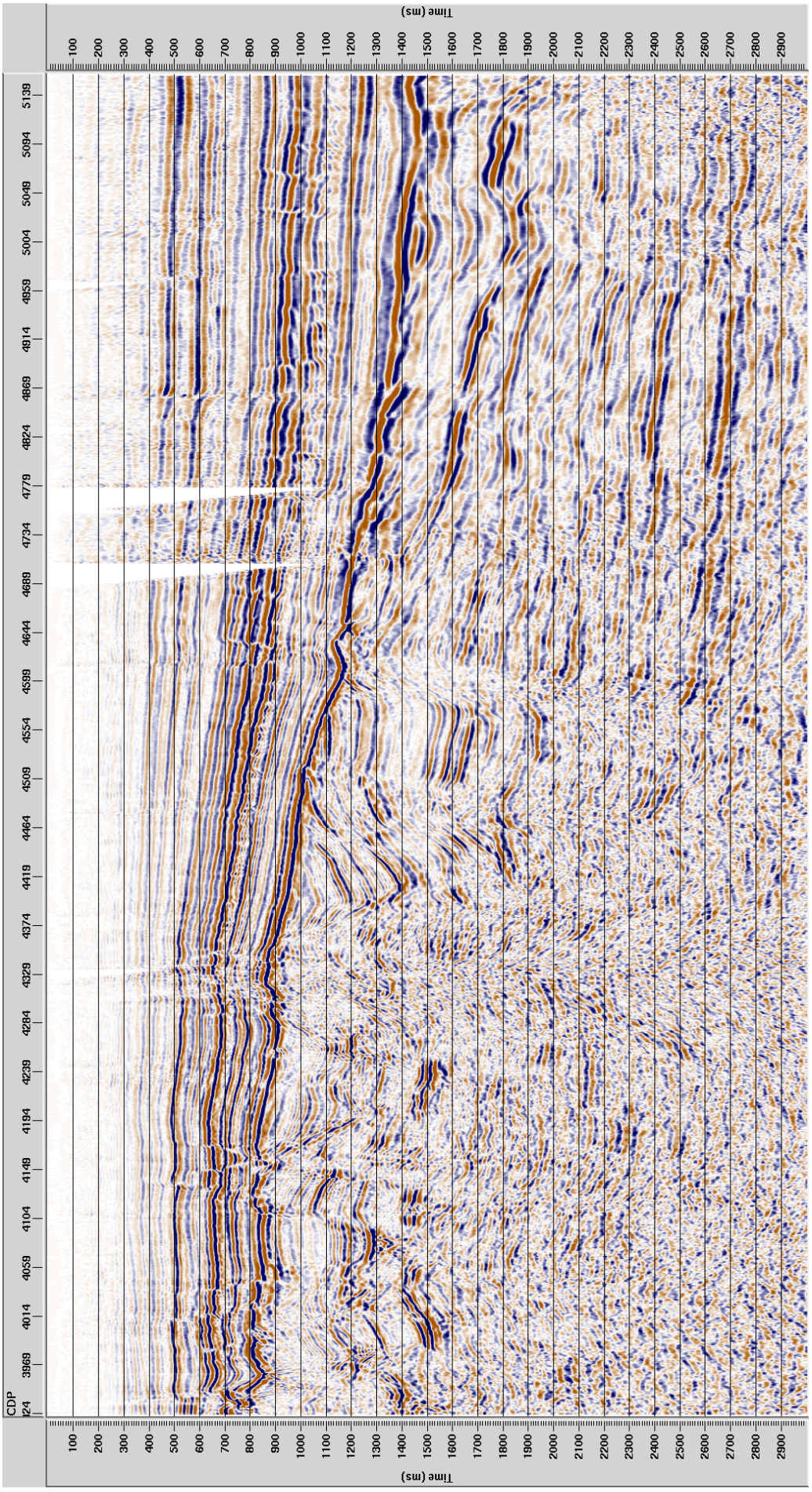

Fig. 68. NAM-DEEP vintage seismic section (legacy processing): PoSTM with time variant scaling applied before stack and after post-processing (according to the archive SEG-Y Header).

11. Summary

The key objectives of reprocessing were:

- produce the seismic image for structural interpretation and preserve true amplitudes as much as possible, especially in the poor image areas related to complex structures,
- decrease the subsurface uncertainty in order to delineate conditions needed for the successful development of geothermal projects in the area of interest,
- resolve the structural complexities and avoid erroneous interpretation results due to distorted images,
- accurate placement of reflectors at their actual sub-surface positions, in time domain of the seismic images,
- produce seismic velocities with reasonable geological meaning.

Time domain processed data achieved expected quality which was due to sophisticated and customized processing. During work to meet processing objectives, the main processing workflow was adjusted and parameters were selected according to current test results. The final image was improved by advanced procedures e.g. *LSS Trace Interpolation* (which also provided higher quality input for pre-stack time migration, *Radon Filter* (manually picked muting was variable along the survey and was one of the key to achieve a good result), Pre-Stack Time Migration with *VTI anisotropic moveout* option (improved the quality of migration). The comparison of current reprocessing and legacy processing results is provided at Figure 67 and Figure 68.

The most time-consuming stage was preparing of navigation data - mostly manual. The creation of a uniform geometry for many lines of different types (single, triple) and with different acquisition parameters was a big challenge. Due to the abovementioned reasons and additional work, processing took much longer than the time provided for in the Contract.

Close cooperation between the processing team and Client representatives was especially important for the successful completion of the project.

The main objectives of reprocessing were achieved.

GEOFIZYKA TORUN S.A.

ul. Chrobrego 50

87-100 TORUN

TEL.: +48 (56) 6593-277

FAX.: +48 (56) 6593-311

E-MAIL: seisproc@GTservices.pl

WWW Page: http://www.GTservices.pl